Nano-DNA induced target assemblies - detection of small targets of DNA by forming networks

Chenze Lu

Communauté
UNIVERSITÉ Grenoble Alpes

THÈSE

Pour obtenir le grade de

DOCTEUR DE LA COMMUNAUTÉ UNIVERSITÉ GRENOBLE ALPES

Spécialité : **Biologie Structurale et Nanobiologie**

Arrêté ministériel : 25 mai 2016

Présentée par

Chenze LU

Thèse dirigée par **Eric PEYRIN** et
codirigée par **Arnaud BUHOT, Didier GASPARUTTO**

préparée au sein du **CEA Grenoble**
Institut Nanosciences et Cryogénie (INAC)
Service : SYstèmes Moléculaires et nanoMatériaux pour l'Energie et la Santé (SyMMES)
Groupe : Chimie pour la Reconnaissance et l'Etude des Assemblages Biologiques (CREAB)
de l'Université Grenoble Alpes

Nano-assemblages d'ADN induites par des cibles – Détection de petites cibles par formation de réseaux d'ADN

Thèse soutenue publiquement le **« 13 Novembre 2017 »**,
devant le jury composé de :

M. Eric Defrancq
Prof. UGA et présent aux CST, Président

Mme. Maria Minunni
Prof. Univ. Florence, Rapporteur

M. Benoît Limoges
DR CNRS, UPMC, Paris, Rapporteur

Mme. Valérie Pichon
Prof. ESPCI Paris, Examinateur

M. Eric Peyrin
Prof. UGA, Directeur de thèse

M. Didier Gasparutto
CEA, Co-Directeur de thèse

M. Arnaud Buhot
CEA, Encadrant de thèse, Invité

Table of Contents

Abbreviation

Au	Gold
Au NP	Gold Nanoparticle
bp	Base pair
CCD	Charge Coupled Device
dsDNA	Double strand DNA
DNA	deoxyribonucleic acid
EIS	Electrochemical Impedance Spectroscopy
FET	Field Effect Transistor
FRET	Fluorescence Resonance Energy Transfer
HPLC	High Performance Liquid Chromatography
K_D	Dissociation constant at equilibrium
LED	Light Emitting Diode
LoD	Limit of Detection
MIP	Molecular imprinted polymer
OD	Optical Density
PCR	Polymerase Chain Reaction
QCM	Quartz Crystal Microbalance
RNA	Ribonucleic acid
SAMs	Self-Assembled Monolayers
SELEX	Systematic Evolution of Ligands by EXponential enrichment
SPR	Surface Plasmon Resonance
SPRi	Surface Plasmon Resonance imaging
ssDNA	Single strand DNA
TEMED	Tetramethylethylenediamine
UV	Ultraviolet

Résumé de la thèse

La détection de petites molécules contribue au développement de nombreux domaines tels que la sécurité alimentaire, la sécurité intérieure, le diagnostic, le contrôle de l'environnement, etc. Cependant, la petite taille dees cibles et leur faible concentration rendent difficile leur détection. Pour pallier à cela, des biocapteurs avec des sondes appropriées et des stratégies d'amplification du signal sont nécessaires. Parmi les éléments de reconnaissance couramment utilisés, les aptamères présentent l'avantage d'une synthèse aisée et de grandes possibilités de modification, ainsi qu'une dénaturation réversible à haute température et une tolérance élevée à la concentration en sel et au pH dans le milieu de travail. Plus important encore, la petite taille des aptamères en fait un choix idéal pour créer des structures adaptées pour la détection de petites cibles. La possibilité de couper la séquence de l'aptamère a fourni d'autres approches d'amplification de signal. Il existe deux catégories de méthodes de détection basées sur des aptamères : analyse hétérogène lorsque l'aptamère est immobilisé sur la surface ou analyse homogène lorsque le test est réalisé en solution. Nous proposons dans cette thèse une approche appliquable aux deux stratégies. L'adénosine a été utilisée comme une cible modèle pour cette preuve de concept. La détection de l'adénosine a été obtenue en combinant l'auto-assemblage de dimères d'oligonucléotides avec des extrémités pendantes correspondantes à l'aptamère coupé. Nous avons construit des structures auto-assemblées d'ADN (de 1D à 3D) avec l'adénosine comme déclencheur d'un changement structurel. La première méthode décrite dans ce travail consiste à utiliser de telles structures d'ADN combinées à l'imagerie par Résonance de Plasmons de Surface (SPRi). La SPRi est une méthode sensible à la variation d'indice optique produite par l'interaction entre les sondes immobilisées sur le prisme de l'or et la cible dans la solution. En présence d'adénosine, la structure d'ADN s'auto-assemble sur la surface de l'or et un signal a été créé. La limite de détection de l'adénosine atteinte par cette méthode est de 10 µM. La deuxième méthode homogène consiste à analyser les variations d'absorbance UV de la solution contenant les structures d'ADN puisque l'absorbance UV de l'ADN monocaténaire et du duplex ADN hybridé est différente. En raison de cet effet, la température de fusion des brins d'ADN peut être déterminée par la dérivée de l'absorbance UV mesurée. Les structures d'ADN combinant les extrémités pendantes de l'aptamère coupé couplées à des oligonucléotides complémentaires présentent deux températures de fusion caractéristique de la dissociation de chaque partie. L'une correspond à

l'oligonucléotide hybridé et l'autre à l'aptamère coupé liant l'adénosine. En présence d'adénosine dans la solution, la stabilité de la structure augmente et le pic de fusion de l'aptamère coupé est décalé à une température plus élevée tandis que le second pic de fusion reste identique et peut servir de référence interne. La limite de détection atteinte pour cette méthode est de 1 µM. Les structures d'ADN que nous avons proposées s'auto-assemblent de manière linéaire ou bi- ou tri-dimensionnelle. La structure 1D est une chaîne d'ADN formée par un enchainement de dimères connectés par des extrémités formées de l'aptamère scindé. La structure en 2D est une structure en forme de Y formée par un ADN simple brin avec une extrémité aptamère scindé sur chaque branche du "Y". La structure 3D est un tétraèdre formé par quatre simple brins d'ADN avec des extrémités aptamère scindé sur les quatre sommets. En présence d'adénosine, les structures 2D et 3D peuvent s'auto-assembler et ainsi former un réseau avec les extrémités pendantes. La structure 1D a été mûrement développée pour les deux méthodes, les structures 2D et 3D ont été de efficaces pour la détection, mais nécessitent encore plus d'efforts pour permettre une détection optimisée.

Chapter 1 Introduction

Les biocapteurs jouent un rôle important dans des domaines comme le diagnostic, la délivrance de médicaments, la surveillance de la santé, la sécurité alimentaire, le contrôle de l'environnement, la sécurité intérieure, etc. Ce chapitre présente les dernières recherches portant sur les biocapteurs. Les biocapteurs ont été triés par leurs éléments de reconnaissance et leurs transducteurs, afin de donner un aperçu des avantages et des inconvénients de ces différentes méthodes de détection. En particulier, nous nous sommes concentrés sur la comparaison des biocapteurs conçus pour la détection de petites molécules. Une grande part des méthodes de détection actuelles repose sur la fonctionnalisation des éléments de reconnaissance sur des nanoparticules d'or ou de l'utilisation d'un marquage fluorescent pour obtenir une bonne détection. Le but de ce travail est de développer de nouvelles méthodes de détection qui ne nécessitent ni nanoparticules d'or ni marquage fluorescent, en utilisant des structures d'ADN 1D à 3D combinées à des séquences aptamères possédant un site de reconnaissance simple brin. Parmi les différents éléments de reconnaissance présentés dans ce chapitre, l'ADN aptamère a été sélectionné dans notre travail en raison de ses avantages dans la détection de petites cibles et des propriétés de liaison spécifique exceptionnelles. Plus important encore, sa nature de brin d'ADN nous a permis de construire des structures de reconnaissance sélectives de type aptamériques. Nous avons proposé d'utiliser de telles structures d'ADN complexes comme moyen d'optimiser les méthodes de détection. Deux méthodes de détection différentes ont été rapportées dans cette étude: une méthode hétérogène utilisant l'imagerie par Résonance Plasmonique de Surface (SPRi) et une méthode homogène utilisant la spectroscopie UV-Vis.

1.1 History and introduction of biosensor

The purpose of a sensor is to convert physical, chemical or biological information into other kind of signal to offer a better understanding of the detected system. The parameters sensed could be the weight, temperature, movement of the material or the presence of other objects. The first sensor could be dated back to the invention of barometer in 1594, whereas the pressure of the surrounding air is converted into the height of the mercury pillar. Nowadays the finest instruments depend highly on these sensors to monitor the condition of vital components or trigger certain response according to the external stimulate. The stimulation was received by the sensor and recognition element will recognize the change before and after the stimulation and output the signal. Sensors can be sorted into chemical sensor, physical sensor and biosensor depending on the principle of the recognition.

Biosensors use sensitive biological elements that are able to recognize specific analyte to transduce biological interactions into physicochemical signals. We can get an understanding of their bio-composition, structure and function by converting a biological response into an electrical signal. People started focusing on developing biosensors since 1960s, when Clark and Lyons built their first generation glucose oxidase biosensor. [1] Using this technology the first commercial biosensor emerged in 1975, the Yellow Springs Instruments Company analyzer (Model 23A YSI analyzer) for the direct measurement of glucose based on the amperometric detection of hydrogen peroxide.[2] But the application of this model was greatly impeded by the high cost of the platinum electrode and limited only to clinical laboratories uses. In the coming decades, we saw one after another milestone in the research of biosensors. (**Table 1.1**)

Year	Breakthrough in biosensor history
1962	Clark and Lyons first proposed glucose enzyme electrodes [1]
1975	Fiber-optic biosensor for carbon dioxide and oxygen detection by Lubbers and Opitz [3]
1975	First microbe-based immunosensor by Suzuki et al. [4]
1982	Fiber-optic biosensor for glucose detection by Schultz [5]
1983	First Surface plasmon resonance (SPR) immunosensor by Liedberg et al. [6]
1984	First mediated amperometric biosensor: ferrocene used with glucose oxidase for glucose detection[7]
1990	Commercialized SPR-based biosensor by Pharmacia BIAcore[8]
1992	Handheld blood biosensor by i-STAT[8]

Table 1.1 Milestones in biosensor development between 1960 and 2000[9]

In the beginning of 21st century, the development of biosensor stepped into a new era. The thriving improvement of other scientific fields has given more abundant choices in designing biosensor devices. Biosensors were combined with BioMEMS, Quantum dots, nanoparticles, nanowire, nanotube, etc. [10] Thus, despite the term "bio" in the name, building a biosensor requires knowledge in multiple research fields. In the past decade, more and more papers were published with the key word "biosensor". We collected the number of paper sorted under the category of biosensor in the "Web of Science" database during the last decade (**Figure 1.1**). The date showed that the paper published each year has been increasing for the past ten years, these papers covered various field of scientific studies and applications. In medical applications, biosensors could be used for monitoring the vitals of patients, developing new drugs and diagnose of the diseases.[11–13] In public services, biosensors could be used for monitoring the environment, such as the quality of water and air.[14–16] Moreover, these sensors play an important role in civil life by controlling food safety and homeland security. [17–20]

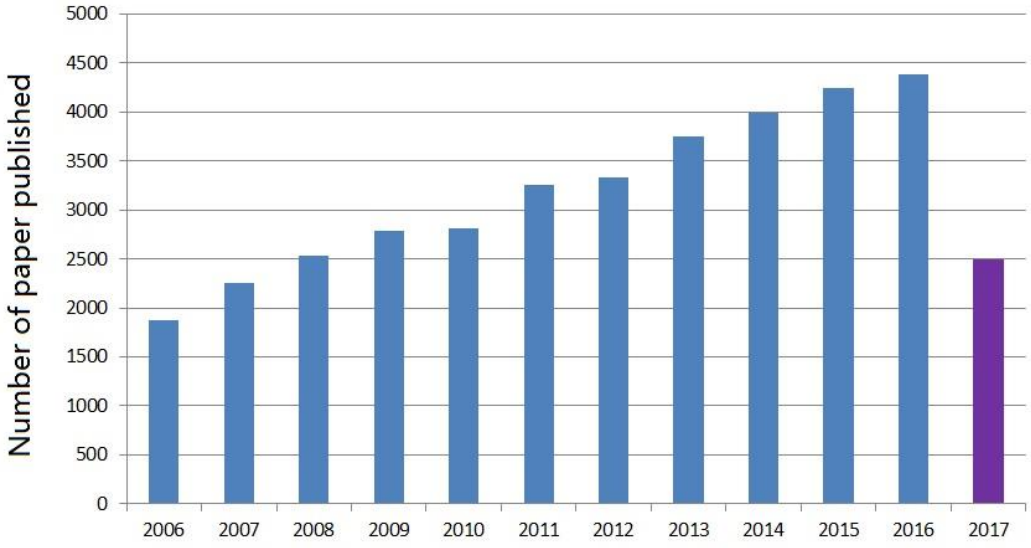

Figure 1.1 The number of paper published in the field of biosensor (2006-2017). The number was the search result of the paper categorized under the topic "Biosensor", the number showed a continuous increase during the last decade. The number in the year 2017 only represent the number obtained in August and was marked in purple.

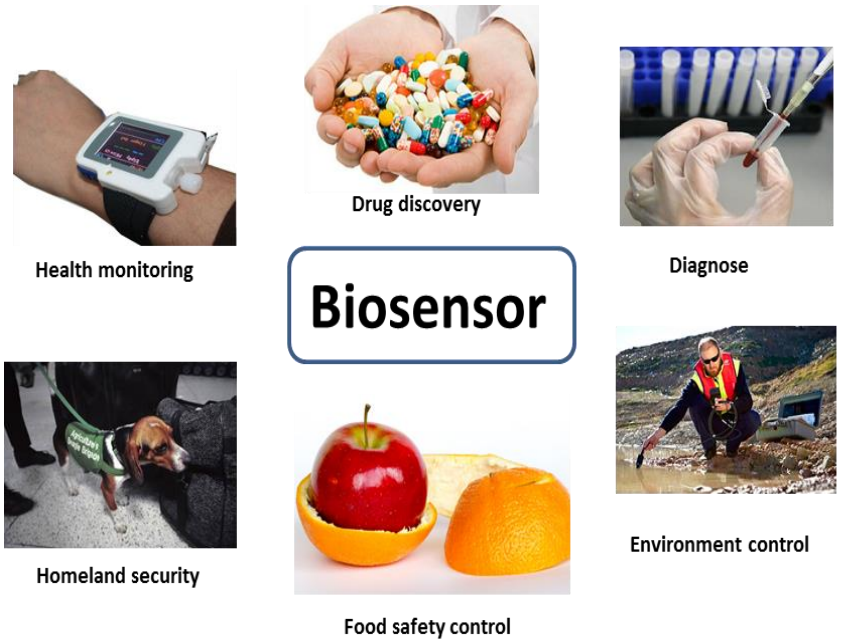

Figure 1.2 The common applications of biosensor [11–20]

1.2 The varieties of transducers

A sensor consists of four parts (**Figure 1.3**): the signal input, recognition element, transducer and user interface. The recognition elements specifically interact with the analyte and capture the analyte to generate the signal in forms of light, heat, change in pH or mass, etc. The recognition element determines the selectivity of the sensor. Selectivity is the ability of a sensor to recognize the right target among many different species, it is the most important feature of biosensor and the foundation of the detection. In order to improve the performance of biosensor, its recognition element should have high specificity and affinity to the target as well as considerable lower cost and simpler production process during the manufactory. The pros and cons of each recognition element in today's sensing technology will be compared in the following section.

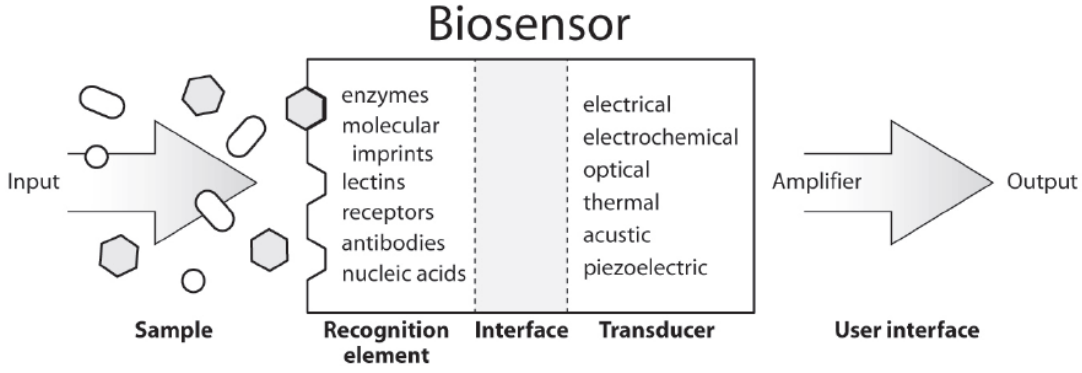

Figure 1.3 The five main elements composting a biosensor [21]

The first step of the detection process was to capture the target in the sample by with the recognition element. In order to observe this process, the recognition element is usually immobilized on an interface through which it is connected to the transducer. The commonly used interface includes metal surface, semiconductors, crystal etc. The recognition process will create a change in certain property of the interface and the transducer monitors this property and converts the change into another form of signal that is easier to be observed, measured and recorded. Different variations of biosensors are usually sorted by the technology used in the transducer, such as: optical sensor, electrochemical sensor, electronic sensor, piezoelectric sensor, pyroelectric sensor, gravimetric sensor, affinity sensor, etc.[22,23] The quality of the transducer

determines the reproducibility and stability accuracy of the sensor. Sensors with higher reproducibility tend to provide the same result under the same conditions and the stability is the sensor's resistance against perturbations in the environment. One could see that the performance of the biosensor depend highly on the transducer.

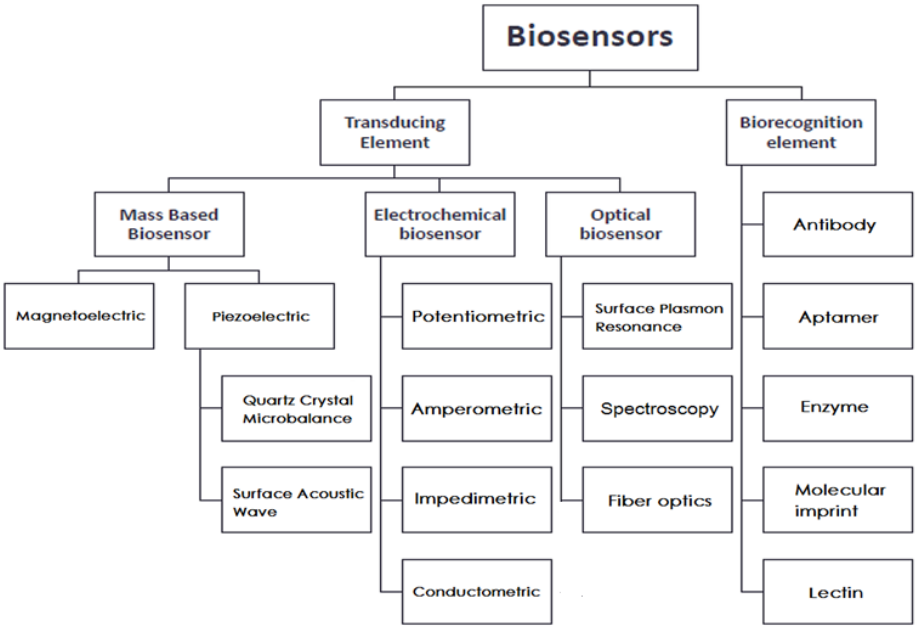

Figure 1.4 The three categories of transducer with their branches and five commonly used biorecognition elements [22,23]

To briefly sum up the different types of biosensor, they could be sorted into three categories: electrochemical detection, optical detection and mass detection. The three branches can be further divided into several techniques. The commonly seen recognition elements include: antibody, aptamer, molecular imprinted polymer, enzyme and lectin. These transducers and recognition elements have their own advantages and disadvantages and the choice of the combination varies according to the purpose of the sensor.

1.2.1 Electrochemical biosensor

Electrochemical biosensor was the first biosensor designs built and commercially available in the market. The idea was based on the work of Clark in 1962, where the enzyme was immobilized on the surface as chemically modified electrode. [1] So far, electrochemical biosensor is still considered the most mature and commercially

available type among the biosensors. The general principle of this kind of sensor is that the chemical reactions between the biomolecule immobilized and the target will either produce or consume ions and electrons in the solution, this will change the electrical property of the solution like electric potential or create a current. It can be divided into four categories: conductometric, amperometric, impedimetric and potentiometric electrochemical sensor.

Conductometric biosensors

The sensing of condutometric biosensors are based on the change in the ionic composition of the sample or the creation of charged objects during the recognition reactions involved.[24,25] Its principle has a wide range of application for the chemical system since a great portion of chemical reactions are related to the production or consumption of ions.

The advantages of this kind of sensor includes: 1) the thin-film electrodes are easy for mass production at reasonable cost; 2) the system requires no reference electrode; 3) the transducer is not sensitive to light; 4) the system can work under low voltage to consume less power. However, since the measurement of the conductance is non-specific against all the ions in solution, conductometric biosensors needed to overcome the lack in specificity. [26] Various attempts were made to solve this problem, for instance, in 1994 Watson et al developed a method to monitor only the conductance produced by the catalytic action of enzymes immobilized over a planar conductance cell.[27] In more recent studies, this problem was overcame with integrated micro biosensor using a differential measuring scheme that can substrate the changes in background conductivity, ruling out the influence of other parameters in the environment, such as the temperature. [28,29]

Amperometric biosensors

Amperometric biosensors are also known as enzyme electrodes, they combine the high selectivity of enzymes with electrochemistry methods. A constant potential is applied between the sensing or working electrode and the counter electrode in the testing environment. The current as the result of an electrode reaction is measured and it is proportional to the concentration of the target. The voltage should exceed the

threshold to make sure the ongoing reaction is the desired reaction. This requires a reference electrode that has repeatable stable surface at fixed potential (for example Ag/AgCl). [26]

Earlier two-electrode models amperometric biosensor with only working and reference electrodes faced the problem of losing linear range due to the limited control of the potential on working electrode at high current. [30] Later on an auxiliary electrode was added to form the three-electrode model. When the voltage is applied between working and reference electrodes, the current is flowing between the auxiliary and working electrodes instead of the reference electrode. More recently, the detection system was combined with microarrays to further improve the performance. For example, an alkaline phosphatase based electrochemical hybridization assay for the detection of HCMV-amplified DNA was reported to have successfully increased the sensitivity and lower the detection limit. [31,32]

The detection limit provided by amperometric biosensor is typically low (in the range of 10^{-7} to 10^{-8} M). The mass production is also easier compared to other electrochemical biosensors like impedimetric biosensor, conductometric biosensors and potentiometric biosensors. The most mature application of amperometric biosensor is the detection of glucose, which is not only effective but has also been successfully commercialized and widely used. [33]

Impedimetric biosensors

Impedance (Z) is a parameter related with resistance (R) and capacity (C). The detection of impedimetric biosensors is based on the direct measurement of the impedance or its two components R and C. [30] Impedimetric biosensors are based on electrochemical impedance spectroscopy (EIS). It started with the work of Newman and Martelet in 1980s [34,35], since then the research of impedimetric biosensor has greatly improved but still limited in academic area, not yet available in market. The most common impedimetric sensor is enzyme immunosensor. The ions created in the enzymatic reaction can significantly increase the impedance, the transducer capture this change to analyze the solution.

The most widely used impedimetric biosensors are lock-in amplifiers and frequency response analyzers (FRA) [36]. Impedimetric sensors based on lock-in

amplifiers are very sensitive and the noise can be effectively suppressed, harmonic distortions are minimized. Its limitation is that the measurement takes much time and it is difficult to be used for standalone measurement, the frequency range is also not wide. Impedance tests based on FRA, on the other hand, could be used for quick tests with wide frequency range, remove harmonic distortions. However its sensitivity is limited and the cost is higher for FRA based systems.

Potentiometric biosensors

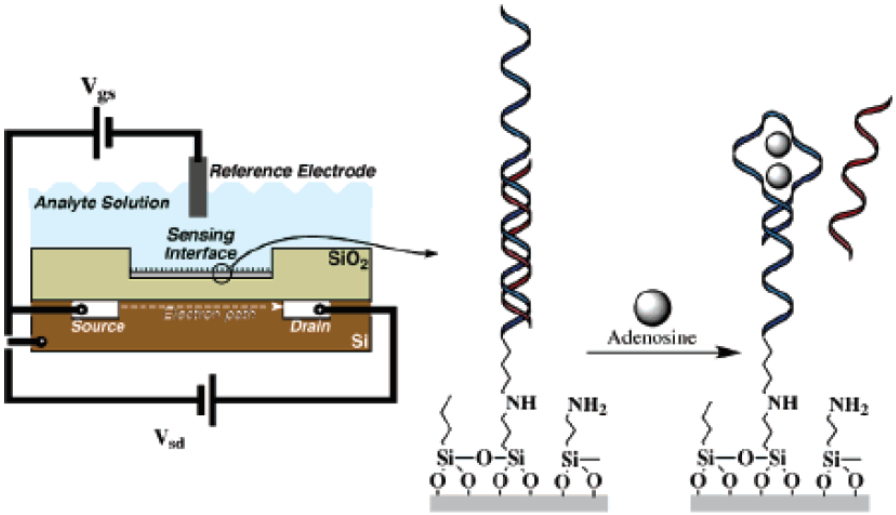

Figure 1.5 A label-free, reagentless sensor for Adenosine using an ISFET device. The sensing interface was functionalized with aptamer probes and a short oligonucleotide was hybridized onto the probe. With the target (Adenosine) in the solution, the aptamer will fold and releasing the short strand and alters the source-to-drain current.[23]

Potentionmetric biosensors use the accumulation of charge density at an electrode surface and the increase of the potential at that electrode to realize the measurement. The whole process is non-faradic and without current in the system. The idea first came with the invention of field effect transistor (FET). The usual gate metal electrode in the traditional metal–oxide–semiconductor field-effect transistor (MOSFET) was replaced by membrane or a reference electrode and turned into ion-selective field effect transistor (ISFET). The bio-recognition element could be either immobilized on the outer surface or captured inside the membrane. The modern semiconductor technology provided more profound foundation for ISFET. The potential drives the current through the semiconductor layer, the gate surface of the

transistor is covered with ion-selective membrane, for example Si_3N_4, Al_2O_3, ZrO_2 for detection of pH. [37] The output signal is the result of the ions accumulated at the ion-selective membrane interface. [38] The advantage of Potentiometric biosensors are their low detection limit, independence of sample volume. [39–41] In **Figure 1.5** we gave an example of a label-free reagentless sensor based on ISFET device. [23] The surface was functionalized with aptamer probes which were partly hybridized. The aptamer bended and released the short DNA fragments hybridized on the aptamer probes with the presence of Adenosine molecules. In the meantime the change of the mass on the surface due to the release of the DNA fragments caused a difference in the source-to-drain current.

1.2.2 Mass based biosensor

Mass based biosensors normally use the receptor to capture the target, to cause a change in the mass on the surface on which the receptors were immobilized. The signal output will be affected by this change and enable the detection. [42] One example is the piezoelectric biosensor which uses a chemical interactive membrane in contact with piezoelectric material, the detection is based on the change in resonance frequency caused by the change in mass. The mass based biosensor could also use magnetic force to sense the analyte. Magnetic beads have been used as label to realize the sensing process. The advantage of mass based biosensor is the easy quantification of target due to the fact that its signal is proportional to mass.

Piezoelectric biosensor

The piezoelectric phenomenon, that is, the generation of an electrical potential between two deformed surfaces when a pressure is applied on quartz plates in certain direction, was discovered by Curie brothers in 1880. [43] This phenomenon could not be used in the sensing research until Sauerbrey established an equation to describe the relationship between frequency and mass in 1959 known as the Sauerbrey equation.[44]

There are two different sensing methods with piezoelectric material: quartz crystal microbalances (QCM) device and surface acoustic wave (SAW) device. They both measure the change in the resonance frequency of the material to determine the

mass change on the surface. The main difference between these two methods is that the acoustic wave is transmitting inside the crystal in the case of QCM device, and for the SAW device the acoustic wave is transmitting on the surface. In general, SAW device has lower detection limit and higher mass sensitivity compared to QCM device, and the material and set up required for QCM is cheaper and hence easier to be commercialized. The recent research works are focused on the development of SAW device to achieve better performance.

The sensors based on QCM device operate with bulk acoustic wave (BAW). Among all the materials that exhibit the piezoelectric effect, quartz crystal is the most common crystal type used.[45] The piezo quartz crystal is placed between two electrodes, usually done by thermal evaporation of gold or silver onto the quartz surface. By controlling the potential on two electrodes and the electric field generated during this process, the crystal will display a mechanical oscillation of a standing shear wave across the bulk of the quartz. The first application of QCM in chemical analysis was reported in 1964 by King et al where QCM was used as a gas chromatograph sorption detector. [46] Same as SAW sensors, QCM sensor also needed years to overcome the difficulty while detecting in solution phase. The first liquid phase detection was made in 1980 by Konash and Bastiaans [47]. Over the coming years, people worked hard to broaden the applications and improve the sensitivity of the sensors. The modern biosensors based on QCM device uses bio-receptors immobilized on the surface to capture the target in the solution, the additional mass of the target attached to the surface will lead to a change in the oscillating frequency. For example, in **Figure 1.6** is the work of Liss who immobilized biotinylated aptamer on the sensing interface as recognition element on gold coated quartz crystal. [48] The aptamer was specific for an antibody IgE and the sensor was used to study their aptamer-protein binding properties. Once IgE was captured by the aptamer, the change in the mass will create a noticeable difference in the oscillating frequency.

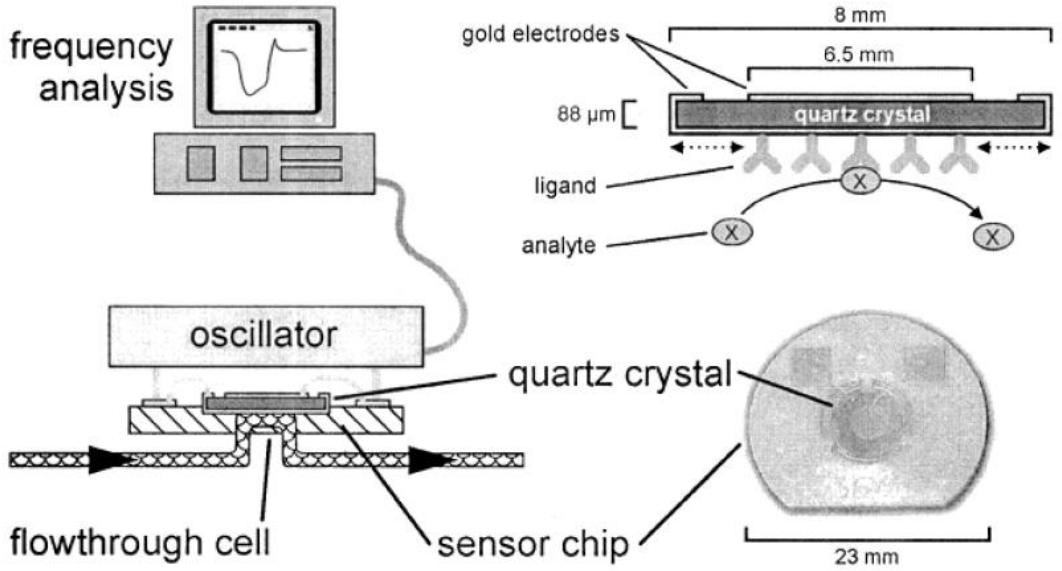

Figure 1.6 A label-free, reagentless QCM aptasensor for IgE detection. The gold coated quartz crystal was functionalized with biotinylated aptamer strands. With the target (IgE) in the solution the aptamer on the surface will capture the target. The mass on the surface was increased and caused a change in the oscillating frequency at the same time. This change was detected and recorded by the frequency analysis system. [48]

There are two common approaches to build sensor with piezo quartz crystal. The first is to use the crystal itself part of the oscillator circuit. In return, the crystal vibrates at the frequency determined by the material. The second way is to connect the crystal to an external device that can apply alternating voltage and pass various frequencies across the crystal.[45,49] The benefit of the second approach is the vibration frequency is not limited by the crystal. But most of the QCM sensors used the first method due to the difficult set up for the second approach.

SAW devices can generate or detect acoustic waves with transducers on the surface of the piezoelectric crystal. Unlike BAW device, the acoustic energy is confined at the surface in the range of the acoustic wavelength regardless of the thickness of the crystal. [50] The acoustic wave is sensitive to the change on the surface, such as mass, viscosity and conductivity. The first SAW sensor was proposed by Wohltjen and Dessy in 1979 using the Rayleigh-type SAW.[51] In their work, the device was coated with sensitive polymer layer which was used for organic gas detection. Since then SAW sensor was widely used in gas detection.

However, when people first attempted to use SAW sensors for detection of bio components, the Rayleigh-type model failed to show the same efficiency in gas detection while immersed in biological buffer. The poor performance was due to the immense attenuation caused by the displacement components perpendicular to the surface.[52] To overcome this problem, the model of acoustic plate mode (APM) was proposed. In this mode, the acoustic wave is trapped by multiple reflections between the two surfaces and substrate. This way, the acoustic wave is kept on the back side of the device, away from the sensing front side which has to be immersed in buffer. [53] However, this method has another drawback: it is difficult to operate the device in standard oscillator circuit.

Magnetic biosensors

Magnetic biosensors usually involve microfluidic channels for detection of magnetic micro or nano particles based on the magnetoresistance effect. Its application in medical diagnose is very versatile. It could be used as label for detection using magnetometer, or as a tool to separate and enrich the wanted target. [54,55] The use of magnetic biosensors focused on medical applications because of the natural absence of magnetic elements in bio-system. The other advantages include: (1) stability, the magnetic nano particles are stable labels, unlike fluorescent dyes that will bleach over time; (2) the particles could be used in opaque media like blood or tissue; (3) it is harmless to human body; (4) the particles could be manipulated with magnetic field; (5) low time consuming detection is possible.

The materials used for magnetic nanoparticles could be magnetite (Fe_3O_4), greigite (Fe_3S_4), maghemite (γ-Fe_2O_3) or ferrites (MeO·Fe_2O_3, where Me=Ni, Co, Mg, Zn, Mn, etc.)[56] Their size and magnetic properties were modified to pursuit the best sensing in applications. The improvement in detecting technique based on magnetic labels was remarkable during the first decade of 21st century. In 1999, magnetic nanoparticles were used to separate cells marked with magnetic label in solution under a gradient of magnetic field by Safařík and Šafaříková. [54] In addition to that, magnetic immunoassay was also built to make full use of the magnetic label. In the work of Richardson's group coated paramagnetic particles were used as a physical label for the detection of human transferrin.[55]

There are two main principles used in magnetic biosensor, the magnetic relaxation sensor and magneto resistive sensor. In the field of magnetic study, the term relaxation describes how signals change with time. The nanoparticles binded to specific molecules serve as the contrast agent and produce local inhomogeneity in the applied magnetic field in the tissue being tested. The signal will decrease over time, when the magnetic field is turned off. This time is named the relaxation time. [57] There are two relaxation mechanisms named Brownian relaxation and Néel relaxation. The effective relaxation rate is expressed as the sum of the Brownian relaxation rate and the Néel relaxation rate.[58]

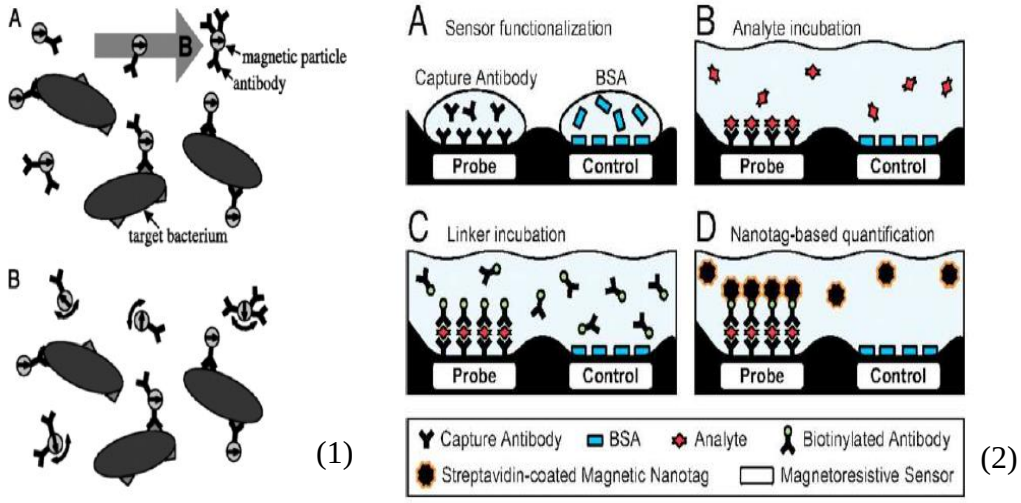

Figure 1.7 The principles of two magnetic biosensors. [58] 1) magnetic relaxation sensor: (A) the magnetic field gave the magnetic labels an orientation, (B) the relaxation time between the free labels and attached labels were different, which enabled the detection ; 2) magneto resistive sensor: (A) the surface was functionalized with capture antibody; (B) the analyte was captured by the antibodies. (C) biotinylated antibodies binded onto the analyte and formed a sandwich assay. (D) streptavidin-coated magnetic label binds onto the second batch of antibody and enabled the detection by changing the current in the magneto resistive sensor.

The relaxation of particle magnetic moments can be measured by Superconducting Quantum Interference Devices (SQUIDs). The detection can be based on the time difference between Brownian relaxation and Néel relaxation, some early applications involved the design of an immunoassay and detection of bacteria.[59,60] A magnetic field orients the magnetic moments of the nanoparticles, once the field is removed the Brownian motion will randomize the magnetic moments of the unbinded particles, but not the binded particles. The Brownian relaxation time of

the unbinded magnetic particle is extremely short and out of the detect range of the SQUID (1ms~1s), whereas the Brownian rotation of the particles bounded to the target is restricted. The Néel relaxation is in the detection range of SQUID, it can be used to determine the relaxation time of surface bounded particles. The sensitivity could be further improved by switching the magnetometer to a gradiometer by two-order of magnitude. [61]

Magneto resistive sensor collects the electrical current changed due to a difference in the magnetic fields and uses it for detection. The difference in the magnetic field is caused by the binding of magnetic particles on the sensing surface. There are direct and indirect mechanisms in binding of particles. The direct binding usually uses the streptavidin-biotin interaction or complementary DNA sequence recognition to direct grasp the magnetic particle in the contacting solution. The indirect approach, which is more commonly used, builds a sandwich structure on the surface for the binding. The surface is first functionalized with receptor, for example antibody, and then the analyte binds onto the surface due to the antibody-antigen recognition. After that recognition, another patch of biotinylated antibody bind onto the surface to form the sandwich. In the end the biotinylated antibody draws the streptavidin coated magnetic particles onto the surface as label. [62]

1.2.3 Optical biosensor

Spectroscopy based biosensor

Spectroscopy studies the interaction between the analyte and radiations most commonly as a function of its wavelength or frequency. Spectroscopy is widely used in physical and analytical chemistry for detection, identification and quantification of atoms and molecules based on their unique spectra. The detection methods using spectroscopy do not require functionalization of the recognition elements on the surface, and the equipment can be suitable for multiple targets without any further modification. The optical methods provide another benefit as well, the sample could be protected and recycled because light is non-invasive to the analyte.[63] In some cases, the sensor measures directly the light emitted by the target. [64,65] Sorted by the nature of the interaction, spectroscopy can be classified into three categories: absorption spectroscopy, emission spectroscopy and scattering spectroscopy.

UV-Vis spectroscopy is an absorption spectroscopy that records the amount of light at a certain wavelength absorbed by the sample. Quantification of the sample is also possible following the Beer–Lambert law. [66] Recent advances in optical devices have greatly promoted the performance of UV-Vis spectrometers. As the result, the detecting range of the wavelength can be from UV light to near infra-red. This technique combines high sensitivity, compactness and scanning speed with low cost, for these reasons it is very commonly used in industrial applications. Noui et al used a high-resolution UV spectrometer to monitor different kinds of bioprocesses. [67] Their sensor was able to monitor several targets simultaneously because the detector was built with concave holographic flat field diffraction grating and a charge coupled device allowed measurement of a continuous spectrum. Today the direction of improvement for UV-Vis techniques lies in developing a new method for monitoring the reaction process to study the interactions between the subjects. For example, the

work of Nomikos provided a way to identify the reaction schemes, stoichiometry and kinetics based on a set of concentrations measured and recorded in a timeline. [68] In the case of this work, we used the absorption of UV light (at 260nm) to analyze the formation and dissociation process of DNA structure. The presence of Adenosine can be detected through the difference in the melting curve derived from the UV absorbance, as commonly reported. More details will be discussed in Chapter 4.

Fluorescence is arguably the most widespread optical method. Fluorescent spectroscopy uses light to excite the electrons in the fluorescent dye and causing an emission of light at certain wavelength, the emission is detected to analyze the sample. Fluorescent biosensors can detect various targets including ions, metabolites, DNA and protein biomarkers with high sensitivity. It is even possible to provide not only the presence but also the status of the targets.[42] The analyte needs to be labeled with fluorescent dye through molecular interactions or chemical modifications. Here we give an example of using the fluorescent emission to observe the energy transfer caused during an interaction between the recognition element and the target which enabled the detection. FRET, short for "Fluorescence Resonance Energy Transfer", is a powerful method for measuring protein-protein interaction, enzyme activity and small molecules. [69] FRET transmits the photo excitation energy from a donor fluorophore to a receptor fluorophore for the detection. [70] The efficiency of this energy transfer is related to the distance between the donor and acceptor fluorophore with very high sensitivity. The measurement of the FRET efficiency could be used to determine the distance between the two fluorophores. For example, in **Figure 1.8** was the work of Komatsu et al. in which they linked yellow fluorescent protein (YFP) with cyan fluorescent protein (CFP). With constant light stimulation of 433 nm wavelength, when the ligand domain was not connected to the sensor domain they observed light emission with wavelength of 475nm due to the excitation of the CFP. However when the ligand domain is attached with the sensor domain due to the recognition process, the two proteins formed dipole–dipole coupling which led to the FRET process, the light emitted was 530nm in wavelength instead of 475 nm. [71]

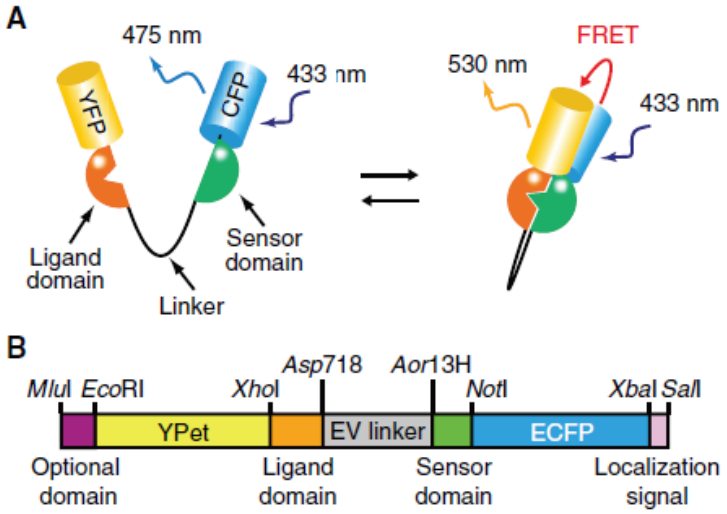

Figure 1.8 The scheme of a FRET biosensor. (A): YFP and CFP were connected with a linker that will bind with the target. (B): The detail of the linker. Without the presence of the target , the CFP is excited to emit light at 475 nm wavelength, while in presence of the target, the two domains will bind and causing the FRET between the two proteins, changing the emitted light wavelength to 530 nm. [71] The detection of the target can be realized by measuring the wavelength of the light emitted.

Raman spectroscopy is another well-developed and powerful technique in analytical application. It is a scattering spectroscopy which can identify the molecules and study their chemical bonding. When molecules are excited with monochromatic light, due to the inelastic collision of photons with the molecule, a shift in the scattering wavelength is observed. Raman spectroscopy is based on this phenomenon. It can offer biochemical information about the target and is a good choice for analyzing cells, especially for the toxic examination. Other than the conventional Raman spectroscopy, numerous methods were used to enhance the signal, such as resonant Raman spectroscopy [72], surface enhanced Raman spectroscopy [73] and coherent anti-stokes Raman spectroscopy [74]. A recent example is Qian's work accepted this July using surface-enhanced Raman spectroscopy for detection of DNA. A peptide nucleic acid was functionalized as recognition probe, after the target DNA hybridize with the probe the silver ions in the solution are adsorbed due to the negative charge of the DNA skeleton. The silver nanoparticles are later grown on the surface with a silver enhancement step. The grown silver nanoparticles along the DNA skeleton induced sufficient interactions between the bases and the substrate to yield a sensitive Raman signal. The detection limit reached 34 pM for this new detection method that requires no label and dye. [75]

Optical fiber

Optical fiber biosensor was widely used in biomarker detection for medical diagnostics and pathogen and toxin detection in food and water. Optical fiber was originally designed to suppress the loss of light during propagation to the minimum, but when the light is interacting with the fiber's surroundings it could also be used for sensing purposes. Optical fibers were used as the transduction element and the signal is exclusively dependent on the optical transduction mechanisms. [76] Optical fibers is made by silica cylindrical core and a surrounding cladding, the core is doped so that the refraction index of the core is slightly higher than the surrounding making the total refraction inside the fiber possible. The light propagating through the fiber consists of the guided field in the core and the evanescent field in the cladding and if the fiber is uniform-diameter, the light cannot interact with the surrounding. To enable the detection, the cladding is partly removed or displaced to let the evanescent field in contact with the surrounding. The modification is often done by tapering, bending the fiber into a different shape or removing part of the cladding like the examples in **Figure 1.9**.

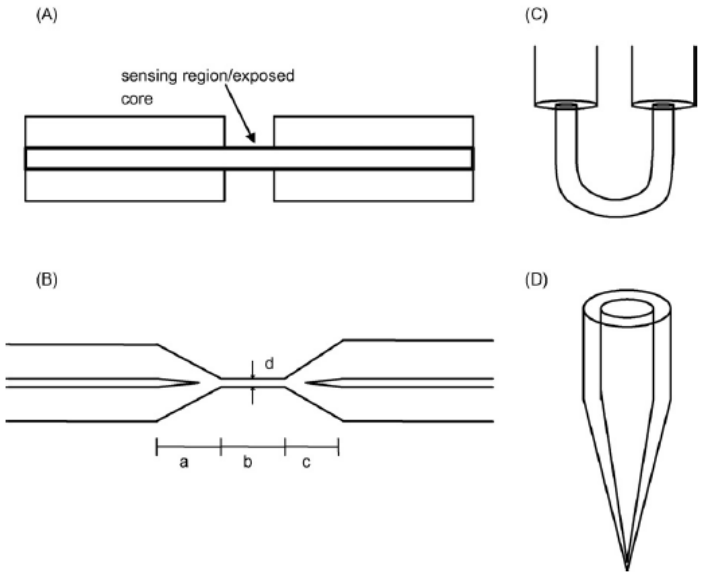

Figure 1.9 Different modified shape of optical fiber: (A) De-cladded optical fiber. (B) Tapered optical fiber. (C) U-shape bended probe. (D) Tapered tip. [76]

The detection with optical fiber could be controlled by multiple parameters, the angle of the light, the way the fiber was modified and the wavelength. Usually additional transduction mechanisms need to be applied to the system to amplify the

signal. The factors that could be used for detection include: change in the output power; evanescent field absorption; fluorescence and surface plasmon resonance. [77–79] We give two biosensor examples using evanescent field absorption and fluorescence dye, and will discuss more about surface plasmon resonance in the later chapters.

Guo's group studied the evanescent field of the optical fiber and they compared the performance of the uniform and tapered fibers. [80] They discovered that when the light is transmitted through the tapered fiber, the evanescent filed could interact with the surrounding region of the tapered area. This phenomenon has been used for the design of biosensor. The transmission shows a decrease when the analytes absorb the energy. The scale of the decrease is related to the concentration of the analyte. The light source should provide the wavelength that will be absorbed by the analyte.

As mentioned before, fluorescent dye could also help the detection with optical fibers. The indirect strategy of a sandwich assay is the frequent choice. For example, the primary antibody was covalently binded to the surface of the fiber as the recognition element, the target biomolecule was then binded on the antibody. To visualize this binding, a secondary fluorescent antibody was injected and also binded onto the target. While the incident light from the evanescent wave came, the fluorescent antibody would be excited and gives the signal.[77]

Surface Plasmon Resonance

Since its first demonstration of Surface Plasmon Resonance (SPR) being used for detection purpose by Liedeberg and Nylander in 1982 [6,81], SPR has emerged as a promising new technique for biosensor application, some of which have already been successfully commercialized.[82,83] SPR biosensors have become popular in fundamental biological studies, health science research, drug discovery, clinical diagnosis, and environmental, food and agricultural monitoring. [84–90] SPR measures kinetics and affinity of bimolecular binding in real-time. More importantly, compared to radioactive or fluorescent labeling methods where the label may impair the binding, SPR is a label-free technique and the binding will not be affected during the detection. Other advantages of SPR are low reagent consumption and direct measurement of binding constant and affinity.

A surface plasma wave (SPW) is an electromagnetic wave which propagates along the boundary between a dielectric and a metal layer. In order to fulfill the requirements to create the SPW, the metal layer is normally noble metal such as silver and gold. [91,92] SPW is a transverse-magnetic (TM) wave excited by a light wave whose magnetic vector is parallel to the plane of interface. [91] This condition is achieved by means of prism coupling, waveguide coupling or grating coupling. Prism coupling is the most commonly used among the three coupling methods, a light wave passes through a high refraction index prism and totally reflected at prism-metal interface. An evanescent wave penetrating the metal layer is generated (**Figure 1.10**). The evanescent wave propagates along the interface and by controlling its incident angle the propagation constant of the evanescent wave could be adjusted to match the SPW. [93] The angle of incident light is plotted against the intensity of the reflected light in **Figure 1.10.** The intensity of the reflected light decreased when the evanescent wave is generated on the surface, the angle corresponding to the lowest intensity of reflected light is the resonance angle.

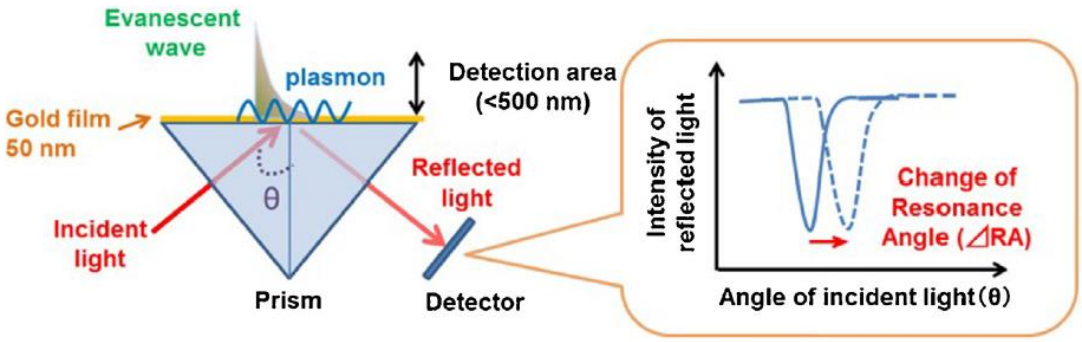

Figure 1.10 The schematic of one SPR biosensor, the light came through the prism and created an evanescent wave that propagated along the gold surface. The reflected light was captured by the detector. Any interaction taking place on the gold surface will affect the reflectivity of the solution, causing a shift in the resonance angle. [94]

The majority of the SPW is concentrated in the dielectric, thus the propagation constant of SPW is very sensitive to the change in the refraction index of the dielectric. This property is the fundamental of affinity SPR sensors. The recognition elements on the surface of the metal recognize and capture the target and produce a local increase in the refraction index at the metal surface. The propagation constant of the SPW increases with the refraction index. The increase in the refraction index led to a shift in the resonance angle and can be accurately measured by optical means. As

a result it is possible to keep track of the interactions on the metal surface. This principle for SPR bio-sensing is shown in **Figure 1.11**. The surface was functionalized with the recognition element as probes prior binding. Once the analyte was introduced to the solution and in contact with the metal surface, the interaction between the probes and the analyte (analyte binding) will cause a change in the refraction index. The setup of one kind of SPR biosensor is shown in **Figure 1.10**, the light source emitted a light wave under the prism and the reflected beam is collected by the detector. The gold surface of the prism is functionalized with recognition element probes interacting with the flowing sample solution. Once the targets are binded on the probes, a change in the incident angle was detected due to the series changes mentioned before.

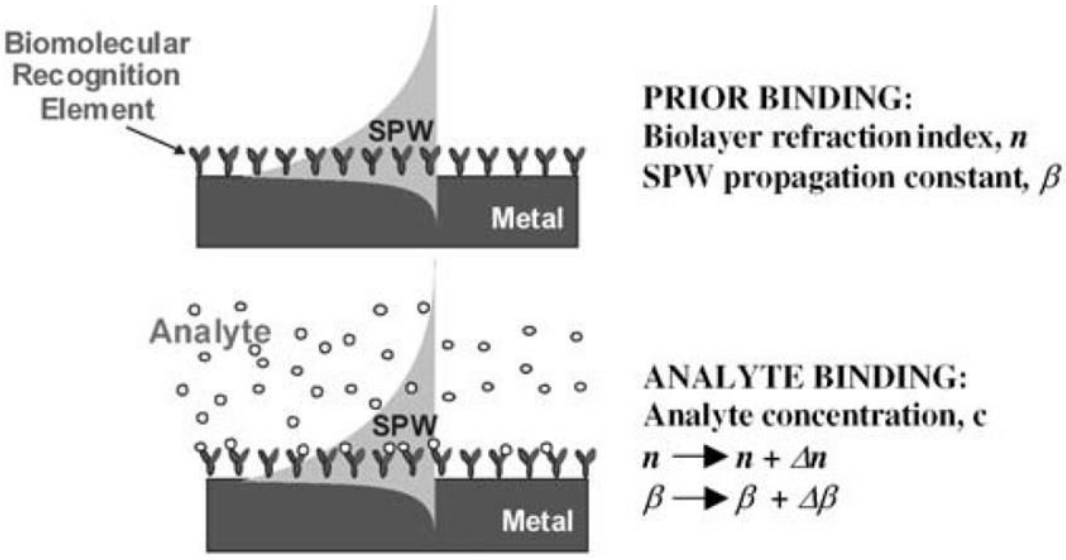

Figure 1.11 The working principle of SPR biosensor. The metal surface was first functionalized with biomolecular recognition elements as probes. The biolayer had an initial refraction index and the SPW had an initial propagation constant. Once the analyte interacted with the probes on the metal surface, a change in the mass caused the change in the refraction index and the propagation constant and as a result created the signal. [91]

There are three detection modes based on the principle of SPR. The first mode known as angular SPR keeps track of the change of resonance angle induced by SPR, the example given in **Figure 1.10** was using this detection mode. The second mode known as spectral SPR measures the changes of resonant wavelength induced by the

SPR. These two detection modes can be used to study the interaction of one spot on the surface. When the interaction took place either the incident angle or the wavelength was varied in order to maintain resonance thus offering information about the binding process. The drawback of these two detection modes is they can only study the interaction on one spot. The third detection mode allows the monitoring of multiple spots at the same time by fixing both the incident angle and the wavelength while measuring the change in the reflectivity. Surface Plasmon Resonance imaging (SPRi) is a method using this detection mode. It can visualize the whole biochip via a CCD camera and enables simultaneously detection of all the active spots prepared on the biochip. SPRi experiments have three modes of data collection: fixed angle, angle scanning and wavelength scanning. [95] A broad-beam monochromatic polarized light emitted from a light source illuminates the whole functionalized area of the biochip surface mounted within the detection chamber. The signal is collected and analyzed in real time for all the spots, which makes it a highly efficient method consumes less reagent and time.

Many detection techniques were coupled to SPR, such as SPR-mass spectroscopy (SPR-MS), surface plasmon resonance electrochemical impedance spectroscopy (SPR-EIS), SPR microscopy, etc. SPR-EIS uses interdigitated metal electrodes (IDEs) that provide supporting structure for surface plasmon in a simplified setup. IDEs reflect white light into diffraction orders and the direct spectral analysis based on surface plasmon can be achieved through the first order of diffraction. SPR-EIS is very promising in stationary and miniaturized platform. [96] SPR-MS is used for quantitative and qualitative analysis of proteomics based investigations. SPR is used for the quantification and interaction analysis of protein while mass spectroscopy is used to deduce the protein structure. [97] The imaging of the surface of the biochip is essential to study the cell's position and morphology. SPR imaging can be achieved by using a microscope objective to couple light and SPW. [98] SPR microscopy allows the observation of extra-and intracellular processes in real-time. [99]

1.2.4 The methods chosen for the project

We gave a non-exhaustive overview about the prolific choice of transducers in sensing techniques. After comparison of each method, we could summarize the key factors in valuing the biosensor: sensitivity, repeatability, the mode of measurement, detection limit, cost both in the setup and experimental process, the quickness of the detection, requirement of label, etc. There are two categories of detection methods, heterogeneous format that involves the usage of a surface on which the recognition element is immobilized and homogeneous format that is carried out directly in solution. In our work, we chose two methods mentioned above, Surface Plasmon Resonance imaging and UV-Vis spectroscopy, in order to build a reporting mode for small molecules. SPRi is a heterogeneous method where the DNA sequence is immobilized on a surface. On the other hand, UV-Vis spectroscopy is a homogeneous method where the DNA structures are free in solution.

Among the methods mentioned above, some require the use of a label to enable the detection. In some cases the labeling process was quite simple, the fluorescent dye solution was directly mixed with the sample solution, whereas in other cases the labeling process may involve the production of antibodies marked with fluorescent labels. The complex labeling process consumes more time and money for the preparation of the experiments. The two methods we chose are label-free techniques that can simplify the whole process. Also, they are both influenced by multiple parameters during the detection, such as the target concentration, temperature, salt concentration. This gives many ways to improve the performance of the sensor to perfection. The detection using SPR is fast and can be used for quick detection, it is also able to quantify the analyte by its mass due to the linear relationship between the mass increased on the surface and the signal created.

Despite the advantages the two methods share, they have their own features as biosensor. The sensing could be categorized by the time element. Surface plasmon resonance imager is a real-time monitoring detecting device. We can observe the interaction on gold surface when the reaction was taking place. On the other hand UV-Vis spectroscopy records the absorbance of incident light during the entire

heating/cooling procedure. By plotting the absorbance with temperature it is possible to analyze the temperature required for formation or dissociation of the binding.

In summary, we chose two label-free analyzing methods to build biosensors with multiple controlling parameters, they are both able to quantify the analyte. These two methods also offered different detection mode with real-time monitoring of probes on surface or a timeline recording of free units in solution, thus offering more options according to the application and target molecule.

1.3 The varieties of recognition elements

Recognition element is the crucial part determining the working principle of the biosensor. It also has a great impact on the overall performance, advantages and shortcomings of the device. In the history of biosensor, recognition elements isolated from living organs such as antibody and enzyme were first used and studied. Later on, the artificial recognition elements synthesized in the laboratory such as DNA, aptamer and molecular imprinted polymer were brought into sight and being tested and improved. There has been a growing need in rapid diagnosis and improvements in sensing characteristics, such as selectivity, stability, and cost-effectiveness. In order to fulfill that need, researchers were seeking new ways to improve the performance of these recognition elements and used combinations of them. Moreover, modern nano-techniques have provided more tools and methods for amplifying the signal harvested from these recognition elements. Thanks to these efforts, the analytical performance of biosensors has improved in key parameters like sensitivity, selectivity, limit of detection (LOD), and signal to noise ratio.

An ideal recognition element has high binding affinity for the target as well as stability. The size of targets and their binding mechanisms between the recognition elements are different and thus the optimal choice of recognition element is highly dependent on the nature of the target. In **Table 1.2** we listed the advantages and limitations of the most commonly used recognition elements for biosensors.

Recognition element	Type of sensor	Advantages	Disadvantages
Enzymes	Enzymatic biosensor	- Specificity - Simple apparatus and procedures	- Purification is costly and time consuming - Poor stability - Efficient only at optimum pH and temperature
Antibodies	Immunosensor	- High affinity - Specificity	- Laborious production - Lack of stability -Difficult for modification
Molecularly-imprinted polymers (MIPs)	MIP sensor	-High thermal, chemical, and mechanical tolerance - Reusability - Low cost	- Complex fabrication methodology - Time-consuming process - Incompatibility with aqueous media - Leakage of template molecules -Non-specific binding
Aptamers	Aptasensor	- Easy to modify and design structure - Possibility to denaturalize and to rehybridize - Possibility to distinguish targets with different functional groups - Thermally stable - In-vitro synthesis	-Non-specific binding -The complexity of SELEX process -Lack of bio-stability

Table 1.2 The advantages and disadvantages of four common recognition elements. [100]

1.3.1 Antibody

Antibody is one of the earliest choices as the recognition element. Even nowadays the majority of biosensor is still using the antigen-antibody interaction for recognition and quantification of the target. Antibody is a large Y shape protein, it is naturally produced by the immune system of animals. The tip of the Y shape contains a paratope that is specific to one particular epitope on an antigen. The paratope and epitope could be regarded as the lock and the key, which gives the binding very high precision and specificity. The molecular forces involved in the binding are weak interactions like electrostatic forces, hydrogen bonds, hydrophobic effect, and van der Waals forces, which makes the binding between antigen and antibody reversible.

In 1975, Kohler and Milstein's work on massive production of antibody has drawn even more popularity to it. [101] Since the antigen-antibody interaction is naturally discovered in the immune system, biosensors using antibody for recognition are therefore named "Immunosensor". The antibody is immobilized on surface, once the target is recognized it will bind with the antibody and changing the properties of the surface. The signal is then amplified and analyzed.

Besides the easy production, another advantage of immunosensor is that the antigen, or in the sensor aspect the analyte requires no purification. However, antibody also has its shortcomings. First of all, the generation of antibody starts with a lab animal, which means if the target is toxic to living creatures it may be very difficult to synthesis the antibody against the toxic target. Secondly, in the application of drug discovery, the antibodies obtained from lab animals could trigger interaction with heterophilic antibodies, a kind of antibody that target non-human origin antibodies, providing very likely false positive results.[102] Despite the massive and simple production of antibody, the performance of the antibodies produced varies from batch to batch. In order to have good sensitivity and repeatability, the parameter of the sensor need to be calibrated. The working condition of antibody is another limitation, the pH and salt concentration must be in-vivo parameters and antibody structure will be irreversibly denatured by high temperature.

1.3.2 Enzyme

Enzymes are macromolecular biological protein catalysts that accelerate biological reactions. Catalytic enzyme based sensor are able to measure reaction products generated in the catalytic process, including protons, electrons, light and heat. Enzyme sensors are widely used in medical and environmental control applications, for example the urea sensor reported by Barhoumi et al. [103] Nowadays, the most commonly used and best developed enzyme biosensor is glucose biosensor. It is very important for clinical application related to diabetes. Although different designs have been proposed, the detection principle remained the same. The detection is based on the reaction shown below. The setup is displayed in **Figure 1.12**

$$\text{glucose} + O_2 \rightarrow \text{gluconolactone} + H_2O_2$$

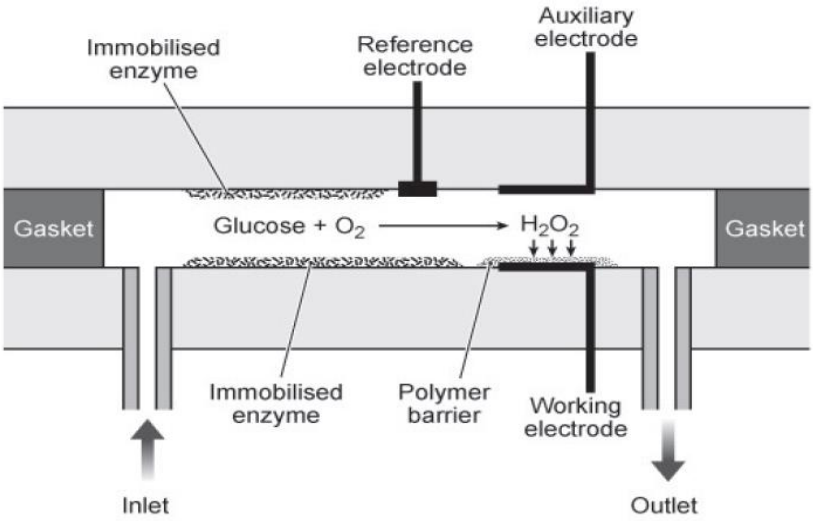

Figure 1.12 The setup of an enzyme biosensor: the enzyme was immobilized on the walls of the reaction chamber, glucose with O_2 will create H_2O_2 with the help of the enzyme, and the H_2O_2 could then be detected by the electrochemical sensor near the exit. [21]

For a glucose biosensor, the glucose oxidase is used as the recognition element that catalyzes the oxidation of glucose to gluconolactone. The enzyme was immobilized on the surface. If there is glucose in the chamber, the enzyme would catalyze the reaction and in the other side of the chamber the H_2O_2 produced is detected by an electrochemical sensor.[21]

The advantage of enzyme biosensor is that the enzyme is promoting the reaction, making the detection more sensitive at very high level. The time required for the detection is also reduced for the same reason. The disadvantage of enzyme as recognition element is the rather high cost in producing enzymes. And its activity will be reduced when immobilized on surface, which limited the following treatment to enhance the signal. The storage of enzyme also faces the difficulty that the enzyme will lose activity due to deactivation in the relatively short time if not kept in the appropriate conditions.[104]

1.3.3 Molecular imprinted polymer

Molecular imprinted polymer (MIP) is a method using molecular templates to create selective binding sites in synthetic polymers. It was introduced by Wulff and

Sarhan as a new synthetic methodology for preparing specific receptor sites in cross-linked polymers in 1972. [105] The process involves the formation of a template-monomer complex and the polymerization with crosslinking agents. The geometry of the self-assembled template-monomer complex is captured in the growing polymer matrix during the polymerization. Once the polymerization is finished, the template is removed from the matrix, leaving cavities with its shape. In the end, synthetic polymer with predetermined selectivity is obtained. The shape of the cavity and position of the binding sites are very important to the recognition process.

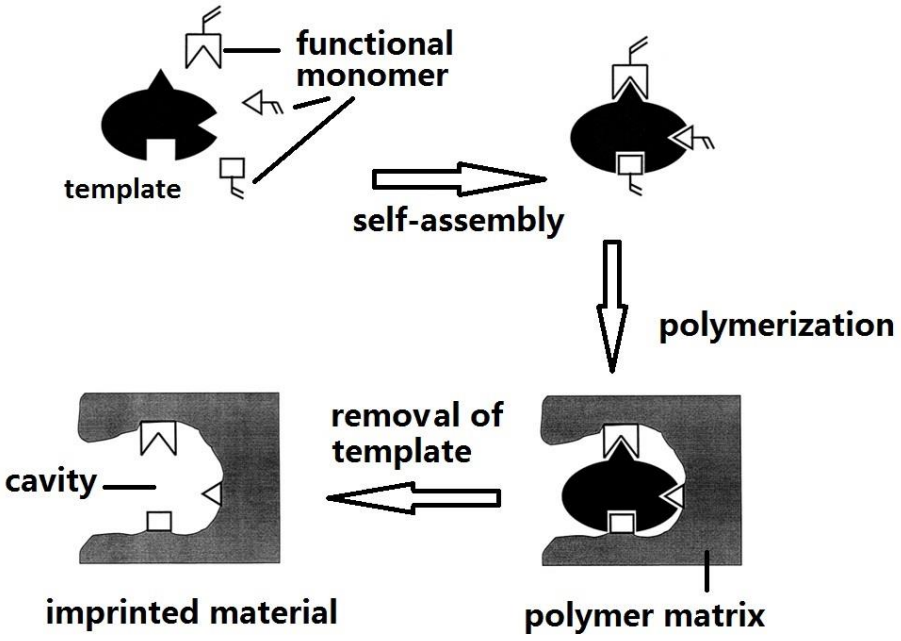

Figure 1.13 the preparation of synthetic polymer with predetermined selectivity. [106] The template was self-assembled with functional monomers, which were later polymerized with the polymer matrix. After removal of the template, a cavity was formed in the imprinted material.

The most evident advantage of MIP is that theoretically it could be used for the detection of any target. The strength of the binding could also be altered on purpose. In general, two binding sites on the matrix with static force inside the cavity are sufficient to provide the binding for good recognition. [107] This method also has very high selectivity. But the complex procedure of designing and preparation of the polymer matrix is the drawback of the method. MIP is a way to mimic antibody and enzyme, but more stable, robust, reproducible and engineerable.[108–110] Since it is

designed according to antibody and enzyme, the transducers used for these two elements could also be adjusted for MIP, which makes the MIP sensors very versatile.

1.3.4 Aptamer

Aptamers are high affinity ligands (DNA or RNA) that would form specific binding with the target molecules. The selection and amplification of these ligands were first made by two groups independently, the group of Gold and Szostak, in 1990 [111,112]. Later on, these ligands were named as "aptamer", as in Latin for "to fit". In 1992, the group of Szostak continued their work and expanded to the domain of DNA [113]. This provided us with more choices when determining the targets and ligands, and more importantly, the higher stability makes DNA a better potential pharmacological reagent compared to RNA. In the next two decades, a large variety of aptamers have been identified for all kinds of targets (i.e. proteins, peptides, amino acids, metal ions and small molecules). Its high selectivity and affinity has made it a rising element in applications such as biosensor, diagnose and selection technology.

Compared to other recognition elements, aptamer has many advantages and is rising as a strong competitor. Antibody or enzyme based assays are regarded as standard and well-established tool for the detection of proteins and small chemicals, but their applications are limited to targets such as toxicants or non-immunogenic compounds. In another aspect, small target detection using mass sensitive methods often requires a way for signal enhancement due to the low mass of the target. The steric hindrance between small targets and large antibody or enzyme poses a challenge in detection applications, especially at low concentration. [114] Aptamer is a small molecule, which makes it more suitable for the detection of smaller targets with the ability to fold around the targets. Being more effective against the small target, aptamer could also be used for big targets like protein or even cells. The fact that antibody and enzymes are proteins also renders their low tolerance of heat and non-physiological environment, while aptamers could be used under non-physiological conditions and its denaturation at high temperature is reversible. Moreover, the performance of aptamer between each batch is also very small, thus no requirement for calibration between different batches. Superior to antibody and enzyme, both

aptamer and MIP could be customized for special application, but MIP typically displays high cross-reactivity and is difficult for chemical modifications. [115,116]

Due to the reasons listed above, we chose aptamer as the recognition element in our study. More historical events and current research interest will be discussed in the next section.

1.4 Aptamer and aptasensor

1.4.1 SELEX process

Aptamers are selected by a process named "SELEX" (Systematic Evolution of Ligands by Exponential Enrichment). This process was established in 1990 by Tuerk and Gold in their work that started the new era of aptamers.[111] SELEX is an in-vitro selection and amplification process that is able to identify and separate the sequences that can bind onto the target with high affinity from the oligonucleotide library.

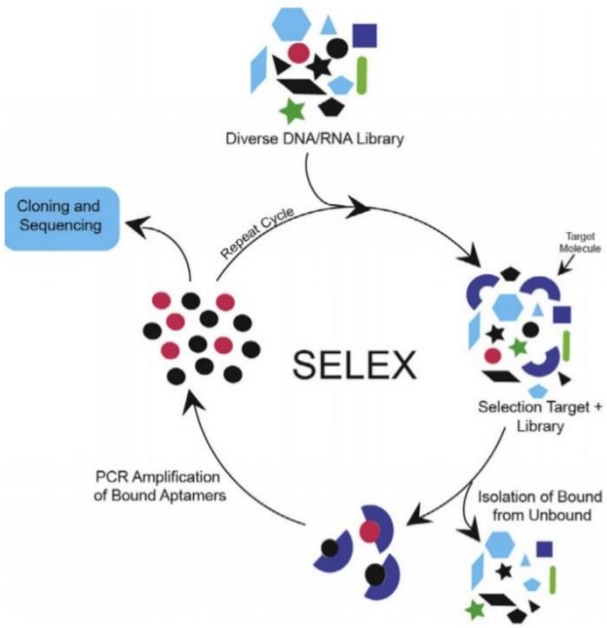

Figure 1.14 The SELEX process, the randomly synthesized DNA/RNA library is mixed with the wanted target. The strands that can bind onto the targets are isolated from the mixture then go through purification and amplification. This cycle is repeated for several times until finally enough amount of sequence is obtained to analyze the sequence of the aptamer.

The SELEX process begins with a randomly synthesized single strand oligonucleotide library. The library should contain huge amount of different oligonucleotides (on the scale of 10^{15}) to maximize the success rate of finding the aptamer that targets the desired material. [117] The library of random oligonucleotides was synthesized through combinatorial chemical synthesis, and then the target of interest was mixed into the initial pool. The next step, the sequences that can bond with the target were selected and purified due to their high affinity against the targets. The interaction between aptamer and target is the combination of multiple molecular interactions including van der Waals forces, hydrogen bonding and electrostatic interaction. Due to the principle of SELEX process the binding between aptamer and target is not specific. In some cases aptamers can also bind with other structures similar to the target, which is one of the drawbacks of aptamer. Different aptamers fold in various manners with their target. For instance, the anti-Adenosine aptamer we selected in our study bond with Adenosine molecules in a hairpin structures, an anti-thrombin aptamer fold with thrombin into a G-quadruplex structure and another anti-cocaine aptamer fold into a three-way junction in presence of cocaine. [117–119]

After the purification these selected sequences were then amplified by polymerase chain reaction (PCR, if the potential aptamer is DNA) or reverse transcription PCR (if the potential aptamer is RNA) to harvest enough amount of oligonucleotide for the next cycle. PCR is a technique that amplifies a few copies of a segment of DNA by several orders of magnitude and generates thousands to millions copies of this particular DNA sequence. [120] This selection and amplification process were repeated for several times (8-15 times based on the affinity of the binding and the kind of separation process), during which the amount of potential aptamers was increased exponentially. As a result, one can analyze the final solution to determine the sequence design of the aptamer. Once the sequence is confirmed, it is considerable easy to produce the precise aptamers with chemical synthesis methods.

1.4.2 Aptamer used for separation application

Due to the high affinity aptamers present, they are often used in separation techniques as immobilized ligands.[121] This application of aptamers has a long history and has been well developed during the last two decades. The target varied from large

targets including cells, antibodies, proteins to small molecule targets.[122,123] There are many techniques for separating target using the high affinity of aptamers. For instance, High-performance liquid chromatography (HPLC) is an effective way for separation in analytical research. The liquid solvent with the sample was pumped through a column at high pressure. The column was filled with absorbent material, which will interact with each component in the solvent. The components were separated due to the difference in their affinity against the absorbent material. In HPLC applications, aptamers served as the absorbent material in the column. In the work of Geiger's group, a RNA aptamer was used to select an amino acid d-arginine from its enantiomer l-arginine because the aptamer binded with the latter enantiomer 1200 times better. [124] Other than these traditional ways of using HPLC, there are new emerging techniques to broaden the applications. For example, in the work of Kim et al, aptamers were placed inside liposome to selectively remove the contaminants in tap water.[125] Chromatographic strips using quantum dots and gold nanoparticles (Au NP) as labels were also developed for detection purposes. [126,127]

There are other separation methods than HPLC that take advantage of the high affinity of aptamer. In 2015 Dong et al reported new affinity purification method using streptavidin-binding RNA aptamer S1to isolate endogenously-assembled viral RNA binding proteins (vRNPs) from crude mammalian cell. [128] Another study by Madru et al used solid phase extraction (SPE) to selectively extract cocaine from human plasma. [129] An anti-cocaine aptamer was immobilized on a solid support as selective SPE sorbents and an extraction recovery close to 90% was obtained

Another example of aptamers being used in smaller target is a study by Roming et al. in 1999 to purify a recombinant human l-selectin–Ig fusion protein obtained from hamster. [123] Other than amino acid and protein, aptamers were also effective for small molecules. Kennedy's group published their work in 2001 to separate Adenosine and its derivatives with a bead-packed capillary column. [130] The streptavidin-modified bead was functionalized with biotin-labeled DNA aptamers binding to Adenosine before they were packed into the column.

Other than these traditional ways of using HPLC, there are new emerging techniques to broaden the applications. For example, in the work of Kim et al, aptamers were placed inside liposome to selectively remove the contaminants in tap

water.[125] Chromatographic strips using quantum dots and gold nanoparticles (Au NP) as labels were also developed for detection purposes. [126,127]

1.4.3 Aptasensor applications

Aptasensor refers to those biosensors whose recognition is based on the interactions between aptamers and their targets. Aptamer can be easily modified and customized to adapt to different analytical methods, as a result many aptasensors were developed for indentifying and determining the concentrations of proteins, small molecules, metabolites and ions, etc. [131–133]

There has been a growing interest in developing aptasensors for the purpose of detecting small molecules. Small molecules plays an important role in some of the living organisms, thus are crucial to applications related to diagnose and monitoring biological functions. However, their small size and low concentration are the two key points limiting the outcome of the detection. To achieve detection with amplified signal and more rapid and accurate feedback, aptamers are often immobilized on a surface. There are also applications in which the aptamers are free in the solution. In some cases the aptamer would be cut into several halves as "split aptamer" to improve the design. Here we sort the aptasensors into heterogeneous detection and homogeneous detection based on the state of the aptamer during the detection. For each kind of aptasensor we provide one example of using the aptamer directly as reconigtion element and another example of dividing the aptamer into splits before use.

Heterogeneous detection with aptamers

As mentioned in the advantages of aptamer against enzyme and antibody, it is rather easy to modify the aptamer to serve the purpose. Aptamers after modification could take an indirect approach to obtain better results in the strength of signal or sensitivity. The easy modification made the immobilization of aptamer on surfaces more accessible, for example the aptamers with thiol modification could be attached to gold surface without much effort. [134] Monitoring the changes of the surface is more convenient compared to direct detection of aptamers in solution.

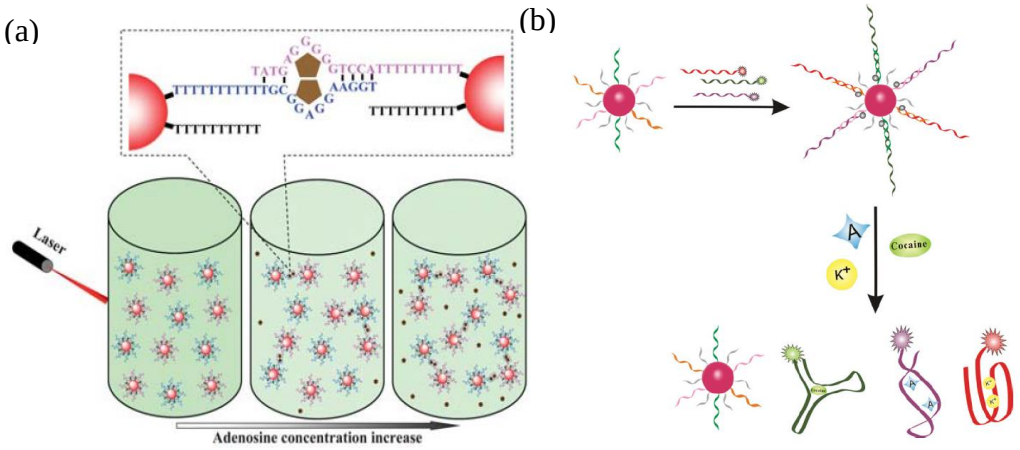

Figure 1.15 The detection principle of two aptasensors. (a) Two split-aptamers were functionalized on gold nanoparticles and these nanoparticles were monitored the with dynamic light scattering. With the presence of Adenosine, the split-aptamers formed binding and the nanoparticles aggregated. The prescence of Adenosine was detected due to the change in diameter of the cluster of gold nanoparticles. [135] (b) Three aptamers labeld with three different fluorescent dye were hyrbidzied with their complementary DNA sequences on gold nanoparticles. The fluorescent signals were suppressed by the quenching effect of the gold nanoparticles. With presence of the targets in the solution the aptamer folded with the targets and released into the solution and the fluorescent dye was no longer suppressed. Different fluorescent signals can be detected with the release of different aptamers. [136]

Other than 2D gold surface, the detection of aptasensor could be enhanced by functionalizing aptamer on gold nanoparticle (Au NP). In 2011 Yang and his group proposed a method using dynamic light scattering for detection of Adenosine by immobilizing split aptamer fragments on Au NPs. One aptamer targeting Adenosine was separated into two halves and functionalized on two batches of Au NPs, these particles will bind with each other in presence of Adenosine. Dynamic light scattering test was performed on solution with these two batches of Au NPs, whereas the diameter of the nanoparticles could be calculated. When the two different Au NPs were binded with the help of Adenosine, the particles aggregated into bigger cluster of gold particles, which resulted in an increase in the diameter calculated.[135]

Another application of functionalizing aptamers on Au NPs was published by Zhang et al. in 2010, the fluorescent sensor they proposed were able to detect three different targets using the same aptamer-modified nanoparticles. Three different aptamers (against Adenosine, potassium cation and cocaine) were first modified to carry fluorescent dye on the 5', the fluorescent dye and its color were different according to the aptamer. Then Au NPs functionalized with the complementary

sequence of three different aptamers were added into the solution which leads to the hybridization between the probes on gold surface and aptamers in solution. The fluorescent signals of the dyes were suppressed due to the quenching effect of the gold surface. However, if there were targets in the solutions, the formation of the binding between the aptamer and the target will pull the aptamers hybridized on gold surface into the solution. The fluorescent dyes were released from gold surface during this process, and in return the observation on the fluorescent signal and its wavelength could be used to determine which kinds of targets were in the solution.[136]

Homogeneous detection with aptamers

Although immobilizing aptamers on surface is a mature and common method for building a biosensor, the high expense of the substrate (normally gold) and the high end technology required during the manufacture are increasing the cost in time and resource as well as reducing the margin of error for the detection. There are other reported sensing methods that used the aptamers directly in the solution.

A recent paper by Nameghi and Danesh in 2016 gave a new way to detect ochratoxin A with pyramid shape DNA structure and PicoGreen dye. The DNA pyramid was made by four oligonucleotides, in which two sequences contain one fragment that could serve as aptamer targeting ochratoxin A. The four sequences were mixed with PicoGreen dye in the solution, the dye will bind onto the double strand inside the pyramid and its fluorescent signal could be detected. In presence of ochratoxin A, the hybridization on the two edges containing aptamer would break, the dangling aptamer will form self-binding with the target. As a result, the total number of double strands was decreased, so did the intensity of the fluorescent signal. [137]

Yang et al. reported another fluorescent detection using a sandwich-type strategy with split-aptamers based on a signaling macrocyclic host-dye system. The split-aptamer based sandwich conjugated β -cyclodextrin (β-CD) and dansyl at the ends of the two aptamer fragments respectively. The two splits binded with each other when the target is present in the solution. The binding between the two fragments brought the dye and its receptor in close proximity and promoted the inclusion interaction. The host-dye reporter acted as an efficient transducer and a stabilizer of the ternary split aptamer complex as well. Moreover, a dual inclusion reporter strategy was also

proposed by conjugating both ends of the DNA strand with the dansyl dye and β-CD molecule. This dual strategy improved the signal-to-background change and the sensitivity. [138]

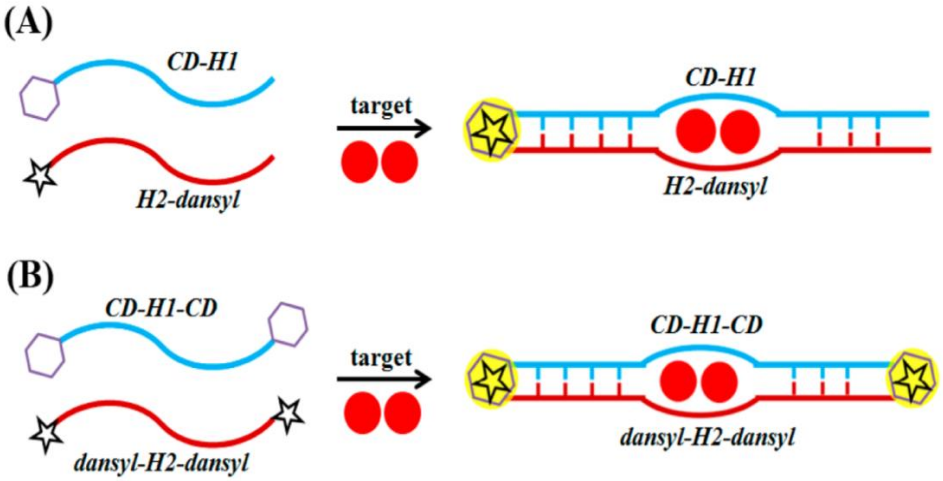

Figure 1.16 The detection principle of a fluorescent based aptasensor. (A) Monovalent and (B) bivalent host-dye reporter sandwich-type aptamer sensing platform. Dansyl and β-cylodextrin were tagged on anti-Adenosine split-aptamers respectively. With presence of Adenosine and formation of duplex or G-quadruplex structures, the fluorescent signal was greatly enhanced due to the host-dye pair. [138]

In conclusion, there are many choices of designs for making an aptasensor and the past work have provided different methods toward each application. However, when we take a look at these methods, we could sort them into two kinds by the state of the aptamer: on surface or in solution. In both cases, two approaches were often required to obtain or enhance the signal: functionalization of aptamers on Au NPs and adding fluorescent label to the aptamers. The whole process was more complicated with these methods and that is why we search for a new method to enhance the signal with neither of the two options. We proposed to build larger DNA structures and take advantage of the increased mass of oligonucleotide itself to enhance the signal for the detection methods on surface. These DNA structures could also provide an internal reference so that we could detect the target without involvement of any label for the detection in solution. The construction of complex DNA structures will be introduced in the next section.

1.5 DNA structure construction

Natural DNA is a molecule that carries genetic information and plays an important role in the growth, functioning and reproduction of human organs. DNA is an organic polymer of four nucleic acid bases: A, C, T, G. These bases can form bonds between the sugar and phosphate to form a long single strand of DNA. If the strand contains N bases the possible sequence of this strand is N^4 combinations. In 1953 the double helix structure of DNA was discovered by Watson and Crick. [139] The double helix is formed by the bases through hydrogen bond, and thanks to this hybridization process, DNA was also considered to be a material with recognition properties.

The idea of using DNA as structural material was first brought up in the 1980s. [140] Self-assembly of DNA is a convenient bottom-up strategy. The interactions between DNA are very specific according to the Watson-Crick complementarity. For that, the DNA strands could be preprogrammed to form the wanted binding and build the designed structure. Nowadays, the self-assembly of DNA strand not only result in DNA duplexes, but also more complex structures or patterns from 1D to 3D. For example a recent study in 2011 built a tetrahedron DNA structure with the self-assembly of four DNA single strands.[141]

In addition to the self-assembly of DNA where multiple strands were mixed to form the structure, another technique named "DNA origami" emerged in the 21st century. This term has drawn more attention since it made the cover story of Nature in 2006. [142] The fundamental of DNA origami is the complementary base pairing of DNA single strands. The mainframe of the DNA structure is a long DNA single strand folded due to hybridization. The structure is further stabilized by attaching DNA staples that provide inter-structural associations. [143] The potential structure and the binding sites of the DNA staples could be simulated by software. With a good design, the structure could be formed simply by mixing the oligonucleotides in proper buffer and a heating-cooling procedure to break and reconstruct the structure to eliminate secondary structures. The sticky-ends will pull the long DNA mainframe into the desired shape during the cooling process. Furthermore, the structure could be observed with various microscope techniques, such as electron microscopy, atomic

force microscopy, or fluorescence microscopy if the strands are already tagged with fluorescent label. The work of Han et al was displayed in **Figure 1.17**, they presented very complex structures like stars and smiling faces built by DNA origami. [144]

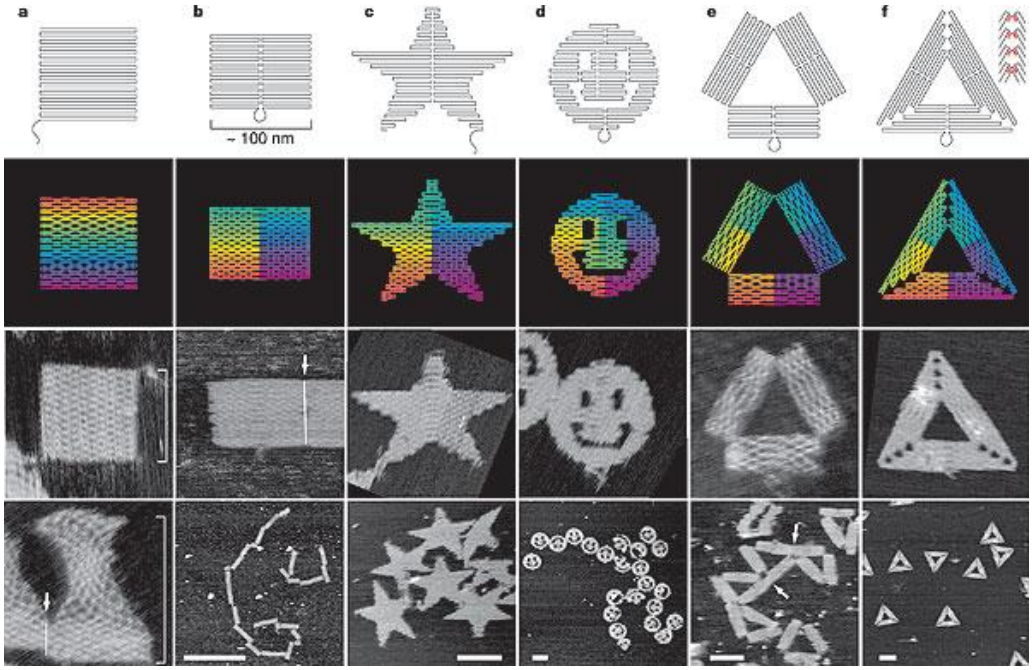

Figure 1.17 Complex structures formed with DNA origami, with the sequence design and their images obtained by microscopy[144]

DNA structures have been used in the development of new drug delivery system. In 2012, Garde et al built a DNA self-assembly origami to carry drug to disease related protein. The structure drug is sealed inside the structure by aptamer staples, however, these aptamer will get loose and release the drug near the infected cells. This method was being tested on diseases like leukemia and lymphoma. [145] It was also used for single molecule detection. In 2008, the first DNA origami structure based detection method was reported. The single molecule hybridization of target RNA to the probes on DNA origami chip was detected by Atomic Force Microscopy (AFM) based on the difference in elastic properties of single and double DNA strands. [146]

DNA structures have already been used in the amplification of detection signal in many studies. Hybridization chain reaction (HCR) can amplify the signal obtained from DNA based biosensor over hundreds of times. Combined with its advantage of isothermal and enzyme-free conditions, HCR has become a promising analytical method for ultrasensitive detection of various targets. In a typical HCR process, the

recognition of the target triggers the chain reaction forming DNA polymeric nanowires which has exponential molecular weight compared to a single DNA structure. HCR can be used in both homogenous and heterogeneous detection methods. The homogenous detection using HCR as amplification strategy uses the hundreds of repeat units to provide an excellent isothermal amplification platform for nucleic acid detection. Various labels can be incorporated to generate signals, mostly in fluorescent and colorimetric assays. In heterogeneous detection methods HCR is implemented on a surface such as electrode, nanoparticles, microfluidic device or glass chip. These assays can separate the analyte from the complex sample matrix and can be applied for optical or electrochemical detection. Complex DNA structures were also used in the amplification of signals. An ultrasensitive detection method for microRNA by combining 3D DNA tetrahedron probes for signal amplification was reported by Xu et al. The tetrahedrons are immobilized on gold nanoparticles and further hybridized with microRNA target to form DNA-RNA heterduplexes. Duplex-specific nuclease (DSN) can recognize the DNA-RNA heterduplexes and ohydrolyze the DNA in the heteroduplexes to produce a specific fluorescent signal corresponding to the microRNA. Moreover, the RNA released during this process can initiate another cycle and significantly increased the signal. [147]

The construction of complex DNA structures with recent advances in DNA origami provided more options in the amplification of signals. In our work, we designed DNA structures from 1D to 3D in order to develop new label-free dye-free detection methods that are not dependent on amplification using gold nanoparticles.

1.6 Purpose of the project

The interest of this project lies in two aspects: first, the development of new sensing technologies based on DNA structures with anti-Adenosine aptamer fragments; second, to build 1D to 3D DNA structures with Adenosine as the shape controlling element. We used Adenosine to set an experimental model. The target could be switched simply by replacing the split-aptamer to another aptamer against the new target.

As mentioned in **Section 1.3**, the current aptasensors depend highly on Au NPs or fluorescent dyes to obtain good signal. What we achieved during these three years is two label-free techniques with no involvement of Au NP. We have built two detection models, one on SPRi platform using DNA probes on gold prism surface to capture DNA structures with split-aptamer dangling ends, another using UV-Vis Spectrophotometer to detect Adenosine with a shift in the melting peak. Both methods were able to detect Adenosine, but they also have their own pros and cons. Thus a choice of method could be made to best serve the application.

Aptasensor using SPR often use Au NPs to realize the detection. In the model we proposed, there is no requirement for Au NPs to enhance the signal. Instead, the signal was enhanced by the mass of the DNA structure itself. This hugely simplified the whole preparation process of the detection, and lowered the cost of this technique. On the other hand, the new method we proposed to use the UV-Vis spectroscopy to detect Adenosine is a label-free in-solution detection technique. This is one advantage compared to the existing models detecting targets directly in solution. We also introduced an internal reference in the detection process, which eliminated the influence of other parameters such as the strand concentration.

We designed DNA structures from 1D to 3D in this study. These structures all combined an anti-Adenosine aptamer with oligonucleotide. The anti-Adenosine aptamer was splited into two halves and the split-aptamers were designed as dangling ends that can bind the DNA structures. The goal was to design and form the DNA basic unit (1D to 3D structures) properly and control these units by adding or removing Adenosine in the environment. The 1D structure was a periodic chain formed by duplexes, the 2D structure was a Y shape structure formed by three single strands, and the 3D structure was a tetrahedron formed by four single strands.

Reference

1. Clark LC, Lyons C. Electrode systems for continuous monitoring in cardiovascular surgery. ***Ann N Y Acad Sci***. 1962;102(1):29-45. doi:10.1111/j.1749-6632.1962.tb13623.x.
2. Yoo E-H, Lee S-Y. Glucose Biosensors: An Overview of Use in Clinical Practice. ***Sensors***. 2010;10:4558-4576. doi:10.3390/s100504558.
3. Photometry F, Pressure O, Analysis G, Gases B. Die pCO2-/pO2-Optode: Eine neue p CO2- bzw. pO2-Meßsonde zur Messung des pCO2 oder pO2 von Gasen und Flüssigkeiten / The pCO2-/pO2-Optode: A New Probe for Measurement of pCO2 or pO2 in Fluids and Gases. ***Zeitschrift für Naturforschung*** C1975:532-533.
4. Suzuki S, Takahashi F, Satoh I, Sonobe N. Ethanol and Lactic Acid Sensors Using Electrodes Coated with Dehydrogenase-Collagen Membranes. ***Bulletin of the Chemical Society of Japan*** 1975;48(11):3246-3249. doi:10.1246/bcsj.48.3246.
5. Schultz, Jerome S. "Optical sensor of plasma constituents." **U.S. Patent** No. 4,344,438. 17 Aug. 1982.
6. Liedberg B, Nylander C, Lunström I. Surface plasmon resonance for gas detection and biosensing. ***Sensors and Actuators***. 1983;4(C):299-304. doi:10.1016/0250-6874(83)85036-7.
7. Cass AEG, Davis G, Francis GD, et al. Ferrocene-mediated enzyme electrode for amperometric determination of glucose. ***Anal Chem***. 1984;56(4):667-671. doi:10.1021/ac00268a018.
8. Vestergaard MC, Kerman K, Hsing IM, Tamiya E. ***Nanobiosensors*** *and Nanobioanalyses*.; 2015. doi:10.1007/978-4-431-55190-4.
9. Mohanty SP. Biosensors : A Tutorial Review Biosensors : A Tutorial Review. *IEEE* ***Potentials***. 2015;25(APRIL 2006):35-40. doi:10.1109/MP.2006.1649009.
10. Sarmishtha GHOSHAL, Debasis MITRA, Sudip ROY DDM. Biosensors and Biochips for Nanomedical Applications: a Review. ***Sensors Transducers*** *J*. 2010;113:1-17.
11. Mittal S, Kaur H, Gautam N, Mantha AK. Biosensors for breast cancer diagnosis: A review of bioreceptors, biotransducers and signal amplification strategies. ***Biosens Bioelectron***. 2017;88:217-231. doi:10.1016/j.bios.2016.08.028.
12. Benvidi A, Dehghani Firouzabadi A, Dehghan Tezerjani M, Moshtaghiun SM, Mazloum-Ardakani M, Ansarin A. A highly sensitive and selective electrochemical DNA biosensor to diagnose breast cancer. ***Electroanal Chem***. 2015;750:57-64. doi:10.1016/j.jelechem.2015.05.002.
13. Belluzo MS, Ribone MÉ, Camussone C, Marcipar IS, Lagier CM. Favorably orienting recombinant proteins to develop amperometric biosensors to diagnose Chagas' disease. ***Anal Biochem***. 2011;408(1):86-94. doi:10.1016/j.ab.2010.09.002.

14. Rodriguez-Mozaz S, Marco MP, Lopez De Alda MJ, Barceló D. Biosensors for environmental monitoring of endocrine disruptors: A review article. ***Anal Bioanal Chem***. 2004;378(3):588-598. doi:10.1007/s00216-003-2385-0.

15. Amine A, Mohammadi H, Bourais I, Palleschi G. Enzyme inhibition-based biosensors for food safety and environmental monitoring. ***Biosens Bioelectron***. 2006;21(8):1405-1423. doi:10.1016/j.bios.2005.07.012.

16. Rodriguez-Mozaz S, Alda MJL de, Marco M-P, Barceló D. Biosensors for environmental monitoring A global perspective. ***Talanta***. 2005;65(2):291-297. doi:10.1016/j.talanta.2004.07.006.

17. Touhami A. Biosensors and Nanobiosensors: Design and Applications. ***Nanomedicine***, 2014: 374-400..

18. Bhalla N, Jolly P, Formisano N, Estrela P. Introduction to biosensors. ***Essays Biochem***. 2016;60(1):1-8. doi:10.1042/EBC20150001.

19. Malekzad H, Jouyban A, Hasanzadeh M, Shadjou N, de la Guardia M. Ensuring food safety using aptamer based assays: Electroanalytical approach. *TrAC* ***Trends Anal Chem***. 2017;94:77-94. doi:10.1016/j.trac.2017.07.001.

20. Alocilja EC, Radke SM. Market analysis of biosensors for food safety. ***Biosensors and Bioelectronic****s*. Vol 18. ; 2003:841-846. doi:10.1016/S0956-5663(03)00009-5.

21. Chambers JP, Arulanandam BP, Matta LL, Weis A, Valdes JJ. Biosensor recognition elements. ***Curr Issues Mol Biol***. 2008;10(1):1-12. doi:10.1016/j.bios.2008.06.007.

22. Mohanty SP, Kougianos E. Biosensors: a tutorial review. *IEEE* ***Potentials***. 2006;25(2):35-40. doi:10.1109/MP.2006.1649009.

23. Zayats M, Huang Y, Gill R, Ma CA, Willner I. Label-free and reagentless aptamer-based sensors for small molecules. ***Am Chem Soc***. 2006;128(42):13666-13667. doi:10.1021/ja0651456.

24. Jaffrezic-Renault N, Dzyadevych S V. Conductometric microbiosensors for environmental monitoring. ***Sensors***. 2008;8(4):2569-2588. doi:10.3390/s8042569.

25. Lawrence AJ, Moores GR. Conductimetry in Enzyme Studies. ***Biochem***. 1972;24(3):538-546. doi:10.1111/j.1432-1033.1972.tb19716.x.

26. Sethi RS. Transducer aspects of biosensors. ***Biosens Bioelectron***. 1994;9(3):243-264. doi:10.1016/0956-5663(94)80127-4.

27. Watson LD, Maynard P, Cullen DC, Sethi RS, Brettle J, Lowe C. A microelectronic conductimetric biosensor. ***Biosensors***. 1987;3(2):101-115. doi:10.1016/S0265-928X(87)80003-2.

28. W Göpel, J Hesse JZ. *Sensors: A Comprehensive Survey*.; 1991.

29. Turner, Anthony, Isao Karube, and George S. Wilson. ***Biosensors: fundamentals and applications***. Oxford university press, 1987.

30. Pohanka M, Skládal P. Electrochemical biosensors – principles and applications. ***Appl Biomed***. 2008;6(2):57-64. http://www.zsf.jcu.cz/jab/6_2/pohanka.pdf.

31. Limoges B, Marchal D, Mavré F, Savéant JM, Schöllhorn B. Theory and practice of enzyme bioaffinity electrodes. Direct electrochemical product detection. *J **Am Chem Soc***. 2008;130(23):7259-7275. doi:10.1021/ja7102845.

32. Rochelet-Dequaire M, Djellouli N, Limoges B, Brossier P. Bienzymatic-based electrochemical DNA biosensors: a way to lower the detection limit of hybridization assays. ***Analyst***. 2009;134(2):349-353. doi:10.1039/B816220D.

33. Rossetti C, Pomati F, Calamari D. Microorganisms' activity and energy fluxes in lake Varese (Italy): a field method. ***Water Res***. 2001;35(5):1318-1324. doi:10.1016/S0043-1354(00)00362-6.

34. Newman A L, Hunter K W SWD. The capacitive affinity sensor: a new biosensor. In: ***Proceedings of the Second International Meeting on Chemical Sensors***;. Bordeaux; France; 1986.

35. Bataillard P, Gardies F, Jaffrezic-Renault N, Martelet C, Colin B, Mandrand B. Direct detection of immunospecies by capacitance measurements. *Anal Chem*. 1988;60(21):2374-2379. doi:10.1021/ac00172a011.

36. Prodromidis MI. Impedimetric Biosensors and Immunosensors. ***Environ Chem Int Semin Anal Sci Pakistan J Anal Environ Chem***. 2007;8(2):69-71. http://www.ceacsu.edu.pk/PDF file/Journal Vol 8 No 1 and 2/69-71-PJAEC-P.pdf.

37. Yuqing M, Jianguo G, Jianrong C. Ion sensitive field effect transducer-based biosensors. ***Biotechnol Adv***. 2003;21(6):527-534. doi:10.1016/S0734-9750(03)00103-4.

38. Blum, Lo¨c J., and Pierre R. Coulet. Biosensor principles and applications. M. Dekker, 1991.

39. Bakker E, Pretsch E. Modern Potentiometry. ***Angew Chemie Int Ed***. 2007;46(30):5660-5668. doi:10.1002/anie.200605068.

40. Bobacka J, Ivaska A, Lewenstam A. Potentiometric ion sensors. ***Chem Rev***. 2008;108(2):329-351. doi:10.1021/cr068100w.

41. Szigeti Z, Malon A, Vigassy T, et al. Novel potentiometric and optical silver ion-selective sensors with subnanomolar detection limits. ***Anal Chim Acta***. 2006;572(1):1-10. doi:10.1016/j.aca.2006.05.009.

42. Mehrotra P. Biosensors and their applications - A review. ***J Oral Biol Craniofacial Res***. 2016;6(2):153-159. doi:10.1016/j.jobcr.2015.12.002.

43. Ngeh-Ngwainbi J, Suleiman AA, Guilbault GG. Piezoelectric crystal biosensors. ***Biosens Bioelectron***. 1990;5(1):13-26. doi:10.1016/0956-5663(90)80023-7.

44. Sauerbrey G. Verwendung von Schwingquarzen zur Waegung duenner Schichten und zur Mikrowaegung. ***Zeitschrift fuer Phys***. 1959;155(2):206-222. doi:10.1007/BF01337937.

45. Deakin MR, Buttry DA. Electrochemical applications of the quartz crystal microbalance. ***Anal Chem***. 1989;61(20):1147A-1154A. doi:10.1021/ac00194a014.
46. King WH. Piezoelectric Sorption Detector. ***Anal Chem***. 1964;36(9):1735-1739. doi:10.1021/ac60215a012.
47. Konash P L BGJ. A SAW device for immunoreactions. ***Anal Chem****, 1980, 52 1929-1935*. 1980;(52):1929-1935.
48. Liss M, Petersen B, Wolf H, Prohaska E. An aptamer-based quartz crystal protein biosensor. ***Anal Chem***. 2002;74(17):4488-4495. doi:10.1021/ac011294p.
49. Ward MD, Buttry DA. In Situ Interfacial Mass Detection with Piezoelectric Transducers. ***Science***. 1990;249:1000-1007. doi:10.2307/2878131.
50. Ballantine DS. Acoustic Wave Sensors : Theory, Design, and Physico-Chemical Applications. Academic Press; 1996.
51. Wohltjen H, Dessy R. Surface acoustic wave probe for chemical analysis. I. Introduction and instrument description. ***Anal Chem***. 1979;51(9):1458-1464. doi:10.1021/ac50045a024.
52. Länge K, Rapp BE, Rapp M. Surface acoustic wave biosensors: A review. ***Anal Bioanal Chem***. 2008;391(5):1509-1519. doi:10.1007/s00216-008-1911-5.
53. Vellekoop MJ. Acoustic Wave Sensors and their Technology. ***Ultrason***. 1998;36(1-5):7-14. doi:10.1016/S0041-624X(97)00146-7.
54. Šafařík I, Šafaříková M. Use of magnetic techniques for the isolation of cells. ***J Chromatogr B Biomed Sci Appl***. 1999;722(1-2):33-53. doi:10.1016/S0378-4347(98)00338-7.
55. Richardson J, Hawkins P, Luxton R. The use of coated paramagnetic particles as a physical label in a magneto-immunoassay. In: ***Biosensors and Bioelectronics***. Vol 16. ; 2001:989-993. doi:10.1016/S0956-5663(01)00201-9.
56. Jianrong, Chen, et al. Nanotechnology and biosensors. **Biotechnology advances** 22.7 (2004): 505-518.
57. Llandro J, Palfreyman JJ, Ionescu A, Barnes CHW. Magnetic biosensor technologies for medical applications: A review. ***Med Biol Eng Comput***. 2010;48(10):977-998. doi:10.1007/s11517-010-0649-3.
58. Koh I, Josephson L. Magnetic Nanoparticle Sensors. ***Sensors***. 2009;9(10):8130-8145. doi:10.3390/s91008130.
59. Chemla YR, Grossman HL, Poon Y, et al. Ultrasensitive magnetic biosensor for homogeneous immunoassay. ***Proc Natl Acad Sci*** *U S A*. 2000;97(26):14268-14272. doi:10.1073/pnas.97.26.14268.
60. Grossman HL, Myers WR, Vreeland VJ, et al. Detection of bacteria in suspension by using a superconducting quantum interference device. ***Proc Natl Acad Sci*** *U S A*. 2004;101(1):129-134. doi:10.1073/pnas.0307128101.
61. Lee S, Myers WR, Grossman HL, Cho HM, Chemla YR, Clarke J. Magnetic gradiometer based on a high-transition temperature superconducting quantum

interference device for improved sensitivity of a biosensor. ***Appl Phys*** *Lett*. 2002;81(16):3094-3096. doi:10.1063/1.1515122.

62. Osterfeld SJ, Yu H, Gaster RS, et al. Multiplex protein assays based on real-time magnetic nanotag sensing. ***Proc Natl Acad Sci*** *U S A*. 2008;105(52):20637-20640. doi:10.1073/pnas.0810822105.

63. Notingher I. Raman Spectroscopy Cell-based Biosensors. ***Sensors***. 2007;7(8):1343-1358. doi:10.3390/s7081343.

64. Lee HJ, Villaume J, Cullen DC, Kim BC, Gu MB. Monitoring and classification of PAH toxicity using an immobilized bioluminescent bacteria. In: ***Biosensors and Bioelectronics***. Vol 18. ; 2003:571-577. doi:10.1016/S0956-5663(03)00039-3.

65. Kim BC, Park KS, Kim SD, Gu MB. Evaluation of a high throughput toxicity biosensor and comparison with a Daphnia magna bioassay. In: ***Biosensors and Bioelectronics***. Vol 18. ; 2003:821-826. doi:10.1016/S0956-5663(03)00027-7.

66. Swinehart DF. The Beer-Lambert Law. ***J Chem Educ***. 1962;39(7):333. doi:10.1021/ed039p333.

67. Noui L, Hill J, Keay PJ, et al. Development of a high resolution UV spectrophotometer for at-line monitoring of bioprocesses. ***Chem Eng Process***. 2002;41(2):107-114. doi:10.1016/S0255-2701(01)00122-2.

68. Kourti T, Nomikos P, MacGregor JF. Analysis, monitoring and fault diagnosis of batch processes using multiblock and multiway PLS. ***J Process Control***. 1995;5(4):277-284. doi:10.1016/0959-1524(95)00019-M.

69. Ai H, Hazelwood KL, Davidson MW, Campbell RE. Fluorescent protein FRET pairs for ratiometric imaging of dual biosensors. ***Nat Methods***. 2008;5(5):401-403. doi:10.1038/nmeth.1207.

70. Shi, Jingyu, et al. "A fluorescence resonance energy transfer (FRET) biosensor based on graphene quantum dots (GQDs) and gold nanoparticles (AuNPs) for the detection of mecA gene sequence of Staphylococcus aureus." ***Biosensors and Bioelectronics*** 67 (2015): 595-600.

71. Komatsu N, Aoki K, Yamada M, et al. Development of an optimized backbone of FRET biosensors for kinases and GTPases. ***Mol Biol Cell***. 2011;22(23):4647-4656. doi:10.1091/mbc.E11-01-0072.

72. Wood BR, McNaughton D. Resonance Raman spectroscopy in malaria research. ***Expert Rev Proteomics***. 2006;3(5):525-544. doi:10.1586/14789450.3.5.525.

73. Kneipp K, Kneipp H, Kneipp J. Surface-enhanced raman scattering in local optical fields of silver and gold nanoaggregates - From single-molecule raman spectroscopy to ultrasensitive probing in live cells. ***Acc Chem Res***. 2006;39(7):443-450. doi:10.1021/ar050107x.

74. Nan X, Potma EO, Xie XS. Nonperturbative Chemical Imaging of Organelle Transport in Living Cells with Coherent Anti-Stokes Raman Scattering Microscopy. ***Biophys*** *J*. 2006;91(2):728-735. doi:10.1529/biophysj.105.074534.

75. Qian, Yong, et al. "Label-free and Raman dyes-free surface-enhanced Raman spectroscopy for detection of DNA." ***Sensors Actuators, B Chem*** 254 (2018): 483-489..

76. Leung A, Shankar PM, Mutharasan R. A review of fiber-optic biosensors. ***Sensors Actuators****, B Chem*. 2007;125(2):688-703. doi:10.1016/j.snb.2007.03.010.

77. Hale ZM, Payne FP, Marks RS, Lowe CR, Levine MM. The single mode tapered optical fibre loop immunosensor. ***Biosens Bioelectron***. 1996;11(1-2):137-148. doi:10.1016/0956-5663(96)83721-3.

78. Mignani AG, Falciai R, Ciaccheri L. Evanescent wave absorption spectroscopy by means of bi-tapered multimode optical fibers. ***Appl Spectrosc***. 1998;52(4):546-551.

79. D'Orazio P. Biosensors in clinical chemistry. ***Clin Chim Acta***. 2003;334(1-2):41-69. doi:10.1016/S0009-8981(03)00241-9.

80. Guo S, Albin S. Transmission property and evanescent wave absorption of cladded multimode fiber tapers. ***Opt Express***. 2003;11(3):215-223. doi:10.1364/OE.11.000215.

81. Nylander C, Liedberg B, Lind T. Gas detection by means of surface plasmon resonance. ***Sensors and Actuators***. 1982;3(C):79-88. doi:10.1016/0250-6874(82)80008-5.

82. Lee J, Jang J, Choi B, et al. A highly responsive silicon nanowire/amplifier MOSFET hybrid biosensor. ***Scientific reports***, 2015, 5: 12286.

83. Jordan L, Xu X, Wittenberg NJ, et al. Measuring binding interactions of neurite-extension promoting antibodies to supported lipid membranes using a multichannel microfluidic plasmonic nanohole array biosensor. In: ***17th International Conference on Miniaturized Systems for Chemistry and Life Sciences****, MicroTAS 2013*. Vol 1. ; 2013:215-217.

84. Karlsson R. SPR for molecular interaction analysis: a review of emerging application areas. ***J Mol Recognit***. 2004;17(3):151-161. doi:10.1002/jmr.660.

85. Chung JW, Kim SD, Bernhardt R, Pyun JC. Application of SPR biosensor for medical diagnostics of human hepatitis B virus (hHBV). In: ***Sensors and Actuators****, B: Chemical*. Vol 111-112. ; 2005:416-422. doi:10.1016/j.snb.2005.03.055.

86. Quinn JG, O'Neill S, Doyle a, et al. Development and application of surface plasmon resonance-based biosensors for the detection of cell-ligand interactions. ***Anal Biochem***. 2000;281(2):135-143. doi:10.1006/abio.2000.4564.

87. Yanase Y, Hiragun T, Yanase T, Kawaguchi T, Ishii K, Hide M. Application of SPR Imaging Sensor for Detection of Individual Living Cell Reactions and Clinical Diagnosis of Type I Allergy. ***Allergol Int***. 2013;62(2):163-169. doi:10.2332/allergolint.12-RA-0505.

88. Kaushik A, Kumar R, Arya SK, Nair M, Malhotra BD, Bhansali S. Organic–Inorganic Hybrid Nanocomposite-Based Gas Sensors for Environmental Monitoring. ***Chem Rev***. 2015;115(11):4571-4606. doi:10.1021/cr400659h.

89. Wu J, Zhu Y, Xue F, et al. Recent trends in SELEX technique and its application to food safety monitoring. ***Mikrochim Acta***. 2014;181(5-6):479-491. doi:10.1007/s00604-013-1156-7.

90. Goh LS, Kumekawa N, Watanabe K, Shinomiya N. Hetero-core spliced optical fiber SPR sensor system for soil gravity water monitoring in agricultural environments. ***Comput Electron Agric***. 2014;101:110-117. doi:10.1016/j.compag.2013.12.008.

91. Homola J. Present and future of surface plasmon resonance biosensors. ***Anal Bioanal Chem***. 2003;377(3):528-539. doi:10.1007/s00216-003-2101-0.

92. Boardman AD. ***Electromagnetic Surface Modes***.; 1982.

93. H. R. Surface plasmons on smooth and rough surfaces and on gratings. ***Springer-Verlag Berlin***. 2013.

94. Singh P. SPR Biosensors: Historical Perspectives and Current Challenges. ***Sensors Actuators, B Chem***. 2016;229:110-130. doi:10.1016/j.snb.2016.01.118.

95. Linman MJ, Abbas A, Roberts CC, Cheng Q. Etched glass microarrays with differential resonance for enhanced contrast and sensitivity of surface plasmon resonance imaging analysis. ***Anal Chem***. 2011;83(15):5936-5943. doi:10.1021/ac200881q.

96. Patskovsky S, Latendresse V, Dallaire A-M, Doré-Mathieu L, Meunier M. Combined surface plasmon resonance and impedance spectroscopy systems for biosensing. ***Analyst***. 2014;139:596-602. doi:10.1039/c3an01685d.

97. Nedelkov D, Tubbs KA, Nelson RW. Surface plasmon resonance-enabled mass spectrometry arrays. ***Electrophoresis***. 2006;27(18):3671-3675. doi:10.1002/elps.200600065.

98. Homola, Jiří. "Electromagnetic theory of surface plasmons." ***Surface plasmon resonance based sensors*** (2006): 3-44..

99. Laplatine L, Leroy L, Calemczuk R, et al. Spatial resolution in prism-based surface plasmon resonance microscopy. ***Opt Express***. 2014;Vol. 22(19):22771-22785. doi:10.1364/OE.22.022771.

100. Justino CIL, Freitas AC, Pereira R, Duarte AC, Rocha Santos TAP. Recent developments in recognition elements for chemical sensors and biosensors. ***TrAC - Trends Anal Chem***. 2015;68:2-17. doi:10.1016/j.trac.2015.03.006.

101. Köhler G, Milstein C. Continuous cultures of fused cells secreting antibody of predefined specificity. ***Nature***. 1975;256:495-497. doi:10.1038/256495a0.

102. Ritter, Mary A., and Heather M. Ladyman, eds. Monoclonal Antibodies. Cambridge University Press, 1995..

103. Barhoumi H, Maaref A, Rammah M, et al. Urea biosensor based on Zn3Al-Urease layered double hydroxides nanohybrid coated on insulated silicon structures. In: ***Materials Science and Engineering C***. Vol 26. ; 2006:328-333. doi:10.1016/j.msec.2005.10.042.

104. Strehlitz, B., Nikolaus N. and Stoltenburg, R.Protein Detection with Aptamer Biosensors. ***Sensors*** 2008, 8, 4296-4307.
105. G W. The use of polymers with enzyme-analogous structures for the resolution of racemates. ***Angrew Chem Intern***. 1972;11(4):341.
106. Andersson LI. Molecular imprinting: Developments and applications in the analytical chemistry field. In: ***Journal of Chromatography B: Biomedical Sciences and Applications***. Vol 745. ; 2000:3-13. doi:10.1016/S0378-4347(00)00135-3.
107. Wulff G, Kemmerer R, Vietmeier J et al. Chirality of vinyl-polymers-the preparation of chiral cavities in synthetic-polymers. ***New J Chem***. 1982;6(12):681-687.
108. Van Dorst B, Mehta J, Bekaert K, et al. Recent advances in recognition elements of food and environmental biosensors: A review. ***Biosens Bioelectron***. 2010;26(4):1178-1194. doi:10.1016/j.bios.2010.07.033.
109. Hillberg AL, Brain KR, Allender CJ. Molecular imprinted polymer sensors: Implications for therapeutics. ***Adv Drug Deliv Rev***. 2005;57(12):1875-1889. doi:10.1016/j.addr.2005.07.016.
110. Piletsky SA, Panasyuk TL, Piletskaya E V., Nicholls IA, Ulbricht M. Receptor and transport properties of imprinted polymer membranes - A review. ***J Memb Sci***. 1999;157(2):263-278. doi:10.1016/S0376-7388(99)00007-1.
111. Tuerk C, Gold L. Systematic evolution of ligands by exponential enrichment:RNA ligands to bacteriophage T4 DNA polymerase. ***Science***. 1990;249(4968):505-510. doi:10.1126/science.2200121.
112. Ellington AD, Szostak JW. In vitro selection of RNA molecules that bind specific ligands. ***Nature***. 1990;346(6287):818-822. doi:10.1038/346818a0.
113. Ellington A, Szostak J. Selection in vitro of single-stranded DNA molecules that fold into specific ligand-binding structures. ***Nature***. 1992;355:850-852. doi:10.1038/355850a0.
114. Gu MB, Kim HS. Biosensors based on aptamers and enzymes. ***Adv Biochem Eng Biotechnol***. 2014;140. doi:10.1007/978-3-642-54143-8.
115. Bui BTS, Haupt K. Molecularly imprinted polymers: Synthetic receptors in bioanalysis. ***Anal Bioanal Chem***. 2010;398(6):2481-2492. doi:10.1007/s00216-010-4158-x.
116. McKeague M, Derosa MC. Challenges and opportunities for small molecule aptamer development. ***J Nucleic Acids***. 2012;2012. doi:10.1155/2012/748913.
117. Tombelli S, Minunni M, Mascini M. Analytical applications of aptamers. ***Biosens Bioelectron***. 2005;20(12):2424-2434. doi:10.1016/j.bios.2004.11.006.
118. Daniel C, Méa ne F, Roupioz Y, Livache T, Buhot A. Real time monitoring of thrombin interactions with its aptamers: Insights into the sandwich complex formation. ***Biosens Bioelectron***. 2013;40(1):186-192. doi:10.1016/j.bios.2012.07.016.
119. Huizenga DE, Szostak JW. A DNA aptamer that binds adenosine and ATP. ***Biochemistry***. 1995;34(2):656-665. doi:10.1021/bi00002a033.

120. Bartlett JMS, Stirling D. A short history of the polymerase chain reaction. ***Methods Mol Biol***. 2003;226:3-6. doi:10.1385/1-59259-384-4:3.

121. Zhao Q, Wu M, Chris Le X, Li XF. Applications of aptamer affinity chromatography. ***TrAC - Trends Anal Chem***. 2012;41:46-57. doi:10.1016/j.trac.2012.08.005.

122. Yang Y, Yin S, Li Y, Lu D, Zhang J, Sun C. Application of aptamers in detection and chromatographic purification of antibiotics in different matrices. ***TrAC Trends Anal Chem***. 2017;95:1-22. doi:10.1016/j.trac.2017.07.023.

123. Romig TS, Bell C, Drolet DW. Aptamer affinity chromatography: Combinatorial chemistry applied to protein purification. ***J Chromatogr B Biomed Sci Appl***. 1999;731(2):275-284. doi:10.1016/S0378-4347(99)00243-1.

124. Geiger A, Burgstaller P, Von der Eltz H, Roeder A, Famulok M. RNA aptamers that bind L-arginine with sub-micromolar dissociation constants and high enantioselectivity. ***Nucleic Acids Res***. 1996;24(6):1029-1036. doi:10.1093/nar/24.6.1029.

125. Kim YS, Niazi JH, Chae YJ, Ko UR, Gu MB. Aptamers-in-liposomes for selective and multiplexed capture of small organic compounds. ***Macromol Rapid Commun***. 2011;32(15):1169-1173. doi:10.1002/marc.201100177.

126. Ruta J, Perrier S, Ravelet C, Roy B, Perigaud C, Peyrin E. Aptamer-modified micellar electrokinetic chromatography for the enantioseparation of nucleotides. ***Anal Chem***. 2009;81(3):1169-1176. doi:10.1021/ac802443j.

127. Xu H, Mao X, Zeng Q, Wang S, Kawde AN, Liu G. Aptamer-functionalized gold nanoparticles as probes in a dry-reagent strip biosensor for protein analysis. ***Anal Chem***. 2009;81(2):669-675. doi:10.1021/ac8020592.

128. Dong Y, Yang J, Ye W, et al. Isolation of endogenously assembled RNA-protein complexes using affinity purification based on streptavidin aptamer S1. ***Int J Mol Sci***. 2015;16(9):22456-22472. doi:10.3390/ijms160922456.

129. Madru B, Chapuis-Hugon F, Peyrin E, Pichon V. Determination of cocaine in human plasma by selective solid-phase extraction using an aptamer-based sorbent. ***Anal Chem***. 2009;81(16):7081-7086. doi:10.1021/ac9006667.

130. Deng Q, German I, Buchanan D, Kennedy RT. Retention and separation of adenosine and analogues by affinity chromatography with an aptamer stationary phase. ***Anal Chem***. 2001;73(22):5415-5421. doi:10.1021/ac0105437.

131. Hamaguchi N, Ellington A, Stanton M. Aptamer Beacons for the Direct Detection of Proteins. ***Anal Biochem***. 2001;294(2):126-131. doi:10.1006/abio.2001.5169.

132. Goluch ED. Microbial Identification Using Electrochemical Detection of Metabolites. ***Trends Biotechnol***. August 2017. doi:10.1016/j.tibtech.2017.08.001.

133. Jarczewska M, Górski Ł, Malinowska E. Application of DNA aptamers as sensing layers for electrochemical detection of potassium ions. ***Sensors Actuators, B Chem***. 2016;226:37-43. doi:10.1016/j.snb.2015.11.139.

134. Liu J, Lu Y. Preparation of aptamer-linked gold nanoparticle purple aggregates for colorimetric sensing of analytes. ***Nat Protoc***. 2006;1(1):246-252. doi:10.1038/nprot.2006.38.
135. Yang XH, Huang JH, Wang Q, Wang KM, Yang LJ, Huo XQ. A one-step sensitive dynamic light scattering method for adenosine detection using split aptamer fragments. ***Anal Methods***. 2011;3(1):59-61. doi:10.1039/c0ay00709a.
136. Zhang J, Wang L, Zhang H, Boey F, Song S, Fan C. Aptamer-based multicolor fluorescent gold nanoprobes for multiplex detection in homogeneous solution. ***Small***. 2010;6(2):201-204. doi:10.1002/smll.200901012.
137. Nameghi MA, Danesh NM, Ramezani M, Hassani FV, Abnous K, Taghdisi SM. A fluorescent aptasensor based on a DNA pyramid nanostructure for ultrasensitive detection of ochratoxin A. ***Anal Bioanal Chem***. 2016;408(21):5811-5818. doi:10.1007/s00216-016-9693-7.
138. Yang C, Spinelli N, Perrier S, Defrancq E, Peyrin E. Macrocyclic Host-Dye Reporter for Sensitive Sandwich-Type Fluorescent Aptamer Sensor. ***Anal Chem***. 2015;87(6):3139-3143. doi:10.1021/acs.analchem.5b00341.
139. Watson J, Crick F. Molecular structure of nucleic acids. ***Nature***. 1953;171(4356):737-738. doi:10.1038/171737a0.
140. Seeman NC. Nucleic acid junctions and lattices. ***J Theor Biol***. 1982;99(2):237-247. doi:10.1016/0022-5193(82)90002-9.
141. Bu N-N, Tang C-X, He X-W, Yin X-B. Tetrahedron-structured DNA and functional oligonucleotide for construction of an electrochemical DNA-based biosensor. ***Chem Commun (Camb)***. 2011;47(27):7689-7691. doi:10.1039/c1cc11628b.
142. Rothemund PWK. Folding DNA to create nanoscale shapes and patterns. ***Nature***. 2006;440(7082):297-302. doi:10.1038/nature04586.
143. LaBean TH, Yan H, Kopatsch J, et al. Construction, analysis, ligation, and self-assembly of DNA triple crossover complexes. ***J Am Chem Soc***. 2000;122(9):1848-1860. doi:10.1021/ja993393e.
144. Han D, Pal S, Nangreave J, Deng Z, Liu Y, Yan H. DNA origami with complex curvatures in three-dimensional space. ***Science***. 2011;332(6027):342-346. doi:10.1126/science.1202998.
145. Fiercepharma.com. DNA origami could allow for “autonomous” delivery.
146. Ke Y, Lindsay S, Chang Y, Liu Y, Yan H. Self-assembled water-soluble nucleic acid probe tiles for label-free RNA hybridization assays. ***Science***. 2008;137:183-186. doi:10.1126/science.1150082.
147. Xu F, Dong H, Cao Y, et al. Ultrasensitive and Multiple Disease-Related MicroRNA Detection Based on Tetrahedral DNA Nanostructures and Duplex-Specific Nuclease-Assisted Signal Amplification. ***ACS Appl Mater Interfaces***. 2016;8(49):33499-33505. doi:10.1021/acsami.6b12214.

Chapter 2 Experimental Methods

Ce chapitre présente les composés, appareils et méthodes utilisés dans ce travail. Les brins d'ADN utilisés et les structures d'ADN formées avec ces brins ont d'abord été introduits. Les structures d'ADN de 1D à 3D ont été formées par hybridation. Ces structures peuvent ensuite créer une chaîne ou un réseau plus complexe en présence d'adénosine. Le protocole expérimental de détection de l'adénosine avec les spectroscopies SPRi et UV-Vis a été exposé en détaillant notamment les principes de détection. D'autres techniques utilisées au cours de ce projet pour la caractérisation des structures d'ADN en solution ont également été présentées. L'électrophorèse en gel, en utilisant deux types de gel différents, a été utilisée pour analyser la taille des structures d'ADN, la spectroscopie de fluorescence et la spectroscopie UV ont été utilisées pour déterminer la courbe de fusion des structures d'ADN. L'existence des structures ADN linéaires ou en réseau a été prouvée par obtention des courbes de fusion à partir des analyses réalisées par spectroscopie UV.

2.1 Sequence design and material

2.1.1 Aptamer and split-aptamer anti-Adenosine

All the DNA structures we used were based on the anti-Adenosine aptamer reported by Huizenga and Szostak [1] in 1995. Adenosine is a component of many biological cofactors. It plays an important part in many biochemical processes, for example, the energy transfer between Adenosine triphosphate (ATP) and Adenosine diphosphate (ADP) or in the signal transduction as cyclic Adenosine monophosphate (cAMP). [2] It is also involved in promoting sleep and regulation of blood flow. [3,4] The detection of Adenosine could be helpful for medical research concerning these interactions. Moreover, Adenosine is a harmless compound with easy access at low cost, which is why we wanted to build the detecting model first with anti-Adenosine aptamer. In future work, the aptamer used in the DNA structures could be switched for the detection of other targets.

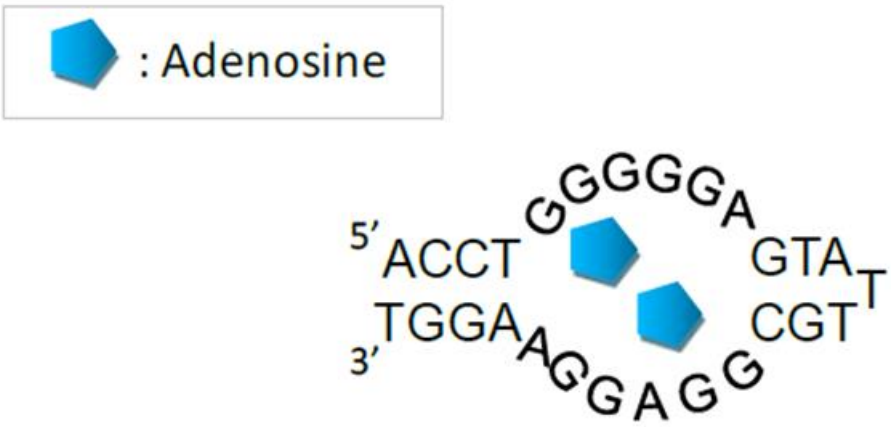

Figure 2.1 The anti-Adenosine aptamer reported by Huizenga and Szostak in 1995, the aptamer consists of 27 nucleotides and folds at two G-quartets with two Adenosine molecules. The binding is referred as an Adenosine bridge.

The DNA aptamer in **Figure 2.1** could bond with Adenosine and ATP. In the original report the author proved with covariation, nucleotide analog substitution and redesigned aptamer that the structure consisted of two small double DNA helices and two G-quartets. The G-quartet structure is four guanosines assembled by hydrogen bonding between the Hoogsteen and Watson-Crick faces of adjacent guanosines. [1] G-quartets can stack on each other to form aggregated structure that could be stabilized with monovalent cations such as Na^+ and K^+. [5,6] The binding formed in **Figure 2.1** is referred as an Adenosine bridge, whereas two Adenosine molecules acted like the bridge to bind the aptamer. The modifications made on this aptamer for the detection of Adenosine will be introduced in the following sections

2.1.2 1D DNA structure sequence design

The 1D DNA structures we proposed were formed by two oligonucleotides. The 1D structure consisted of two parts, a split aptamer dangling end and complementary DNA duplex. The first step for the design of the structure was to remove the T nucleobase in the middle of the anti-Adenosine aptamer to cut it into two halves (**Figure 2.2**). These two short oligonucleotides were splited from an aptamer, thus named “split-aptamer”. This modification will not affect the strands’ ability to bind with Adenosine molecules. The second step was to add complementary oligonucleotide dangling ends acting like a zip so that the two strands could bind with each other through hybridization.

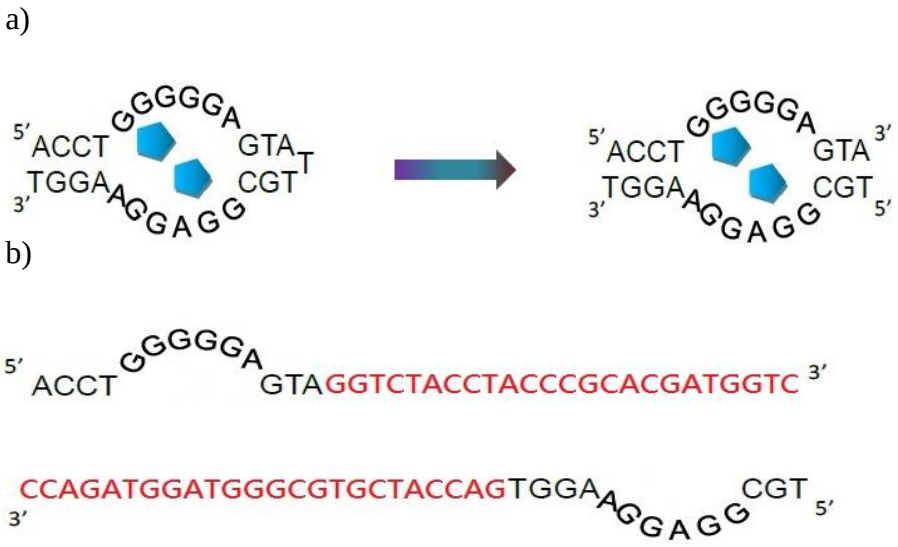

Figure 2.2 (a) The creation of split aptamer anti-Adenosine. The 27-base aptamer was splited into two halves of 13-base oligonucleotide. (b) Split-aptamers with oligonucleotide zips. The oligonucleotide zips (red) were complementary to each other thus could hybridize and form duplex.

Our purpose for modifying the aptamer was to build a 1D DNA chain structure with Adenosine molecules acting as the shape switching element. **Figure 2.3** showed the interactions that took place while the two strands were mixed in solution. The buffer containing salt provided the condition for the oligonucleotide parts to hybridize and form a duplex with split-aptamer dangling ends. With presence of Adenosine molecules in the environment, these duplexes will further bind and form Adenosine bridges. Finally, a 1D chain structure of DNA was formed with two binding mechanisms: hybridization (red part) and Adenosine bridges (blue part). In order to seek the best performance, we modified the split-aptamer part and designed three different 1D DNA chain with different binding strength. The main difference is the number of hybridized base pairs on one side of the Adenosine bridge. While naming the sequences, we referred to one of the split-aptamer part of the sequence "Sx". The "S" was short for "split-aptamer" and "x" was the number of base pairs (x=5, 6, 8) hybridized next to the Adenosine bridges. The other half of the splited aptamer was

named “Sx*”. The two oligonucleotide zip was abbreviated as “Z” and “Zc”, which meant “zip” and “zip complementary”. To sum up, the sequences were named SxZ and Sx*Zc. The structure existed in equilibrium, which meant the 1D chain will deform into duplexes if the Adenosine molecules were removed. The detection of Adenosine could be realized thanks to this selectivity of target in solution.

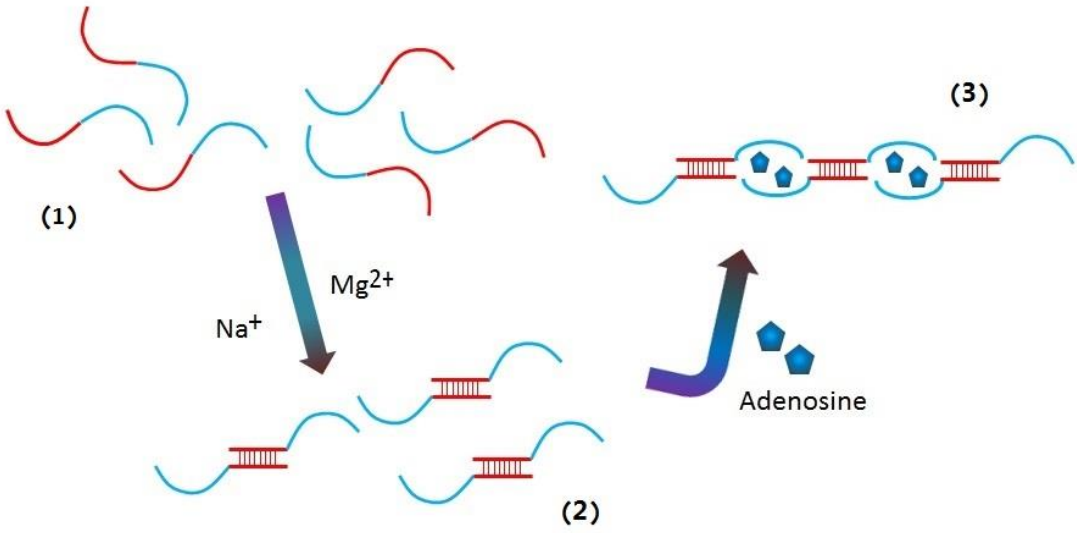

Figure 2.3 the formation of 1D DNA chain structure: (1) the two single strands containing split-aptamer and oligonucleotide zip were mixed in solution; (2) with the salt ions in the buffer, the two single strands were hybridized and formed a duplex with split-aptamer dangling ends; (3) with presence of Adenosine in the environment, the split-aptamer dangling ends formed Adenosine bridges and as a result we obtained 1D DNA chain binded with two mechanisms.

The final step to design the sequence was to rule out possibilities of secondary structures that will bring unwanted interactions to the solution. To eliminate these disturbing secondary structures we used an online simulation tool “Mfold” [7]. The simulation was used to calculate the theoretical melting or self-folding temperature of one single strand or mixture of two strands based on the salt concentration, strand concentration and DNA sequence. The structures with higher self-folding temperature need more energy to disassociate, in other words, are more stable and easier to bring secondary structures into the solution. The simulation condition was set to be close to

the buffer we used for all the tests (Na^+ 150mM, Mg^{2+} 5mM, pH=7.4, 25℃). There were two simulations we ran to rule out the secondary structures. First, the self-folding temperature of each single strand was tested. This test made sure that the sequence will not bind with itself before forming the designed DNA structure. Then, all the possible structures that can be formed with the SxZ and Sx*Zc strands were enlisted to compare their melting temperatures. This test made sure that the designed DNA structure was the most stable structure formed after the denaturation of the DNA mixture.

The 1D chain design we proposed had many potential combinations, the details in sorting these potential possibilities and choosing the best combination will be displayed in the first section of Chapter 3. In addition the sequences were further modified to achieve better performance. The exact sequence could be found in the Appendix of the thesis. There were five different duplexes (ten single strands) used throughout the whole project, two of them were proposed to improve the sensing methods, the others were designed for support experiments that help understand the concept of detection.

2.1.3 2D DNA structure sequence design

To further improve the detection results, we also designed a 2D DNA Y shape structure. The main frame of the structure was a Y shape DNA 2D structure self-assembled by three single strands Ya, Yb and Yc (**Figure 2.4**). The lengths of the three strands varied from 31 to 33 nucleobases. The three strands were hybridized to each other through a junction in the center accompanied by three branches. The structure of the 2D DNA gave six positions where the oligonucleotide could be extended with split-aptamer dangling ends. The Y shape structure was formed by self-assembly of DNA. Same amount of the three strands were mixed in SPR buffer which contained salt to accelerate hybridization. The solution was then heated to 95℃ for

5mins, after the heating process the solution was cooled down at room temperature for at least 30mins. By switching the three strands, the number of the split-aptamer dangling ends could be controlled from 0 to 3.

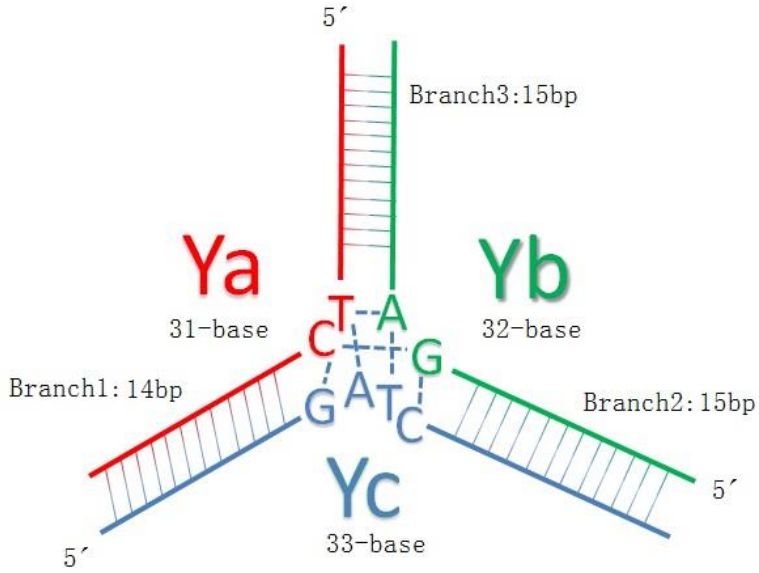

Figure 2.4 The 2D Y shape DNA structure: the Y composed of three DNA strands (Ya, Yb and Yc). In the center of the structure there was a junction through hybridization, some of the nucleobases were attracted by more than one nucleobase. Three branches extended from the junction and formed a 2D DNA structure.

The Ya sequence added with split aptamer was named YaS, and if it was added with the other half of the split-aptamer it will be named YaS*. The dangling ends in the Y could grasp onto the probes functionalized on gold surface or form a network with each other. Our goal of proposing this design was to use such network and its heavier mass effect to further increase the signals on SPRi sensor. Same as the 1D structure, melting profile simulation was carried out to select the best sequence design among the potential choices. The results of the simulation will be discussed in Chapter 5 and the exact sequence of DNA was displayed in the Appendix of the thesis.

2.1.4 3D DNA structure sequence design

Goodman et al. reported a single-step synthesis method of a DNA tetrahedron in 2004.[8] Inspired by their work, we built a 3D DNA tetrahedron structure with split-aptamer dangling ends. The DNA tetrahedron reported by Goodman was self-assembled by four 55-base oligonucleotides. Each of the six edges of the tetrahedron was a 17-base "sub-sequence". Each of the 55-base oligonucleotide had three "sub-sequence" separated by two sets of two-base hinges. The two-base hinges were not hybridized during the self-assembly. The purpose of the hinges was to ensure the flexibility of the DNA strands so that the vertices of the tetrahedron reach an angle of 60 degree between the adjacent edges. The four split-aptamer dangling ends can also form a 3D network and dramatically increase the mass effect. The structure was chiral and had two enantiomers.

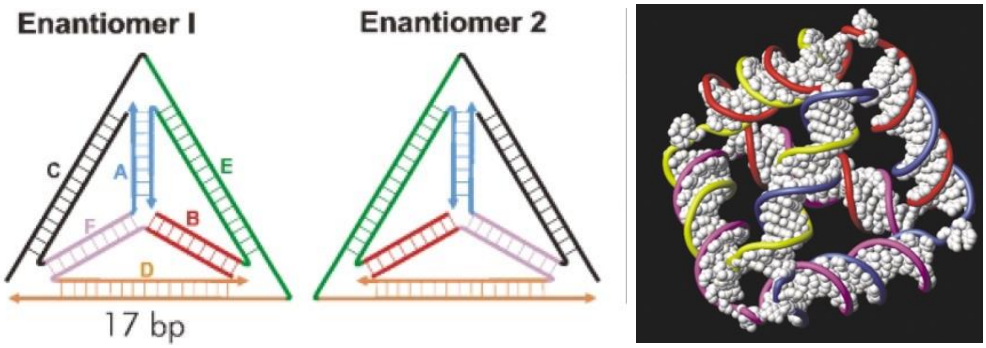

Figure 2.5 The 3D scheme of DNA tetrahedron and its two enantiomers. .[8] The tetrahedron composed of four single strands. Each strand was a 55-base oligonucleotide with three 17-base edge separated by two sets of two-base hinges.

The four oligonucleotides were named T1, T2, T3 and T4. The split-aptamer dangling ends could be added to the four vertices of the tetrahedron. The split-aptamer dangling ends can build a 3D network, which gives the ability to increase detection signal from SPRi for its heavy mass. The thermodynamic simulation to rule out secondary structures will be discussed in Chapter 5.

2.1.5 Reagent and oligonucleotide purchased

Adenosine and guanosine as well as all the reagents used to prepare the buffer and gel were purchased from Sigma-Aldrich (Saint Quentin Fallavier, France). The reagents include NaOH, K_2HPO_4, $MgCl_2$, NaCl, HCl, ammonium persulfate ($(NH_4)_2S_2O_8$), TEMED (Tetramethylethylenediamine), Agarose and Polyacrylamide stock solution (19:1). CH3O-PEG-SH (PEG 2000, MW 2000 Da) was purchased from Rapp Polymere GmbH (Tübingen, Germany). The oligonucleotides were purchased from Eurogentec (Angers, France). The strands used for the functionalization of the gold surface had a thiol modification at the 5' end position. The water used was ultrapure with 18.2 MΩ•cm-1 resistivity. The fluorescent label Gel Red for gel electrophoresis and the Gel prestain loading buffer were purchased from Biotium (Fremont, California, USA) and 10X SYBR Green PCR buffer used in fluorescent spectroscopy was purchased from Applied Biosystem (UK), 10X TBE buffer (1mM Tris, 1mM EDTA, 5mM $MgCl_2$, pH=8) was purchased from Thermo Fisher Scientific (MA, USA). The detail of the buffers prepared from these reagents including the SPR buffer, fluorescent buffer can be found in the Appendix.

2.2 Surface Plasmon Resonance imaging

2.2.1 Introduction

Self-Assembled Monolayers (SAMs) provide a convenient, flexible and simple system to alter the interfacial properties of metals, metal oxides and semiconductors for scientific research. [9,10] It is formed through the adsorption of molecular constituents from solution or the gas phase onto the surface of solid material or liquid. The molecules or ligands that form SAMs have a chemical functionality named as the "head group" who has specific affinity for the substrate, and in most cases the head group also has the ability to displace adsorbed materials from the surface. A molecular chain is normally connected to the head group so that it can be

functionalized on the surface to alter the wetting and interfacial properties. In the field of biosensor, SAMs are widely used in heterogeneous detection methods to immobilize the recognition elements on metal surface. In Surface Plasmon Resonance imaging (SPRi) the first step is to prepare the gold prism immobilized with the probes for detection. The most common protocol for formation of SAMs on metal surface (Au, Ag, Hg, etc.) is to immerse a clean substrate into a diluted solution of thiols for 12-18 hours at room temperature. The Thiol-metal bonds have the strength of 100 kJ/mol. It makes these bonding fairly stable in a variety of temperatures, solvents, and potentials. [11]

SPRi is a technique oriented from SPR technique. Unlike SPR devices in which the angle or the wavelength of the light is fixed and the plasmon resonance absorption peak is detected from varying the other parameter, SPRi devices fix both parameter and measure the change in reflectance on the whole metal surface instead. The benefit of SPRi is that it can make measurement on multiple spots at the same time and the change happening on the surface could be visualized. The detection principle of SPRi is shown in **Figure 2.6**. A micro array was prepared on gold surface and the light beam generated from the light source come beneath the gold prism at fixed incident angle. The beam is reflected and collected by a CCD camera. The camera captures all the reflected light from the surface and automatically processes the data in return for the array image and quantitative data viewed in real time. The interaction between the analyte and the immobilized probes will lead to a change in the reflectivity of the solution in contact with the gold surface. This change is recorded to monitor interaction on the surface. At fixed incident angle the reflectivity will increase with greater mass on the gold surface and the SPR image is obtained. Under optimized conditions, the lateral resolution of SPRi could reach 2μm range, the resolution depends on the optical parameters of the prism, the sample layer and metal surface. The application of SPRi includes the study of bimolecular interactions (DNA, RNA,

peptides, proteins and antibodies) on arrays. Millington et al. also reported their work using SPRi for screening of ligands in affinity chromatography, the binding behavior of the ligands can be monitored 15-fold faster and saves 130-fold target compared to traditional chromatographic methods. [12] There are other studies focusing on the enhancement of the image obtained from SPRi. Dark-field technique and SPR interferometry are two methods to improve the contrast. [13,14] SPRi can also be combined with other analytical method, for example by combing with optical spectroscopy information about the structure of the molecules can be provided at the same time. [15]

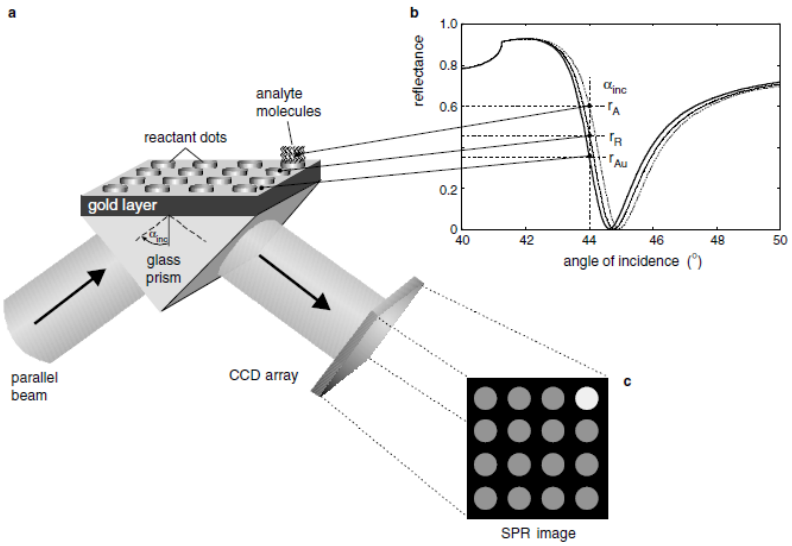

Figure 2.6 The setup and principle of SPRi, (a): The setup of SPRi ; (b): The reflectance calculated, the solid line (rAU) is the pure gold surface with probes, the dashed line (rR) is the spot without analyte, the dotted line (rA) is the spots with analyte attached; (c): the SPRi image obtained because rA > rR > rAu at fixed angle.

2.2.2 Experimental methods

SAMs of oligonucleotides with thiol moiety at the 5' end were formed on gold-coated prisms (Horiba Scientific-GenOptics, Orsay, France) following previously described protocols [16–19]. In brief, the gold surface on top of the prism was cleaned with plasma treatment (0.6 mbar, 75% Oxygen, 25% Argon, power 40 W, 3 min) using a Femto plasma generator (Diener Electronic, Ebhausen, Germany), the night

before the deposition. The grafting solution was spotted onto the surface with a piezoelectric dispensing system sciFLEXARRAYER S3 (Scienion, Berlin, Germany, **Figure 2.7**) which provided precise control of position and volume (4 nL) of the droplets with piezoelectric robot arm.

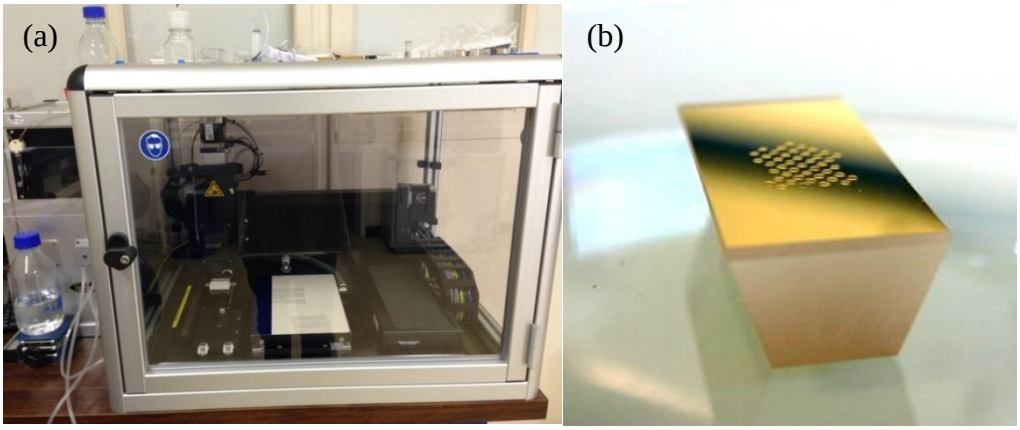

Figure 2.7 (a) The sciFLEXARRAYER used to prepare the SAMs on gold prisms. The spotting solution was automatically loaded and spotted with precise control of the position and volume. (b) The spotted surface of the gold prism.

The grafting solution consisted of H_2KPO_4 buffer (1 M, pH=9.25) with PEG2000 (10 μM) and a mixture of thiolated DNA strands. The total concentration of DNA strands are kept constant at 20 μM incorporating different ratio of DNA probes Z (the same sequence as the oligonucleotide dangling zip) and negative control (NC) in order to control the grafting densities of the probes. The diameters of the spots were around 500 μm and the total grafting density was 8 pmol/cm^{-2}. The density of the grafted probes (Z) was controlled by diluting the strands Z with negative control strands while keeping the total strand concentration at 20 μM. Thus, the probes density varied from 0.4, 0.8, 2, 4 to 8 pmol/cm^{-2} corresponding to the following ratio of Z probes with respect to the total DNA strands (1/20, 1/10, 1/4, 1/2 and 1). For reproducibility studies, at least triplicate spots of each grafting density of probes have been deposited and several microarrays have been produced and analyzed. The atmosphere in which the deposition took place had a controlled humidity of 85%.

The prism was left in the same humid chamber for 2 hours after the deposition. Later the prism was removed from the chamber and kept in dark and dry environment overnight to complete the formation of the SAMs. The second morning, the prism was taken out, the gold surface was rinsed with deionized water and dried with argon flow. Before the first use, the functionalized gold surface was immersed in 150 µM of PEG2000 solution for 90 minutes at room temperature to block the surface from non-specific interactions. After this blocking procedure, the surface was rinsed again with deionized water and dried with argon flow. Between successive experiments, the microarrays were stored dry at 4 ℃. From those initial microarrays with Z probes, the injection of SX*Zc strands lead to a functional microarrays upon hybridization of the Z and Zc strands leading SX* strands as dangling end probes. Thus, the same microarray served to analyze the sequence engineering of split-aptamers with 5, 6 or 8 hybridizing complementary bases (probes S5*, S6* or S8* respectively)

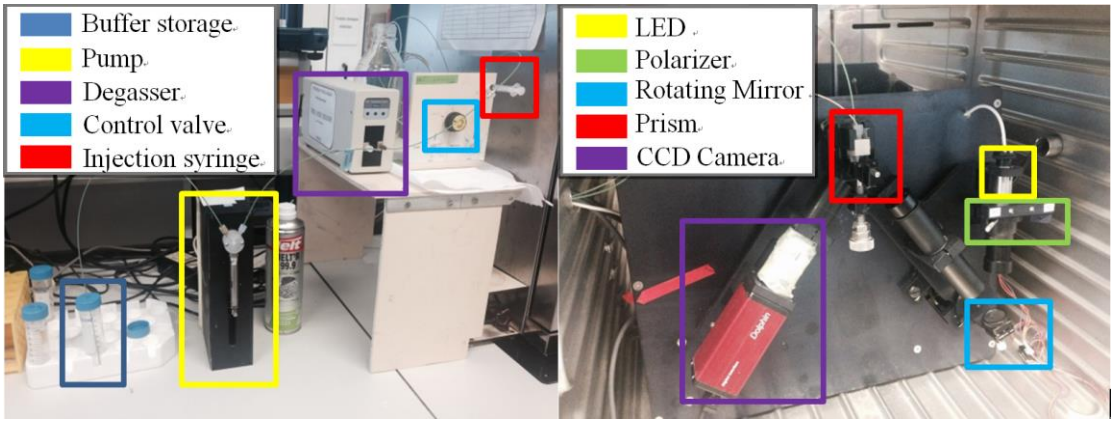

Figure 2.8 The injection system (left) and reaction chamber (right) of SPRi. The buffer was pumped into a degasser to remove the bubbles and then channeled into the injection system where the samples could be added into the buffer. The pipe then directed the buffer with the sample into the reaction chamber. The prism was in contact with a cuvette on top, the light came from beneath and was collected by the CCD camera. The switching stick on the right side controlled the polarization of the light.

The SPRi apparatus used for the experiments was the SPRi-Lab from Horiba Scientific-GenOptics (**Figure 2.8**) with incoherent light source (λ = 635 nm) as in our previous works [16,18]. The flowing solution was first pumped (syringe Cavro pump, Tecan, San Jose, CA, USA) into a degassing system from Alltech (Carquefou, Fance) and then continued into the reaction chamber which consisted in a hexagonal reactor PEEK flow cell with approximately 15 µL of volume. The temperature was set at 25 ℃ for all the experiments. Before each injection, the solution to be injected was loaded into a 1 mL injection loop. The SPR data were acquired using the software from Horiba Scientific-GenOptics. In the following, the changes in reflectivity ΔR (in %) were obtained by the average over the triplicate spot measurements on the same microarray.

The buffer used during the SPRi measurement contained 10 mM HEPES, 5 mM MgCl2 and 150 mM NaCl, the pH of the solution was adjusted to 7.4. The DNA strands to be injected were first mixed in the tube and the buffer was added along with Adenosine solution. The mixture was then heated to 90 °C for 5 mins and cooled down for 30 mins before use. The concentration of the DNA strands was fixed at 1 µM in all the experiments whereas the concentration of Adenosine varied depending on the purpose. Injection of Guanosine at 1 mM was also performed to test the selectivity. The speed of injection during the hybridization process was 0.26 µL/s, each injection lasted for 70 mins, the speed of injection during the interaction between the probes and the sample was 0.83 µL/s, and each injection lasted for 20 mins.

2.3 UV-Vis Spectroscopy

2.3.1 Introduction

Ultraviolet–visible spectroscopy (UV-Vis spectroscopy) is an absorption spectroscopy in the ultraviolet-visible spectral region. It has been used in analytical

chemistry for the quantitative determination of different analytes. Some of the ultraviolet light will pass through the solution and some will be absorbed by the analytes. The more light absorbed by the sample, the higher the concentration of analytes in the sample. The resulting effect is that less light will strike the photodetector and this will produce a higher optical density (OD). The analyte could be transition metal ions, highly conjugated organic compounds, biological macromolecules, etc. In our case, UV-Vis spectroscopy was used as a way to determine the presence of Adenosine in the solution based on a shift in the melting peak of DNA caused by the formation of Adenosine bridges, and the melting temperature of the DNA in solution was calculated from the absorbance of UV light whose wavelength was 260nm. The absorption of such UV light is named "A260" in molecular biology.

"A260" is a quantity measurement for nucleic acids. One A260 unit is the amount of nucleic acid contained in 1 mL and producing an optical density (OD) of 1. The A260 unit is different between single strand DNA (ssDNA) and double strand DNA (dsDNA). The A260 unit for ssDNA is 33 μg/ml but for dsDNA it is 50 μg/ml. This is the fundamental of melting temperature measurement based on the absorbance of UV light. Simply put, the absorbance of dsDNA in the solution is less than the two ssDNA forming the dsDNA in the same solution. By recording the absorbance during heating of the DNA solution, we can find the melting temperature at the point where the increase of absorbance is the fastest. In **Figure 2.9** we gave an example of the melting temperature measurement of an aptamer single strand. The absorbance was increasing with temperature and the peak in its first derivative was considered the melting temperature of this strand.

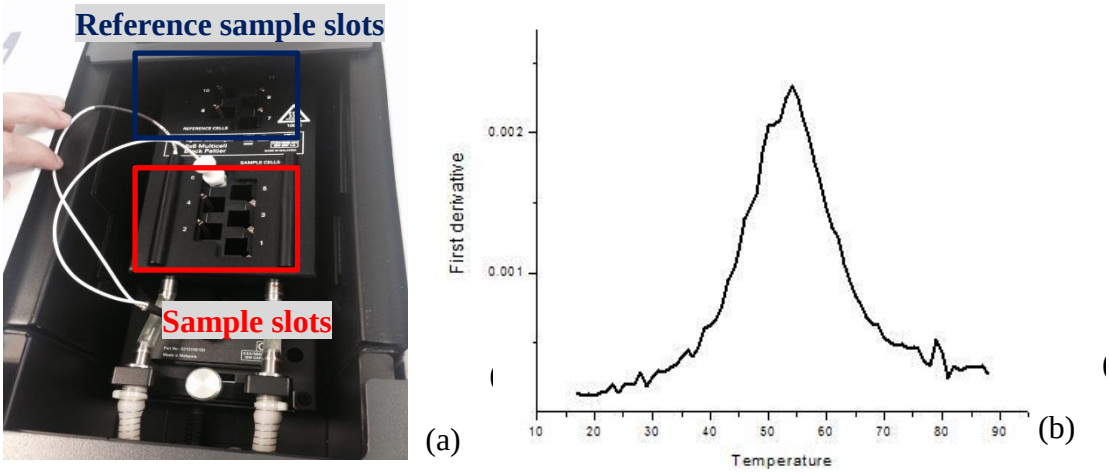

Figure 2.9 (a): The analyze chamber in which the absorbance of UV was measured, the white probe was the sensor to detect the temperature in the chamber. The cuvette containing sample solution and reference solution were placed in the sample slots and reference sample slots respectively. (b): the first derivative of the UV absorbance for an aptamer sequence, the peak of the derivative represented the melting temperature of the aptamer.

2.3.2 Experimental methods

In our work, we used Cary 100 UV-Vis Spectrophotometer (Agilent, Santa Clara, CA, USA) to perform the UV absorbance measurement. With its operating software, this machine offered the ability to measure the absorbance of light with certain wavelength in a pre-programed heating-cooling process.

1mL sample solution was placed inside a cuvette, and then the cuvette was inserted into the sample slots. The sample solution was a mixture of DNA duplex and Adenosine molecules in the same buffer we used in SPRi experiments. The concentration of DNA duplex was kept at 10 ng/μL to maintain good resolution in the absorption curve. Adenosine concentration was varied based on the purpose of the test. Guanosine molecules were used as negative control to verify the selectivity. The reference solution was placed inside a cuvette and inserted into the reference slots as well. The reference solution had the same Adenosine concentration and buffer as the corresponding sample slots, but without DNA duplexes. Before the test, the sample

was heated to 95° C for 5mins and cooled down at room temperature for at least 30mins. The cuvette in which the sample was loaded had a window on two sides to allow light come through. The top of the cuvette was sealed and placed into the chamber. The light source will generate UV light at 260nm wavelength and the light passed through the window on the cuvette. The light was collected and analyzed to provide absorption data. During the tests, a venting system was running to refresh the air inside the chamber and reduce frosting at low temperature.

The sample was kept at 15 ℃ for 10 mins before the scan, then it was heated to 80 ℃. For every 0.2 degree increase in the temperature, the absorbance of UV light was recorded after 1min wait. Once the temperature reached 80 ℃, the samples were heated to 90 ℃, whereas the data was taken for every 0.5 ℃ of increase. The temperature was then decrease to 80 ℃ for each 0.5 ℃ and continued to 15 ℃ for each 0.2 ℃. This process was repeated for 4 times. The different heating/cooling rate reduced the evaporation of samples at high temperature region and eliminated its influence on the accuracy and repeatability of the measurement.

2.4 Other supplementary characterizing methods

2.4.1 Gel electrophoresis

Introduction

Gel electrophoresis is usually used for analytical purposes. Gel electrophoresis uses the negative charge DNA carries to separate DNA strands or structures by their lengths. DNA is negatively charged due to the phosphate groups in its structure. With DNA sample loaded in the gel and voltage applied to the electrodes, DNA would migrate to the positively charged end. The gel acted as an anticonvective and sieving medium. In other words, the gel suppressed the thermal convection caused by the electric field and retarded the movement of the molecules. [20] The migration rate was

different according to the mass of the DNA, thus separating the structures with different length. Agarose gel and polyacrylamide gel are the two kinds of gels commonly used. Polyacrylamide gel is more suitable for smaller DNA fragments (5-500bp) due to its high resolving power. On the other hand, agarose gel has lower power for DNA but has greater range of separation, thus is more suitable for DNA fragments that are longer (50-20000bp). [21] Based on the size of our DNA structures, we chose to use 10% polyacrylamide gel and 2% agarose gel.

In our work we tried to use it to prove the presence of DNA structures in the solution. Both agarose gel and polyacrylamide gel was tested because the length of the dimer was within the range of both gels. The gel was vertically positioned for polyacrylamide whereas the gel was horizontally positioned for agarose. This difference was due to the fact that the polymerization of polyacrylamide gel required isolation from oxygen. This requirement can only be fulfilled by a vertical sandwich space between two plates. An open horizontal mold can be used for agarose gel system.

Experimental methods

The experiments were carried out on a home-assembled system which contained a plastic slot for positioning the gel. The vertical mold and horizontal mold for polyacrylamide gel and agarose gel was shown in **Figure 2.10**. To prepare 100 mL Polyacrylamide gel, 50 mL of 40% acrylamide solution (5% crosslinker), 10mL 10X TBE buffer and 700 μL ammonium persulfate (APS). After the solution was fully mixed, 70 μL Tetramethylethylenediamine (TEMED) was added to increase the rate of polymerization. The solution was quickly mixed again in 5 seconds and poured into the mold, and then waited 20 mins to finish the polymerization. Agarose gel was prepared by dissolving 1g agarose powder into 50mL TBE buffer and heat until bubbles started to appear in the solution. The solution was then poured into the mold to form the gel during the cooling process.

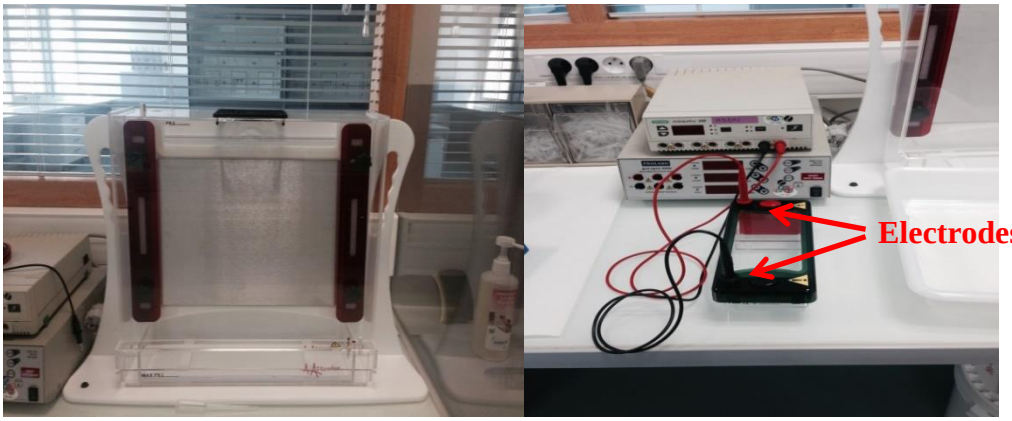

Figure 2.10 The apparatus for polyacrylamide and agarose gel electrophoresis. The mold in which the gel was polymerized and stabilized was vertical for polyacrylamide gel (left) and horizontal for agarose gel (right). The electrodes in the apparatus could be connected to power supplier to apply electoral potential to the electrodes as shown in the figure.

The mold created wells in the gel where the samples could be injected. The sample solution was a 15μL mixture of GelRed nucleic acid gel stain, GelRed prestain loading buffer and DNA strands in SPR buffer. 4μL of GelRed prestain loading buffer (Biotium, USA) was first mixed with 1pmol DNA strands and 1.5μL 10X SPR buffer then diluted to 14μL solution. 1μL of 10X GelRed nucleic acid gel stain was added in the end and the solution was kept in dark containers to avoid exposure of light. The loading buffer had two DNA bands served as the baselines to estimate the position of the sample. Once the gel was prepared and loaded with sample solution, the mold was immersed into TBE buffer and a voltage was applied to the electrodes. Polyacrylamide gel was stabilized under low power (110V, 30mA, 3W) for at least one hour. The power was provided by Biorad PowerPac 300 Electrophoresis Power Supply (Bio-Rad, CA, USA). The stabilization process was not necessary for agarose gel. During the migration, the power was increased (280V, 25mA, 6W). After about 30mins of migration, the gel was collected and put into Molecular Imager Gel Doc XR+ (Bio-Rad, CA, USA) to scan for imaging.

2.4.2 Fluorescence spectroscopy

Fluorescence spectroscopy is an electromagnetic spectroscopy that analyzes fluorescence from the sample. Fluorescent dyes are mixed or functionalized on the sample. A light source generates light, usually UV light, that can excite electrons in molecules of fluorophore and emit light at certain wavelength. As the fluorophore releases a photon, it descends to its ground state. An absorption spectroscopy is combined to help determine the intensity of the emitted light. Compared to other DNA label techniques such as silver staining, radioisotopes and intercalating dye, fluorescent label has multiple choices in the emission wavelength which allowed multiplexing analyze. The materials and methods also have easier access and lower cost, thus fluorescent labeling has become the most popular label chose for DNA analyze.

In order to study the forming and breaking of the binding in the proposed DNA structure, the melting profile of the sample solution was measured and analyzed. The melting curve was based on the quantification of DNA duplex in the solution with a timeline. The amount of DNA duplex was decreased when thermal denaturation happened due to the increase of temperature. The dye/DNA complex was dissociated and fluorescent dye was released into the solution. This change was noticeable by recording the emission of fluorescent signal. The peak in the first derivative of the fluorescent intensity plot indicated the melting temperature of the duplex.

In our search for methods to prove the existence of 1D DNA chain in solution, we tried fluorescence spectroscopy using SYBR Green dye as label. Two different apparatuses were used, a Step-one real time PCR system and a Fluoromax 4 spectrofluorometer. The PCR system was able to record the emission of fluorescent signal during the heating process with fine resolution. On the other hand, the spectrofluorometer could record the emission in both the heating and cooling process. The apparatuses measured the emission of light whose wavelength was 525 nm.

Experimental methods

The protocol of fluorescence spectroscopy using Step-one real time PCR system (Applied Biosystems) is as follow: 20 μL sample solution (0.32 μM DNA mixed with fluorescent buffer) was placed in the PCR system, the solution was first stabilized at 25 ℃ and heated to 95 ℃, the heating rate was 0.3 ℃ /min. After 5 mins, the sample solution was cooled down to 25 ℃ and stabilized for 5mins. Afterwards, the sample was heated again to 95 ℃ at the same heating rate, during which the data was collected to measure the melting curve.

The protocol of fluorescence spectroscopy using Fluoromax 4 spectrofluorometer (Horiba scientific) is as follows: A calibration for each sample was first made to determine the preferable DNA concentration. Based on the strand this value could vary from 1 nM to 10 nM. Then 100 μL of the DNA strands in fluorescent spectroscopy buffer (see Appendix) was injected into a cuvette same as the UV spectroscopy, the cuvette was placed in the spectrofluorometer. The heating-cooling procedure was the same as spectroscopy with PCR system, however the data was collected throughout the whole heating-cooling process.

Reference

1. Huizenga DE, Szostak JW. A DNA aptamer that binds adenosine and ATP. ***Biochemistry***. 1995;34(2):656-665. doi:10.1021/bi00002a033.
2. Sato A, Terata K, Miura H, et al. Mechanism of vasodilation to adenosine in coronary arterioles from patients with heart disease. ***Am J Physiol Heart Circ Physiol***. 2005;288:H1633-H1640. doi:10.1152/ajpheart.00575.2004.
3. Strametz JK, Matulla B, Wolzt M, et al. Role of nitric oxide in adenosine-induced vasodilation in humans. ***Life Sci***. 1998;62(11):1035-1042. doi:10.1161/01.HYP.31.5.1061.
4. Morgan JM, McCormack DG, Griffiths MJ, Morgan CJ, Barnes PJ, Evans TW. Adenosine as a vasodilator in primary pulmonary hypertension. ***Circulation***. 1991;84(3):1145-1149. doi:10.1161/01.CIR.84.3.1145.
5. Betzel C, Saenger W, Hingerty BE, Brown GM. Topography of cyclodextrin inclusion complexes, part 20. Circular and flip-flop hydrogen bonding in .beta.-cyclodextrin undecahydrate: a neutron diffraction study. ***J Am Chem Soc***. 1984;106(24):7545. doi:10.1021/ja00336a039.
6. Sen D, Gilbert W. Novel DNA superstructures formed by telomere-like oligomers. ***Biochemistry***. 1992;31(1990):65-70. doi:10.1021/bi00116a011.
7. The Mfold Web Server. mfold.rit.albany.edu. http://unafold.rna.albany.edu/?q=mfold. Accessed June 15, 2017.
8. Goodman RP, Berry RM, Turberfield AJ. The single-step synthesis of a DNA tetrahedron. ***Chem Commun (Camb)***. 2004;44(April):1372-1373. doi:10.1039/b402293a.
9. Love JC, Estroff LA, Kriebel JK, Nuzzo RG, Whitesides GM. Self-assembled monolayers of thiolates on metals as a form of nanotechnology. ***Chem Rev***. 2005;105(4):1103-1169. doi:10.1021/cr0300789.
10. Christopher Love J, Wolfe DB, Haasch R, et al. Formation and structure of self-assembled monolayers of alkanethiolates on palladium. ***J Am Chem Soc***. 2003;125(9):2597-2609. doi:10.1021/ja028692+.
11. Vos, Johannes G., Robert J. Forster, and Tia E. Keyes. ***Interfacial supramolecular assemblies***. John Wiley & Sons, 2003..
12. Morrill PR, Millington RB, Lowe CR. Imaging surface plasmon resonance system for screening affinity ligands. ***J Chromatogr B Anal Technol Biomed Life Sci***. 2003;793(2):229-251. doi:10.1016/S1570-0232(03)00282-4.
13. Grigorenko A., Beloglazov A., Nikitin P., Kuhne C, Steiner G, Salzer R. Dark-field surface plasmon resonance microscopy. ***Opt Commun***. 2000;174(January):151-155. doi:10.1016/S0030-4018(99)00676-8.

14. Nikitin PI, Grigorenko AN, Beloglazov AA, et al. Surface plasmon resonance interferometry for micro-array biosensing. ***Sensors Actuator****s, A Phys*. 2000;85(1):189-193. doi:10.1016/S0924-4247(00)00386-1.

15. Steiner G, Sablinskas V, Savchuk O, et al. Characterization of self assembly layers of octadecanephosphonic acid by polarisation modulation FT-IRRA spectroscopy mapping. ***J Mol Struct***. 2003;661-662(1-3):429-435. doi:10.1016/j.molstruc.2003.08.031.

16. Melaine F, Roupioz Y, Buhot A. Gold Nanoparticles Surface Plasmon Resonance Enhanced Signal for the Detection of Small Molecules on Split-Aptamer Microarrays (Small Molecules Detection from Split-Aptamers). ***Microarrays***. 2015;4:41-52. doi:10.3390/microarrays4010041.

17. Yang C, Spinelli N, Perrier S, Defrancq E, Peyrin E. Macrocyclic Host-Dye Reporter for Sensitive Sandwich-Type Fluorescent Aptamer Sensor. ***Anal Chem***. 2015;87(6):3139-3143. doi:10.1021/acs.analchem.5b00341.

18. Melaine F, Coilhac C, Roupioz Y, Buhot A. A nanoparticle-based thermo-dynamic aptasensor for small molecule detection. ***Nanoscale***. 2016;8(38):16947-16954. doi:10.1039/C6NR04868D.

19. Chen Y, Xu J, Su J, Xiang Y, Yuan R, Chai Y. In situ hybridization chain reaction amplification for universal and highly sensitive electrochemiluminescent detection of DNA. ***Anal Chem***. 2012;84(18):7750-7755. doi:10.1021/ac3012285.

20. Berg J M TJL. ***Stryer: Biochemistry***. WH Freeman and Company; 2002.

21. Sambrook J, Fritsch EF, Maniatis T. *Molecular Cloning: A Laboratory Manual. Cold Spring Harbor Laboratory Press*.; 1989. doi:574.873224 1/1989.

Chapter 3 Detection of Adenosine with 1D DNA structure and SPRi

Dans ce chapitre, nous avons présenté une méthode de détection hétérogène de l'adénosine basée sur la technique de SPRi et la structure d'ADN 1D présentée au chapitre 2. Cette méthode de détection a permis une détection sans marquage de l'adénosine en temps réel. En outre, la masse de la chaîne 1D a été utilisée pour améliorer le signal obtenu par SPRi au lieu d'immobiliser les éléments de reconnaissance sur les nanoparticules d'or. Les avantages d'une telle conception sont une préparation simplifiée de détection et un coût moindre. Le prisme en or a été fonctionnalisé avec des sondes oligonucléotidiques pour former des monocouches auto-assemblées (SAM), la densité de ces sondes a été contrôlée avec précision en diluant la solution de greffage avec un contrôle négatif. La densité de greffage des sondes s'est avérée avoir un impact important sur le signal obtenu et la longueur de la chaîne ADN 1D formée sur les sondes. Trois modèles de séquence différents ont été utilisés pour cette application. Deux d'entre eux (S5 et S6) ont été efficaces pour la détection et le troisième (S8) a été utilisée comme preuve de concept. Le protocole de détection a été optimisé pour les dimères S5 et S6 afin d'obtenir le meilleur signal. Ces deux dimères ont montré des propriétés spécifiques dans la détection, le signal le plus fort a été obtenu en utilisant des dimères S6 et la meilleure limite de détection a été atteinte avec des dimères S5 à 10 µM.

3.1 Introduction

Surface Plasmon Resonance imaging (SPRi) was widely used in the detection of macromolecules because it is highly sensitive to the change of refraction index caused by the binding of the macromolecules on the gold surface. [1–4] However, in the domain of small molecule detection conventional SPRi lacks the ability to provide measureable signal since the mass of small molecules is not sufficient to create good signal. Therefore indirect measurements were commonly taken to amplify the change of refraction index. [5–9] Gold nanoparticles (Au NPs) were widely used in SPR experiments as a way to enhance the signal for two reasons: the mass effect brought by the heavy mass of Au NPs and the coupling effect between the localized surface plasmon of the particles and the surface plasmon of the gold prism.[10–12] Wang and Zhou reported a detection method using Au NPs to amplify the SPR signal for detection of adenosine.[13] The scheme of their sensor was shown in **Figure 3.1**. The anti-Adenosine aptamer was adsorbed on the gold surface by gold-sulfur affinity. Au NPs were functionalized with the complementary ssDNA of the aptamer and would create a huge signal while in contact with the aptamer probes on the surface. However, if the surface was first immersed in the sample solution which contained Adenosine molecules, the probes on the surface would fold with Adenosine and were no longer able to hybridize with the ssDNA on the Au NPs. As a result, a decrease in the shift of SPR angle was observed and used for detection of Adenosine.

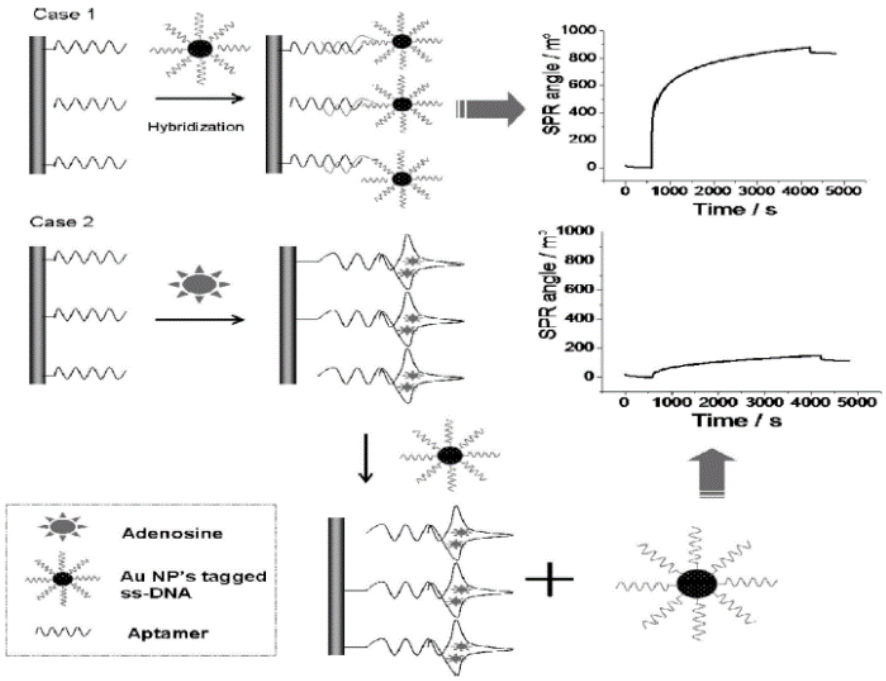

Figure 3.1 The detection principle of a sensor for Adenosine. The surface was functionalized with aptamer probes, the scenario with and without Adenosine was compared in Case 1 and 2. In Case 1, without the presence of Adenosine, the Au NPs functionalized tagged with ssDNA can hybridize onto the aptamer probes. Whereas in Case 2 the probes were folded due to the presence of Adenosine, which prevented the hybridization between the ssDNA on the Au NPs and the aptamer probes and as a result a difference in the signal could be noticed for detection. [13]

Here we give two detection methods reported during the three-year project to present the cutting edge detection methods and the latest trend in SPR signal amplification. In 2015 Qiu's group combined both amplification approaches of using Au NPs conjugation and DNA strand displacement cycle.[14] The detection process was shown in **Figure 3.2**. An aptamer was partially hybridized with a short oligonucleotide c-DNA1, the presence of Adenosine would break this binding so that the aptamer will fold with Adenosine and release the c-DNA1 into the solution. Another DNA strand H-DNA1 was functionalized on the surface of Au NPs and their purple parts were self-hybridized. The release of c-DNA1 caused by the Adenosine will break the self-hybridization of H-DNA1. Only in this state, the H-DNA1 can interact with the H-DNA2 functionalized on the gold prism for SPR test. In conclusion, the detection of Adenosine was realized through a series of changes in the DNA structures both in solution and on gold surface. As the result, a change in the SPR angle was observed only with Adenosine molecules in the solution to trigger the

series of interactions. They managed to get a sensor that has a LOD of 0.21pM, which is about 3 orders of magnitude enhanced compared to other amplification approaches. Even though the combination of aptamers on Au NPs has been the key element in increasing the signal for SPR experiments, its high cost and difficult manufacture were still inconvenient. Among the possible replacement of Au NPs, DNA structure was an outstanding candidate that requires no label and no involvement of enzymes. In 2017 Ding et al reported a DNA detection method based on nonlinear hybridize chain reaction (HCR) amplification, which could also be used for detection of Adenosine. [15] The detection started with capture probes functionalized on gold prism. Similar as the previous example, the aptamer was partially hybridized with a short oligonucleotide which will be released in presence of Adenosine. The released short oligonucleotide triggered the HCR and a network of DNA formed after several cycles. This network of DNA was huge in size and mass, thus led to a significant change in the SPR angle.

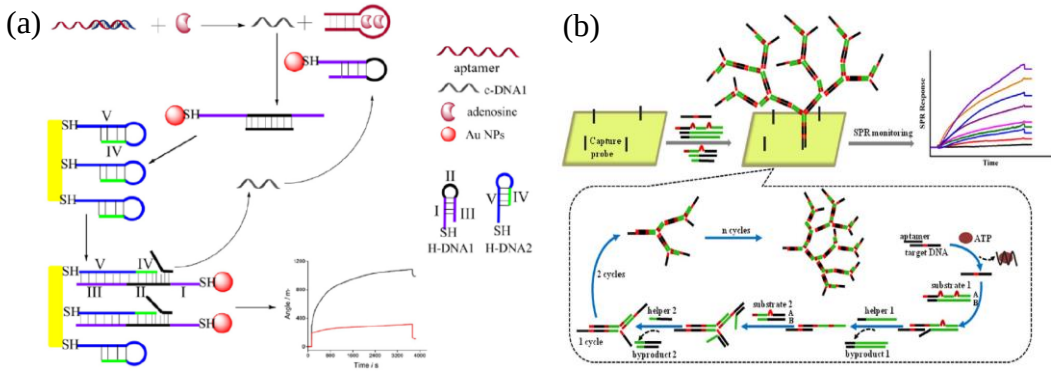

Figure 3.2 Two detection methods for Adenosine. (a) The method reported by Qiu et al, the detection system consisted of aptamer, detection probe (c-DNA1) partially hybridizing to the aptamer strand, Au NPs-linked hairpin DNA (Au-H-DNA1), and thiolated hairpin DNA (H-DNA2) previously immobilized on SPR gold chip. (b) The method reported by Ding et al, the one terminal of target DNA hybridized with specifically designed capture DNA on the sensing chip, and the other terminal triggers the non linear HCR. The HCR could only start when the short strand hybridized with the aptamer was released due the presence of Adenosine. [14,15]

In these examples either Au NPs or self-assembling strategies like the use of hybridization chain reaction was used as an amplification method to achieve higher SPR signal. The shortcoming of traditional signal amplification methods using Au NPs was the preparation for the experiments, including the money and time needed to

produce, purify and functionalize the Au NPs. Self-assembling strategies to amplify the SPR signal by building large scale DNA structures on the gold surface is one promising new approach. In this work we searched for a way that requires no involvement of Au NPs and simplified the sequence engineering as much as possible. In our earlier work we functionalized split-aptamers on the surface of Au NPs which interacted with the probes on gold prism and realized the detection of Adenosine molecules.[10] The working principle of this sensor was displayed in **Figure 3.3**. An anti-Adenosine aptamer was splited into two halves and functionalized respectively on the Au NPs and on the gold prism. The split-aptamers immobilized on the gold prism formed the microarray used for detection of Adenosine. The Au NPs did not interact with the probes on the surface without the presence of Adenosine. When there was Adenosine in the solution the split-aptamer on the Au NPs formed the Adenosine bridge with the split-aptamer on the prism and created a signal. To further explore the potential of this detecting method, we developed an approach based on the self-assembling of oligonucleotide dimers with split-aptamer dangling ends forming linear chains in presence of the adenosine target in order to avoid the complex synthesis and functionalization of Au NPs. The formation of linear chains on the biosensor surface served as an amplification strategy. As a result, this detection method had good selectivity and a detection limit of 10 μM. We also discovered an important role played by the grafting density of the probes during the detection not only in the strength of signal but also in the formation of the 1D chain.

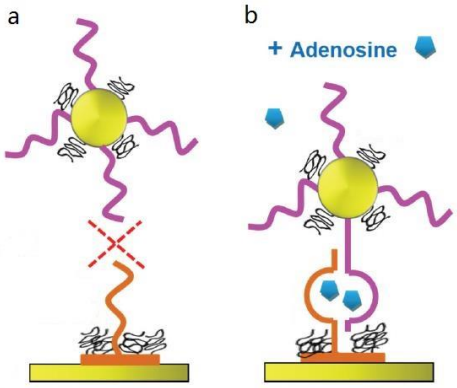

Figure 3.3 The detection principle of the SPR sensor in our previous work. [10] (a): The Au NPs functionalized with split-aptamer did not interact with the corresponding split-aptamer probes on the gold prism. (b): with the presence of Adenosine in the solution, the split-aptamers formed the Adenosine bridge which captured the Au NPs to the surface and created SPR signal.

3.2 Sequence design and characterization

3.2.1 Sequence design of 1D chain structure

The concept of the 1D chain structure has been explained in the introduction. To finalize the sequence engineering, it is vital to rule out the secondary structures. As discussed in Chapter 2, we used online simulation tool "Mfold" to calculate the theoretical melting temperature of the duplex and check its stability. In our design the sequence consisted of two parts, the oligonucleotide zip and the split-aptamer. In earlier work [10,11,16], we have splited the aptamer reported by Huizenga and Szostak [17] and functionalized the split-aptamer on gold surface. Modifications of the base pairs next to the Adenosine bridges were made to alter the strength of binding. Three kinds of split-aptamers were chosen for this project, the S5, S6 and S8 split aptamer. The sequences started with split-aptamer on the 5' and followed by the oligonucleotide zip. In **Table 3.1** we showed "two-state folding" simulation that gave the melting temperature of the structure formed with self-folding of one single strand, and the "two-state melting" simulation that gave the melting temperature of the most stable structure among the possible structures formed by the two strands. The conditions used in these simulations were the same as the SPR buffer we used in the experiments and the temperature was set at room temperature (25 ℃), the strand concentration was set to be 1 μM.

In the simulation results the melting temperatures obtained from two-state folding were all lower than the melting temperatures obtained from two-state melting. This means while the solution was heated to 90 ℃ for denaturation of the duplexes, the duplex will form prior to the self-folding structures during the cooling process. In other words, no secondary structures will interfere with the formation of the 1D DNA chains we desired. Thus we have the sequence finalized for the SPRi experiments. The details near the Adenosine bridge was displayed in **Figure 3.4** for better understanding.

Strand	Two-state folding(°C)	Two-state melting(°C)
S5Z	47.5	74.7
S5*Zc	52.4	
S6Z	43.8	72.0
S6*Zc	52.4	
S8Z	47.5	72.0
S8*Zc	52.4	

Table 3.1 The melting temperature calculated with online tools for the dimers and monomers used for SPRi tests. The simulation result of two-state folding corresponded to the melting temperature of the self-folded structure of the ssDNA. The simulation result of two-state melting corresponded to the melting temperature of the dimers formed by the hybridization of two strands.

Figure 3.4 The DNA scheme near the Adenosine bridge for S5, S6 and S8 dimers. The red bases are part of the oligonucleotide zip, the yellow bases were those not hybridized and the blue bases are the split-aptamer. In the split-aptamer the hybridized bases came in darker blue while the binding pockets were marked light blue.

S5 dimer was the first attempt for this 1D model among the three duplexes. Its design was based on the sequence we used in our earlier study that use Au NPs functionalized with split-aptamer for the detection of Adenosine.[10] On one side of the Adenosine bridge there was a G-T base pair that was not hybridized with each other, which was vital to the formation of Adenosine bridge [17]. On the other side of the Adenosine bridge, there was five hybridized base pairs followed by three non-complementary base pairs. In our previous work we proposed four different sets of

split-aptamers (APT4, APT5, APT6 and APT8), the three non-complementary base pairs were added to make sure the four sets of split-aptamers had the same length. [10] The S5 dimers were successfully formed in the solution and the detection with SPRi showed the curve we expected. But the lack in the binding strength near the Adenosine bridges was limiting the signal of SPR. Based on the feedback from these first experiments with S5 dimer, we decided to design another sequence with stronger bindings. In S6 dimer, the number of base pairs hybridized next to the Adenosine bridges increased to 6. Moreover, the three non-complementary base pairs were removed and two "CC" bases, which was part of the oligonucleotide zip on the 3' end of the sequence was moved to the 5' of the sequence. This modification was shown in **Figure 3.4**, the number of hybridized base pairs in the oligonucleotide zip remained the same and only the position in which the chain was disconnected has changed. As a result, there were five base-pairs (four hybridized) on one side of the Adenosine bridges and six base-pairs on the other side. Compared to S5 dimer, this provided a structure with more balanced binding on both sides of the Adenosine bridges. The S8 dimer had the same modification as S6 dimer, and the number of base pair hybridized was further increased to 8. This sequence was purchased as a proof of concept, since in past experience we already noticed that due to the strong binding the 1D chain tend to form even without the presence of Adenosine. Another duplex was also used as positive control during the project to help prove of concept. The fully complementary S6 dimer (S6c) was designed. Instead of S6* on the 5' of the S6*Zc sequence the fully complementary sequence of the split-aptamer was used. The sequence of this S6cZc sequence was also shown in the Appendix.

3.2.2 Characterization of the 1D chain structure

The 1D DNA chain we described should form successfully based on theoretical calculation and simulation, but yet its existence in the solution needs to be proven by analytical methods with a direct view. During the search for such method, we first tried to directly separate the 1D chain with different length with gel electrophoresis and characterize with the fluorescent dye in the gel. We also tried to measure the melting profile of the solution containing the 1D DNA chain and compare the difference with and without Adenosine to suggest a change in the structure and prove

the formation of 1D chain indirectly. We tried to measure the melting profile with both fluorescent spectroscopy and UV-Vis spectroscopy. Here we discuss the results obtained from the three methods, some of them was not successful result but still helped to achieve better understanding of the 1D DNA chain.

Gel electrophoresis results

Gel electrophoresis can separate DNA structures with different lengths. Since we were expecting 1D DNA chains connected with various number of Adenosine bridges which result in DNA structures with a variety of different lengths, we hoped to find multiple bands as evidence that the 1D DNA chain structure was formed successfully. However, the challenge lies in maintaining the DNA chain structures while they are migrating through the electrophoresis gels. The hydrogen bonding holding the G-quartets in the Adenosine bridges was weaker than the Watson-Crick interactions (C-G or A-T). We added 1mM Adenosine in the gel solution during its preparation, so that the gel would contain sufficient Adenosine. Same amount of Adenosine was also added to the TBE buffer in which the gel was immersed.

Line 1 and 2 in **Figure 3.5** corresponding to the duplex with Adenosine only showed one band in the gel. Judging from the DNA ladder, the size of the structure was around 40bp, which suggested that only 1 duplex was in the solution and they were not connected by the Adenosine bridges. Despite the Adenosine molecules we added into the system, the environment in the gel was different than the solution, thus the Adenosine bridges could not be protected during the migration in the gel. Another reason that may cause the failure was the competition between the fluorescent label and Adenosine molecules in the space between the two split-aptamers. In Line 3 and 4 we gave the agarose gel electrophoresis of the positive control: a fully complementary duplex formed by S6cZc and S6Z ssDNA. The 1D chain formed by these dimers was connected through only one binding mechanism, which was the hybridization of DNA. There were multiple bands observed in the gel representing 1D DNA chain structures with different lengths. If the Adenosine bridges were successfully preserved during the migration, its pattern should be similar to the results of the positive control.

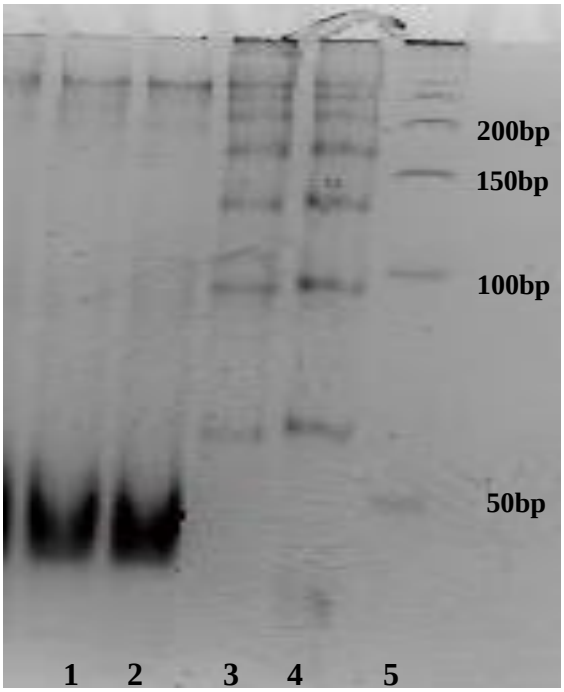

Figure 3.5 The agarose gel electrophoresis of S6 dimers and fully complementary S6 dimers (S6Z+S6cZc). The wells on top of the gel contained 10 pmol of DNA in 15 μL sample before the migration started. Line 1 and 2 were the S6 dimers solutions with 100μM Adenosine, Line 3 and 4 were the fully complementary S6 dimers and Line 5 was the DNA ladder to estimate the scale of the structure. The DNA ladder contained DNA structure whose size was measured and verified. The first band corresponded to DNA structure composited of 50 base pairs (bp) and the difference between each band was 50 bp.

Melting temperature measurements

Fluorescent spectroscopy was also used to analyze the DNA structures existing in the solution. SYBR Green was a fluorescent dye known to interact not only with DNA duplexes but also with ssDNA and G-quadruplex, even though the affinity was lower.[18–20] By recoding the emission of the fluorescent signal during the heating and cooling process, the melting profile of the DNA structures could be determined. We expected two melting peaks to prove the existence of the 1D DNA chain. Based on the simulation result, the first peak we expected corresponding to the hybridized oligonucleotide zip at around 75 ℃. The second peak we expected was a melting peak of the Adenosine bridge formed by the split-aptamers. Because this binding was due to aptamer-target interaction but not hybridization of ssDNA, the approximate value of its melting temperature could not be calculated by the software. We expected the peak to be at a temperature lower than 75 ℃ because the split-aptamer is shorter in length compared to the oligonucleotide zip and its binding is weaker than the

hybridization of DNA. However, the result of the fluorescent spectroscopy showed only one melting temperature at 76 ℃, the melting temperature expected for the dissociation of the Adenosine bridges was not discovered.

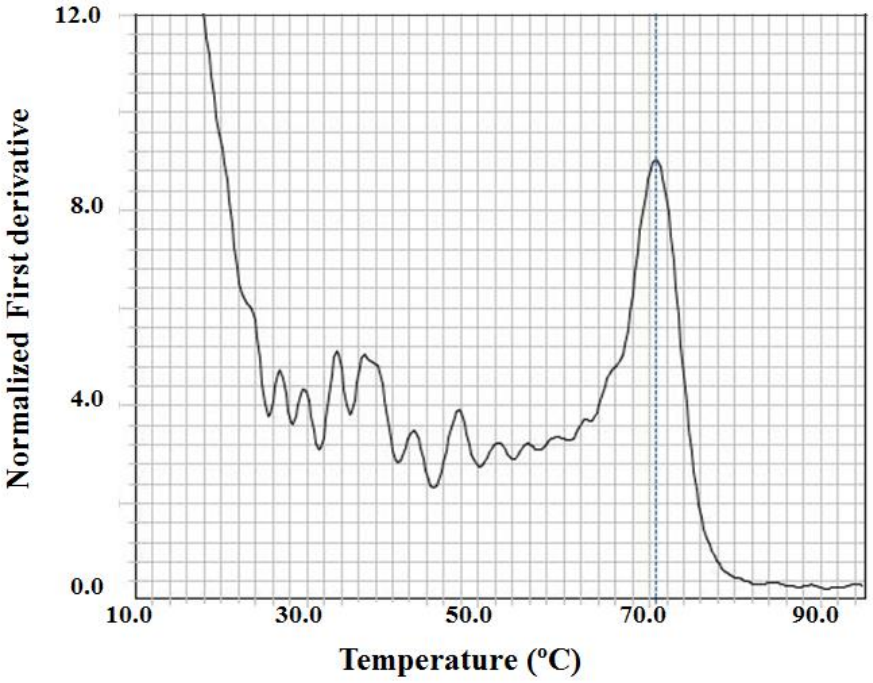

Figure 3.6 The normalized first derivative of the fluorescent signal obtained from fluorescent spectroscopy using step-one real time PCR system. The 20 μL sample was prepared by mixing 0.32 μM DNA (S6Z+S6*Zc) in fluorescent buffer with 100 μM Adenosine. Only one clear peak was observed at 72 ℃ which corresponded to the melting temperature of the oligonucleotide zip.

The reason why we observed only one melting temperature was the competition between the fluorescent dye and the Adenosine molecules in the space between two split-aptamer dangling ends. This competition was reported in a study of fluorescence anisotropy probe for DNA-based bioassays.[21] In **Figure 3.7** the SYBR Green fluorescent dye were attached to the anti-Adenosine aptamer. The dye was released when Adenosine molecules were interacting with the aptamer to form the Adenosine bridge. To obtain an accurate melting curve the release of the fluorescent dye need to have one exclusive reason: the dissociation of the dsDNA. But in our case SYBR Green dye can be released due to both the dissociation of the dsDNA and the formation of Adenosine bridge. As a result the measurement of melting profile with fluorescent dye was not reliable.

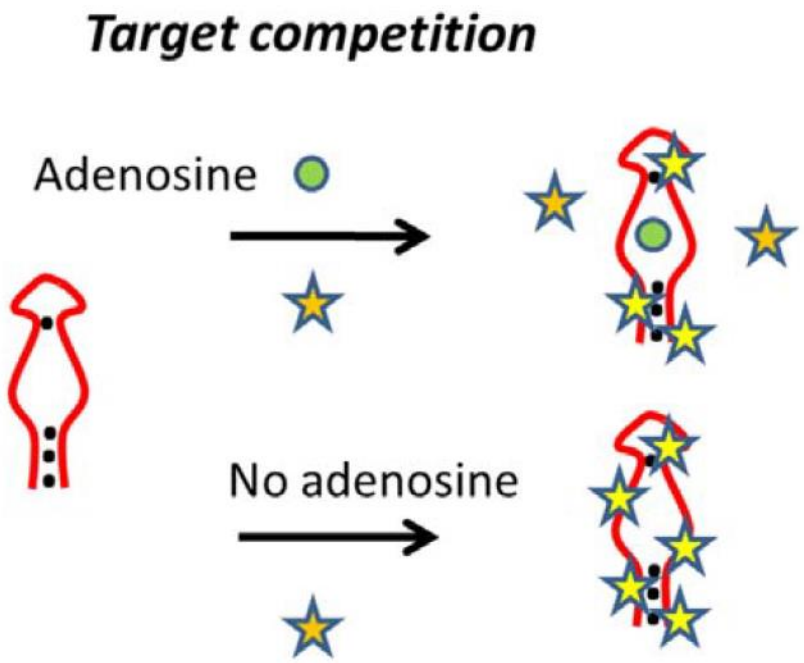

Figure 3.7 The competition between the Adenosine and fluorescent dye at the bindng pocket of full anti-Adenosine aptamer. When without Adenosine the fluorescent dye binded to the aptamer. When Adenosine was presented in the solution, the Adenosine molecules competed with the fluorescent dye and the dye was released. [21]

UV-Vis spectroscopy can also be used to measure the melting profile of the solution, the principle was similar to fluorescent spectroscopy. The absorbance of UV light at 260 nm wavelength for single strand DNA and double strand DNA were different. The A260 for ssDNA is 33 μg/ml whereas for dsDNA the A260 is 50 μg/ml. This means when the dsDNA is dissociated the absorbance of UV light increased by a factor of 1.32 (66/50). Unlike fluorescent spectroscopy, no fluorescent label is required for this measurement and we successfully obtained the melting profile of the S5 duplex in the figure below. Only one peak was observed for the sample without Adenosine (black curve) at 77℃, which is the melting temperature of the oligonucleotide zip. With the presence of Adenosine (red curve), a second peak was observed for the dissociation of Adenosine bridges at 25℃. This was an evidence that the 1D chain was successfully formed in the solution. Moreover, we further developed this method and turned it into another detecting technique for Adenosine, the details will be discussed in Chapter 4.

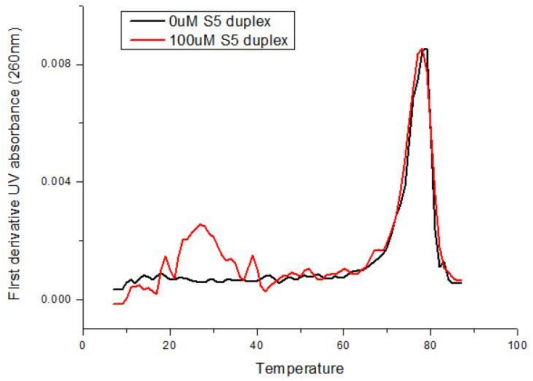

Figure 3.8 The melting curve of S5 duplex with and without Adenosine. The concentration of the duplex was 0.9 μM. The peak corresponding to the oligonucleotide had the same melting temperature in both cases, a new melting peak was observed with the presence of 100 μM of Adenosine. This new peak suggested the formation of the 1D chain was successful.

3.3 SPRi results on 1D DNA structure

3.3.1 SPR detection of adenosine

The interactions on the functionalized DNA probes were shown in **Figure. 3.9**. In Step 1, the stabilization of the microarray with zipper probes Z (red probes on the gold surface) was obtained by a running buffer injection. This initial microarray allowed us to further implement the different engineered sequences of split-aptamers to obtain functional microarrays and to optimize the number of adenosine bridges. In Step 2, the injection of monomer strands SX*Zc (complementary zipper Zc (red) and split-aptamer SX* (blue) sequences) allowed for the hybridization between the Z probes on the prism and oligonucleotide zip Zc in the monomer. As a result, split-aptamer dangling ends on the microarrays at various grafting densities were created (the method to control the grafting densities has been explained in Chapter 2). In order to fully hybridize all the probes on the prism, this step required 2-3 injections of the same monomer solution. In Step 3, the functional microarray with split-aptamer probes was stabilized upon injection of the running buffer. Step 4 corresponded to the detection step with the injection of dimers presenting two split-aptamer dangling ends to form linear chains on the microarray due to bridges triggered by the presence of Adenosine in the injection solution. In Step 5, the injection of the running buffer

destabilized the adenosine bridges and could regenerate the functional microarray for a subsequent dimer injection and Adenosine detection. The regeneration of the microarray was different according to the dimer duplex injected. A complete regeneration of the microarray (back to Step 1) is also possible upon injection of 50mM NaOH solution to dissociate any hybridized strands on the microarray.

The SPRi signal of spots with various grafting concentrations obtained during these 6 steps was also displayed in **Figure 3.9**. The signal was stabilized in Step 1 and increased due to the increased mass on the surface followed by the hybridization of S6 monomers on the initial Z probes. After the spots were fully saturated, the surface was stabilized by buffer flow and no significant change in the signal took place in this step. In the next step, 1μM of S6 dimer with 1mM Adenosine were injected. We expect some 1D DNA chain already formed in the solution and could bind to the probes on the surface with the formation of a new Adenosine bridge. The 1D chain formed on the probes and led to a second increase in the SPRi signal. When the injection was finished the running buffer flushed the Adenosine away and broke the connection between the dangling split-aptamer and the dimers. The signal decreased during this step. Unlike S5 dimers which can regenerate the probes in 30 mins simply through the flowing buffer. The regeneration of the probes connected to S6 1D chain took hours to finish. Thus an injection of 50mM NaOH was made in Step 6 to completely regenerate the probes. The signal dropped rapidly after the injection and can be stabilized back to the level in Step 1 with injection of the SPR buffer.

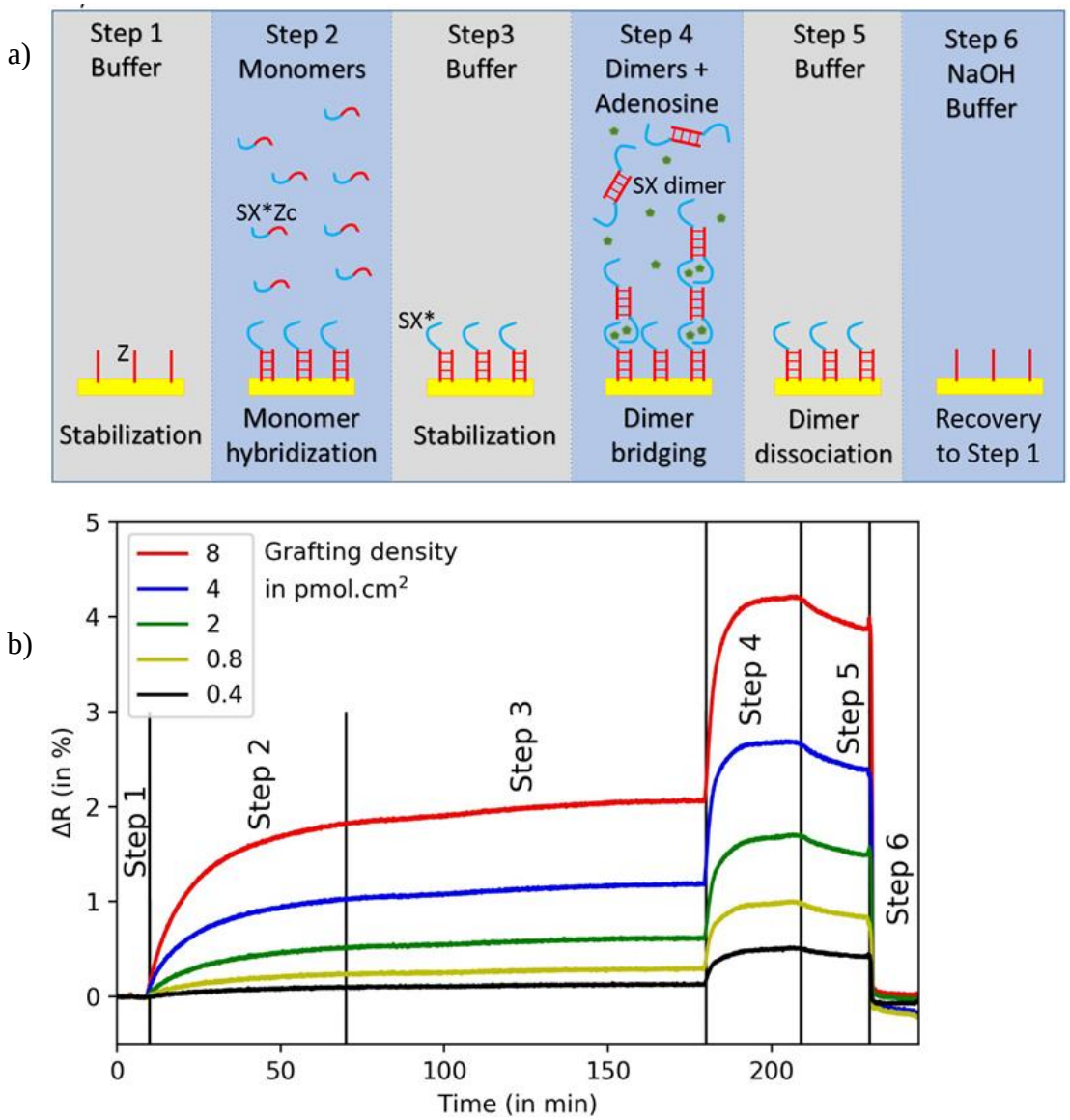

Figure 3.9 Various injection steps considered for the detection of adenosine and the determination of the number of dimer bridges. (a) Schematic representation of the various steps and (b) Corresponding SPR signal. Step 1: Stabilization of the universal initial microarray with zipper probes (red) by a running buffer injection. Step 2: Injection of 1µM monomer strands with complementary zipper (red) and split-aptamer (blue) sequences for hybridization and fabrication of functional microarray. Step 3: Stabilization of the functional microarray with split-aptamer probes under buffer injection. Step 4: Injection of 1µM dimers with two split-aptamer dangling ends to form linear chains on the microarrays due to Adenosine bridges. Step 5: Injection of running buffer removed the Adenosine bridges and could regenerated the functional microarray for a subsequent dimer injection and Adenosine detection. Step 6: Injection of 50mM NaOH buffer removed the hybridized DNA strands to recover the initial microarray (Step 1).

3.3.2 The SPRi result and key parameters

The reproducibility of the hybridization process

The grafting density of the probes had a non-linear relationship with the concentration of the grafting solution. But the grafting density can be controlled by diluting the grafting solution with negative control. By mixing zipper strands Z and negative control sequences NC, we managed to reach grafting densities in the range 0.4 to 8 pmol·cm^{-2}. The determination of these grafting densities was made by radioactive quantification in previous work. [22] After the SAMs were well formed and rinsed, the initial microarray of Z probes was prepared and it was possible to address any DNA sequence as probes by its simple coupling with Zc, the complementary strand of Z, and further hybridization on the microarray. For the detection of Adenosine, the Z probes functionalized on the surface was hybridized with one of the monomers forming the Sx duplex to be ready for detection purpose (Step 2). The hybridization process was done by injecting 1μM of monomer at 0.26 μL/s, each injection took 1 hour so that 90% of the solution in the injection loop can be injected. The injection was stopped to refill the injection loop with monomer solution before the entire loop was injected. The purpose was to avoid injection of pure buffer into the chamber. The hybridization was completed after 2 injections, but a third injection was made to ensure saturation of the hybridization of the probes.

The interest of this Step 2 was two-fold for a detailed analysis of the amplification method. First of all, from the initial microarray, we were able to obtain functional microarrays with various split-aptamer sequences depending on the monomer strands injected SX*Zc. Thus, with strong efficiency, the sequence engineering of the split-aptamers was tested on the same microarrays by either injecting S5*Zc, S6*Zc or S8*Zc. An overall regeneration of the microarray is possible by injecting NaOH solution to remove the monomer strands SX*Zc and to recover the initial microarray (Step 6). Secondly, Step 2 also served as a calibration step since the SPR signal observed was useful to further determine the number of bridges and the length of the DNA chains formed in the detection step (Step 4). In order for this calibration to be effective, the hybridization of the monomers SX*Zc should be complete (100% hybridization) on every spots and for each grafting density.

In the recent literature, the saturation effects due to crowding of the probes have been tested and experimentally observed [23–25] as well as theoretically analyzed [26–28].

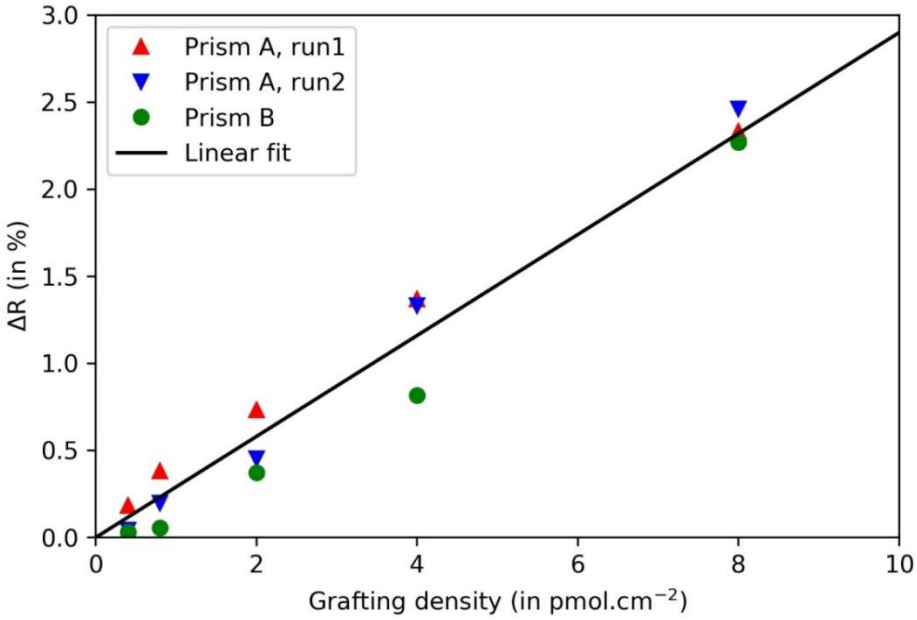

Figure 3.10 SPR signal obtained following hybridization of monomer injection (S6*Zc) at 1µM concentration as function of the grafting density. Two injections on the same prism A separated by NaOH regeneration (red and blue triangles) and on a different prism B (green circles) confirmed the reproducibility.

In our study, it seemed that the use of PEG molecules on the probe surfaces favored the probe hybridization even at large grafting densities. This was confirmed by the linear SPR signal ΔR observed as function of the grafting density shown in **Figure 3.10**. The lack of saturation at high grafting densities suggested that 100% of the probes had been hybridized independently of the grafting density. The linear fit of the SPR signal ΔR presented a vanishing value when the grafting density was extended to 0 pmol·cm^{-2}. In other words, when no probe was grafted on the surface, the signal of hybridization was correctly predicted to ΔR = 0%. This further confirmed that the hybridization of the probes was complete on all the range of grafting densities studied. Thus, the same grafting density of the functional probes SX* were present at the surface of the microarray than the initial grafting density of the probes Z. Furthermore, the maximum grafting density tested in this study (8 pmol·cm^{-2}) was sufficiently low to avoid crowding effects of the probes and the saturation of the hybridization reaction. More importantly, the results in **Figure 3.10**

was gathered from more than one prism, which suggested the hybridization had good intra- and inter-microarray reproducibility

Detection of Adenosine

The detection of Adenosine target was based on the SPR signal obtained from the second injection (Step 4). The detection signal obtained from different sequence designs and approaches were analyzed. The maximum signal obtained for two different dimers (S5 and S6) and an image obtained during the detection were shown in the figures below. The signal observed for S6 dimer in presence of 1 mM of Adenosine was stronger than that for S5 dimer (red circles compared to red triangles in **Figure 3.11**). The main reason for this increased signal may be inferred from the presence of one more binding base pair in the split-aptamer stem inducing stronger interactions with Adenosine. However, by increasing the number of hybridizing bases, interactions may also occur even without Adenosine due to simple hybridization of the split-aptamer dangling ends. This was explicitly observed for the S6 and S8 dimer injections without Adenosine target (**Figure 3.11a**).

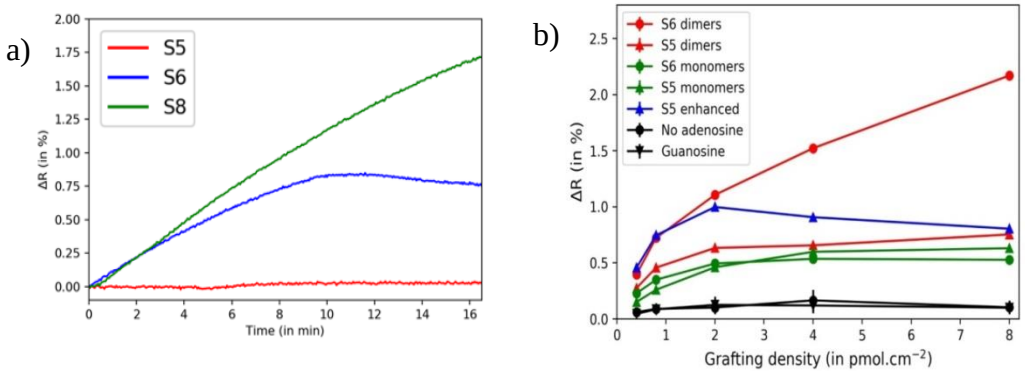

Figure 3.11 The SPR signal and image obtained, (a) the signal obtained in step 4 after an injection of 1µM dimers with no Adenosine. Among the three dimers, S5 dimer showed no signal increase, S6 dimer showed an increase about 0.8% and the signal was significantly higher for the S8 dimers. (b) the signal obtained for different dimers at various grafting densities. The concentration of Adenosine was 1mM and the strand concentration was 1µM for all these injections. As a control, we also represent the SPR signal following injection of 1 mM of adenosine and 1µM of monomers (green) with split-aptamer dangling ends with respectively 5 or 6 hybridizing bases (S5Z monomers in green triangles or S6Z monomers in green circles). Results for the enhancement strategy with S5Z monomers injection are depicted with blue triangles. Negative controls (in black) correspond to the injection of dimers without targets (circles) or 1 mM concentration of guanine (down triangles) to test the selectivity.

Error bars have been determined from the standard deviation of the response of the replicate spots on the microarray.

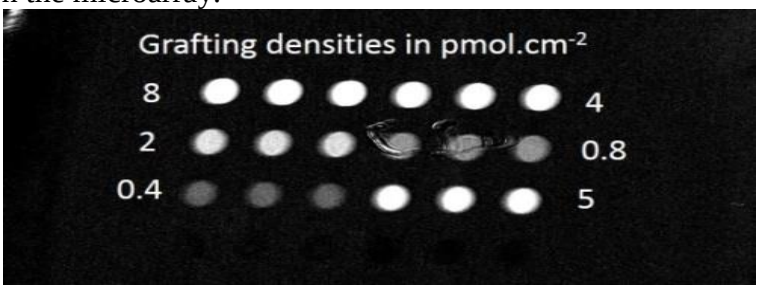

Figure 3.12 The SPR image obtained during the injection of 1µM of mixture (S6Z+S6*Zc) with 1mM Adenosine, the brightness of the spots shows the strength of signal. The spots were in six series with different grafting densities of the probes, the gold prism was functionalized with Z probes and hybridized with S6*Zc ssDNA to form the probe for detection.

With an increase of the grafting density, more probes were available inside the spots. A linear increase of SPR signal after the first injection (Step 2) was observed in **Figure 3.10**. A similar increase of the SPR signal with the grafting density could be observed as well during the second injection (Step 4) in the SPR results shown in **Figure 3.11b**. However, we observed a non-linear behavior with saturation for larger grafting densities. This was consistent with a crowding effect during chain formation leading to shorter chains at larger grafting densities. Thus, the increased number of probes was counter-balanced by the reduced length of the linear chains formed on the biosensor. This result was also confirmed by the average number of Adenosine bridges per probes present on the microarray as function of the grafting density (see next section).

There were two negative controls used in this study to confirm the detection of Adenosine and the selectivity, respectively. In both cases, the test started with hybridization of S5*Zc monomer sequence on the probes Z to obtain a functional microarray. Then, for the confirmation of Adenosine detection, S5 dimers were injected without Adenosine (black circles in **Figure 3.11b**). The SPR signal observed after the injection, around 0.1%, was comparable to the biosensor noise and was significantly lower than the signal observed upon injection of Adenosine at 1 mM with S5 dimers. This effectively confirmed the detection of Adenosine, more details on the detection limit will be discussed in the next section. To control the selectivity of the biosensor, S5 dimers were also injected with 1 mM of Guanosine. Guanosine is a molecule with similar structure as Adenosine but without binding affinity toward

split-aptamer of Adenosine. Effectively, the SPR signal observed (black down triangles in **Figure 3.11b**) was similar to the signal of negative control without any target in the buffer, confirming the selectivity of the biosensor toward Adenosine.

In order to assess the interest of the linear chain formation in the signal amplification, we also compared the SPR signal upon injection of monomers instead of dimers to avoid the formation of linear chains. We observed similar SPR signals for both S5Z and S6Z monomer injections (sequences S5Z green triangles and S6Z green circles respectively in **Figure 3.11b**) with 1mM of Adenosine. Those signals were increased compare to the two negative controls (lack of Adenosine or Guanosine injection) especially for grafting densities higher than 2 pmol·cm^{-2} where the SPR signal reached 0.5% more than three times the noise signal noise. The injection of S6 dimers (red circles in **Figure 3.11b**) produced even larger SPR signals than S6Z monomers confirming the interest of the self-assembling of linear chains to amplify the sandwich assay in the detection of the small molecule Adenosine. However, this enhancement was not recovered for S5 dimer injections which suggested that sequence engineering was necessary to optimize the formation of linear chains.

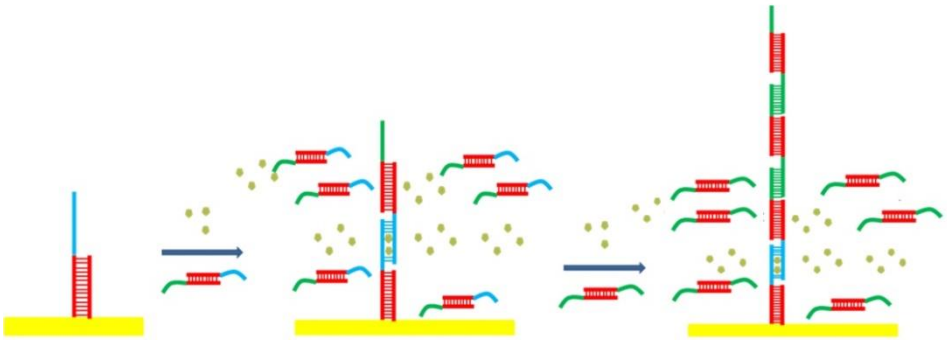

Figure 3.13 The enhancement of S5 dimer signal. After the Z probe was hybridized with S5 monomer, instead of an injection of the dimer formed with "S5*Z9c+S5Z", an injection of 1µM "S5Z+S6cZ9c" was made, the dimer formed Adenosine bridge just like S5 dimer, but the split-aptamer dangling ends was replaced by a dangling end fully complementary to S6 split-aptamer. Another injection of the S6 dimer was made to extend the DNA chain on the gold surface. 1 mM of Adenosine was kept in the buffer throughout the whole process in order to maintain the interaction between the 1D chain with the probes on gold prism.

Since S5 dimer injection did not improve the SPR signal as compared to S5Z monomer injection, we developed an enhancement strategy, whose results were shown as "S5 enhanced" in **Figure 3.11b**. The process of the enhancement was

shown in **Figure 3.13**: First, similarly as for the classic approach, the S5*Zc sequence was injected to hybridize on the probes immobilized on the gold surface to form S5* functional probes. Then, instead of injecting the duplex formed by S5Z and S5*Zc couple, the duplex formed with S5Z and S6cZc was injected as well as Adenosine molecules. This dimer still formed binding with the split aptamer dangling ends S5* on the surface but was limited to only one Adenosine bridge formed on each probe and led to a S6c sequence as dangling ends. Then, another injection of the complementary S6c dimer from mixtures of S6Z and S6cZc sequences was made to enhance the SPR signal. In order to remove the initial Adenosine bridge, the presence of 1 mM of Adenosine was conserved upon this second injection. The complementary S6c dimer formed linear head-tail self-binding chains where the split aptamer dangling ends are replaced by self-complementary oligonucleotide dangling ends (S6-S6c) to further increase the binding affinity of the bridges. To sum up, this strategy enhanced the SPR signal of S5 dimer by changing the classical Adenosine bridges self-assembling mechanism by two kinds of binding mechanisms: 1) Adenosine bridges for the first bound dimer and 2) standard DNA hybridization for the following extension of the linear chains. In **Figure 3.11**, the SPR signal obtained from "enhanced S5" was 50% higher than the S5 dimer injections at low grafting density of probes (below 2 pmol·cm^{-2}), even close to the S6 dimer injections. However at larger grafting densities (8 pmol·cm^{-2}), the enhancement was not efficient. The spots with 8 pmol·cm^{-2} grafting density had the same SPR signal for S5 dimer injections and enhanced S5 strategy. Therefore, the optimal strategy remains the injection of S6 dimers at every grafting density to perform longer chains.

Regeneration of the microarrays

The regeneration of the microarrays is essential for multiple consecutive detections of Adenosine. As can be seen form **Figure 3.9**, the dissociation of the adenosine bridges formed by S6 dimers in Step 4 is relatively low in Step 5 and do not allow a full regeneration of the functional microarray back to Step 3. Thus, consecutive detections of Adenosine would require the regeneration to the initial microarray back to Step 1 by the injection of NaOH solution (Step 6) and the further injection of SX*Zc monomers to recover a functional microarray.

In the case of Adenosine detection by injection of S5 dimers, the recovery of the functional microarray directly to Step 3 after a buffer injection was possible (**Figure 3.14**). It allowed another Adenosine detection followed by the previous one. The main reason for the fast regeneration to a functional microarray is the lower stability of the Adenosine bridges of S5 dimers compared to the S6 and S8 dimers due to the sequence engineering and the lower number of hybridizing bases (5 compared to 6 and 8 respectively).

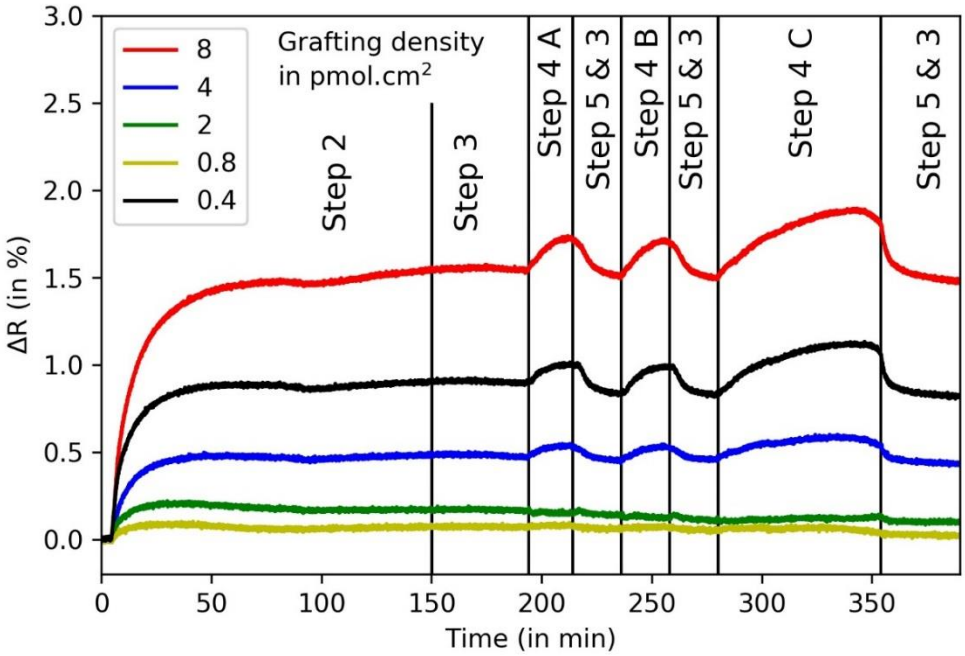

Figure 3.14 The SPR signal obtained from S5 dimers and their regeneration observed after several injections. The probe was first hybridized with S5 monomer and two injections of S5 dimer with 10µM Adenosine was made, the SPR signal decreased to the same level before the injection after the Adenosine was flushed by the buffer. Then another injection of S5 dimer with 100µM Adenosine was made. The signal was higher than the first two injections, yet the probes were regenerated after the injection was finished. In the image, three Step 4 (A, B and C) corresponded to three detecting process and the probes were regenerated and stabilized during "Step 5&3"

Number of adenosine bridges

During Step 2, the monomers SX*Zc were hybridized on the initial probes Z leaving a split-aptamer dangling end SX* as functional probes for the detection of Adenosine. The second injection involved oligonucleotide dimers with SX-SX* split-aptamer dangling ends (Step 4). Its injection combined with the presence of Adenosine induced the formation of linear DNA chains attached to the functional

probes via Adenosine bridges. Since the signal increased in SPR measurement was proportional to the mass increase on the surface, the signal from Step 2 and Step 4 injections could be used to determine the average length of the linear chains or the average number of Adenosine bridges. The SPR signal increase from Step 2, ΔR(mono), was proportional to the total mass of the monomers attached onto the surface and thus to the mass of the monomers and the number of initial probes since the hybridization is complete (100% hybridization). The signal increase from Step 4, ΔR(dimers), was proportional to the total mass of the dimers that formed the linear chains and thus to the mass of the dimer (twice the mass of the monomer), the number of functional probes (similar to the number of initial probes) and the number of adenosine bridges. Finally, the average number of adenosine bridges, N(bridges), on each probe may simply be determined by the ratio between ΔR(dimers) and ΔR(mono) as N(bridges) = ΔR(dimers) /2·ΔR(mono). The factor 2 was due to the fact that the mass of the dimer is twice the mass of the monomer.

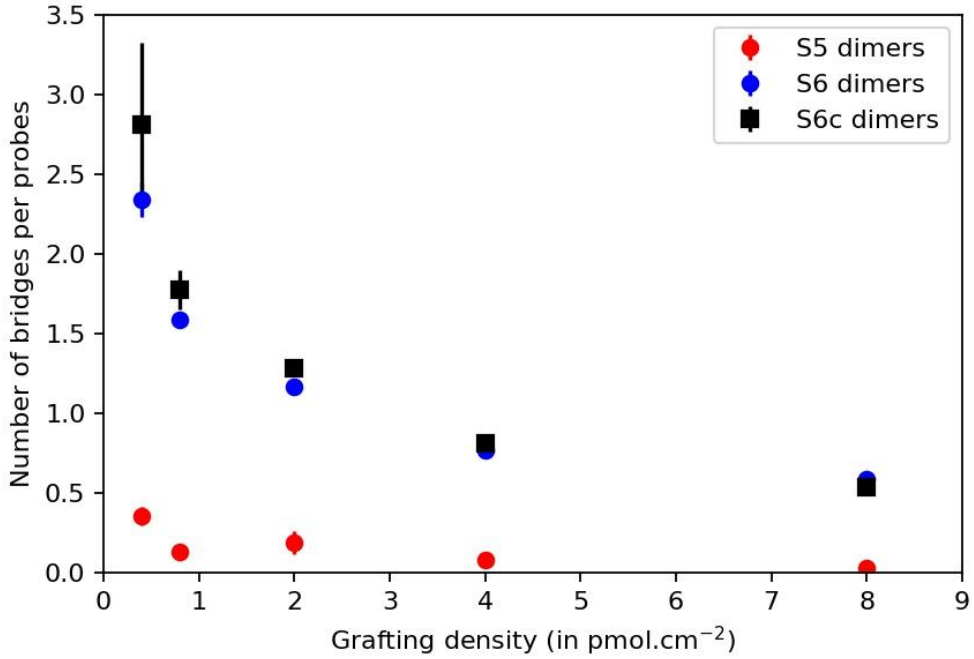

Figure 3.15 Average number of adenosine bridges as function of the grafting density for an injection of S5 and S6 dimers (red and blue circles) with 100 µM of adenosine and for an injection of S6c dimers (black squares) with S6 and S6c complementary dangling ends. Error bars have been determined from the standard deviation of the response of the replicate spots on the microarray.

The impact of grafting density on linear chain formation was further studied through the average number of Adenosine bridges listed in **Figure 3.15**. A change in the grafting density not only modified the total amount of probes available, but also the average distance between the probes. The fact that the number of bridges was decreasing with the grafting density drew the conclusion that given more space between probes the linear chain had better conditions for growing in length. However, the loss in the number of probes led to a decrease in the overall SPR signal, regardless of the longer 1D chain on each probe.

In order to assess that the length of the linear chains was not limited by the concentration of Adenosine, we used the injection of the fully complementary S6c dimers as positive control. Since the formation of the bridges is due only to hybridization of self-complementary strands S6-S6c and Z-Zc for the S6c dimers, we expected to obtain the maximum number of bridges. Electrophoresis analysis have shown that while linear chains formed for S6c dimers in solution, they were not stable enough to be observed for S6 dimers even in presence of 1 mM Adenosine. However, we observed that S6 and S6c dimers led to similar results suggesting that the number of bridges observed upon injection of S6 dimers is not limited by the concentration of Adenosine and the strength of the Adenosine bridge for the formation of linear chains at the surface of the biosensor. On the contrary, the results observed for the S5 dimers have shown that the strength of the Adenosine bridges were not enough to reach the maximum number of bridges.

3.3.3 The selectivity and detection limit of the sensor

Detection limit and selectivity

Despite the fact that S5 dimers were not strong enough for maximal growing length, it led to the best detection limit. In order to assess the detection limit of Adenosine molecules by the current self-assembling strategy of 1D linear chain formations on biosensors, we considered S5 dimer injections at various Adenosine concentrations, the results were plotted in **Figure 3.16**. From the SPR signal obtained in the range 0–50 μM and the signal noise observed, the limit of detection (LOD) was determined to be 10μM. This LOD was determined as the concentration for which the

signal to noise ratio is 3. This value is comparable to the dissociation constant of the full aptamer (K_D=6 µM) [29] and well below the estimated value for the split-aptamer (K_D=50 µM) [30]. The detection range was not limited to the range 10-50 µM but extended up to 1 mM as shown in **Figure 3.16**. An injection of guanosine at 1 mM presented the same signal as the sample without adenosine, which confirmed the selectivity of the method. Higher LODs were observed for the dimers S6 and S8 as the result of the higher background signal (**Figure 3.11a**). The injections of S6 and S8 dimers at 1µM lead to a significant SPR signal even without Adenosine. The numbers of hybridizing bases were large enough to lead to bridges without Adenosine. This effect impaired low detection limits for those S6 and S8 dimer sequences since the increased of signal by a small amount of Adenosine only slightly increased the background signal. On the contrary, the SPR signal for the injection of S5 dimers without Adenosine was close to the noise level. Thus, no bridges were present and a small amount of Adenosine trigger the formation of bridges leading to an observable SPR signal. In conclusion, sequence engineering of the split-aptamer allowed us to obtain a Signal OFF - Signal ON behavior of the biosensor. Better LOD were obtained for the signal OFF (without background SPR signal) to signal ON in presence of Adenosine with the S5 dimers. Similar results were observed for sandwich assays using Au NPs [10].

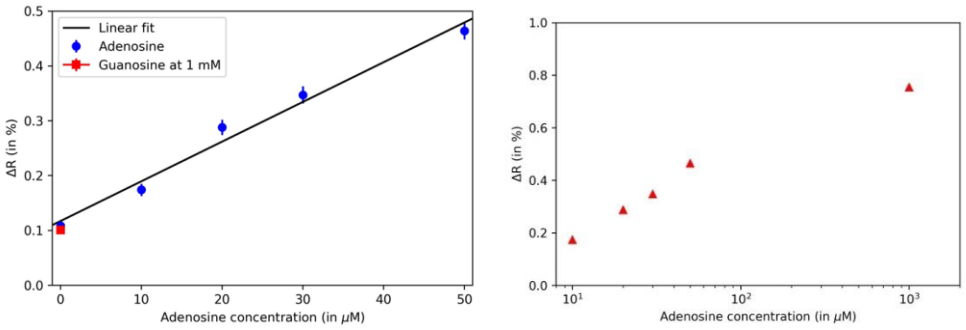

Figure 3.16 SPR signal for S5 dimer injections as function of adenosine concentration (blue circles) for the spot with grafting density of 8 pmol·cm^{-2}. Guanosine injection at 1 mM served as selectivity control (red square). Error bars have been determined from the standard deviation of the response of the replicate spots on the microarray. The extension of this linear increase to higher Adenosine concentrations was shown as the red triangle, up to 1mM Adenosine.

3.4 Conclusion

In order to circumvent the difficulties to detect small molecules with biosensors, we proposed an amplification strategy based on the self-assembly of linear DNA chains triggered by the targets. The benefits of this method are that no Au NPs are needed for the amplification of signal, and the formation of DNA structure is a self-repeating chain instead of complex chain reactions, which makes the adjustment toward another target more tangible since the sequence engineering is less complicated. Oligonucleotide dimers presenting split-aptamer dangling ends were injected with the target Adenosine. The presence of Adenosine target triggered the formation of bridges between the dimers through split-aptamer dangling ends bonding. The effect of the grating density of the probes on the length of the linear chains formed at the surface of the biosensor was analyzed. It was shown that by decreasing the grafting density, the length of the multi-strand chains increased. However, on the SPR signal, this increase is insufficient to counter-balance the reduction in immobilized probe densities. Thus, higher grafting densities constituted the best option even if they led to shorter multi-strand chains. Furthermore, the sequences leading to the strongest signal (S6) were not those leading to the best detection limit of Adenosine. This is principally explained by the existence of bridges with S6 sequences even in absence of Adenosine that impair the detection of low amount of Adenosine. While the detection limit with S5 dimers remains low (LOD = 10 µM), the potential simple regeneration of our approach could be interesting for continuous monitoring of small molecules like recently suggest by Sergelen et al. [28]

In order to enhance the self-assembling amplification, it would be interesting to study the formation of dendritic structures by the use of Y shape or even more complex DNA structures with multiple split-aptamer dangling ends [15,31]. The multiple bindings could help to over-come by cooperative effects the low K_D of the split-aptamers in the formation of large structures linked by Adenosine bridges. The attempts on using such structures in the same technology will be discussed in Chapter 5.

Reference

1. Hoa XD, Kirk AG, Tabrizian M. Towards integrated and sensitive surface plasmon resonance biosensors: A review of recent progress. ***Biosens Bioelectron***. 2007;23(2):151-160. doi:10.1016/j.bios.2007.07.001.
2. Scarano S, Mascini M, Turner APF, Minunni M. Surface plasmon resonance imaging for affinity-based biosensors. ***Biosens Bioelectron***. 2010;25(5):957-966. doi:10.1016/j.bios.2009.08.039.
3. Frasconi M, Tel-Vered R, Riskin M, Willner I. Surface plasmon resonance analysis of antibiotics using imprinted boronic acid-functionalized au nanoparticle composites. ***Anal Chem***. 2010;82(6):2512-2519. doi:10.1021/ac902944k.
4. Vaisocherová H, Yang W, Zhang Z, et al. Ultralow fouling and functionalizable surface chemistry based on a zwitterionic polymer enabling sensitive and specific protein detection in undiluted blood plasma. ***Anal Chem***. 2008;80(20):7894-7901. doi:10.1021/ac8015888.
5. Wang Q, Huang J, Yang X, et al. Surface plasmon resonance detection of small molecule using split aptamer fragments. ***Sensors Actuators, B Chem***. 2011;156(2):893-898. doi:10.1016/j.snb.2011.03.002.
6. Nelson B, Grimsrud T, Liles M, Goodman R, Corn R. Surface plasmon resonance imaging measurements of DNA and RNA hybridization adsorption onto DNA microarrays. ***Anal Chem***. 2001;73(1):1-7.
7. Mitchell J. Small molecule immunosensing using surface plasmon resonance. ***Sensors***. 2010;10(8):7323-7346. doi:10.3390/s100807323.
8. Shankaran DR, Gobi KV, Miura N. Recent advancements in surface plasmon resonance immunosensors for detection of small molecules of biomedical, food and environmental interest. ***Sensors Actuators, B Chem***. 2007;121(1):158-177. doi:10.1016/j.snb.2006.09.014.
9. Liedberg B, Nylander C, Lunström I. Surface plasmon resonance for gas detection and biosensing. ***Sensors and Actuators***. 1983;4(C):299-304. doi:10.1016/0250-6874(83)85036-7.
10. Melaine F, Roupioz Y, Buhot A. Gold Nanoparticles Surface Plasmon Resonance Enhanced Signal for the Detection of Small Molecules on Split-Aptamer Microarrays (Small Molecules Detection from Split-Aptamers). ***Microarrays***. 2015;4:41-52. doi:10.3390/microarrays4010041.
11. Melaine F, Coilhac C, Roupioz Y, Buhot A. A nanoparticle-based thermo-dynamic aptasensor for small molecule detection. ***Nanoscale***. 2016;8(38):16947-16954. doi:10.1039/C6NR04868D.
12. Yao X, Li X, Toledo F, et al. Sub-attomole oligonucleotide and p53 cDNA determinations via a high-resolution surface plasmon resonance combined with

oligonucleotide-capped gold nanoparticle signal amplification. ***Anal Biochem***. 2006;354(2):220-228. doi:10.1016/j.ab.2006.04.011.

13. Wang J, Zhou HS. Aptamer-based Au nanoparticles-enhanced surface plasmon resonance detection of small molecules. ***Anal Chem***. 2008;80(18):7174-7178. doi:10.1021/ac801281c.

14. Yao G-H, Liang R-P, Huang C-F, Zhang L, Qiu J-D. Enzyme-free surface plasmon resonance aptasensor for amplified detection of adenosine via target-triggering strand displacement cycle and Au nanoparticles. ***Anal Chim Acta***. 2015;871:28-34. doi:10.1016/j.aca.2015.02.028.

15. Ding X, Cheng W, Li Y, et al. An enzyme-free surface plasmon resonance biosensing strategy for detection of DNA and small molecule based on nonlinear hybridization chain reaction. ***Biosens Bioelectron***. 2017;87:345-351. doi:10.1016/j.bios.2016.08.077.

16. F.Melaine. Biopuce à aptamères : application à la détection de petites molécules par imagerie de résonance plasmonique de surface. ***Thèse de doctorat UGA*** 2014.

17. Huizenga DE, Szostak JW. A DNA aptamer that binds adenosine and ATP. ***Biochemistry***. 1995;34(2):656-665. doi:10.1021/bi00002a033.

18. Cosa G, Focsaneanu KS, McLean JR, McNamee JP, Scaiano JC. Photophysical properties of fluorescent DNA-dyes bound to single- and double-stranded DNA in aqueous buffered solution. ***Photochem Photobiol***. 2001;73(6):585-599. doi:10.1562/0031-8655(2001)0730585ppofdd2.0.co2.

19. Zipper H, Brunner H, Bernhagen J, Vitzthum F. Investigations on DNA intercalation and surface binding by SYBR Green I, its structure determination and methodological implications. ***Nucleic Acids Res***. 2004;32(12). doi:10.1093/nar/gnh101.

20. Xu H, Gao S, Yang Q, Pan D, Wang L, Fan C. Amplified fluorescent recognition of g-quadruplex folding with a cationic conjugated polymer and DNA intercalator. ***ACS Appl Mater Interfaces***. 2010;2(11):3211-3216. doi:10.1021/am1006854.

21. Chovelon B, Fiore E, Faure P, Peyrin E, Ravelet C. A lifetime-sensitive fluorescence anisotropy probe for DNA-based bioassays: The case of SYBR Green. ***Biosens Bioelectron***. 2017;90:140-145. doi:10.1016/j.bios.2016.11.049.

22. Daniel C, Méa ne F, Roupioz Y, Livache T, Buhot A. Real time monitoring of thrombin interactions with its aptamers: Insights into the sandwich complex formation. ***Biosens Bioelectron***. 2013;40(1):186-192. doi:10.1016/j.bios.2012.07.016.

23. Petty TJ, Wagner CE, Opdahl A. Influence of Attachment Strategy on the Thermal Stability of Hybridized DNA on Gold Surfaces. ***Langmuir***. 2014;30(50):15277-15284. doi:10.1021/la504128h.

24. Chiang H-C, Levicky R. Effects of Chain–Chain Associations on Hybridization in DNA Brushes. ***Langmuir***. 2016;32(48):12603-12610. doi:10.1021/acs.langmuir.6b02990.
25. Macedo LJA, Miller EN, Opdahl A. Effect of Probe–Probe Distance on the Stability of DNA Hybrids on Surfaces. ***Anal Chem***. 2017;89(3):1757-1763. doi:10.1021/acs.analchem.6b04048.
26. Halperin A, Buhot A, Zhulina EB. Sensitivity, Specificity, and the Hybridization Isotherms of DNA Chips. ***Biophys J***. 2004;86:718-730. doi:10.1016/S0006-3495(04)74150-8.
27. Halperin a, Buhot A, Zhulina EB. On the hybridization isotherms of DNA microarrays: the Langmuir model and its extensions. ***J Phys Condens Matter***. 2006;18(18):S463-S490. doi:10.1088/0953-8984/18/18/S01.
28. Harrison A, Binder H, Buhot A, et al. Physico-chemical foundations underpinning microarray and next-generation sequencing experiments. ***Nucleic Acids Res***. 2013;41(5):2779-2796. doi:10.1093/nar/gks1358.
29. Huizenga DE, Szostak JW. A DNA aptamer that binds adenosine and ATP. ***Biochemistry***. 1995;34(2):656-665. doi:10.1021/bi00002a033.
30. Yang C, Spinelli N, Perrier S, Defrancq E, Peyrin E. Macrocyclic Host-Dye Reporter for Sensitive Sandwich-Type Fluorescent Aptamer Sensor. ***Anal Chem***. 2015;87(6):3139-3143. doi:10.1021/acs.analchem.5b00341.
31. Meng H-M, Liu H, Kuai H, Peng R, Mo L, Zhang X-B. Aptamer-integrated DNA nanostructures for biosensing, bioimaging and cancer therapy. ***Chem Soc Rev***. 2016;45:2583-2602. doi:10.1039/C5CS00645G.

Chapter 4 Detection of Adenosine with 1D DNA structure and UV spectroscopy

Dans ce chapitre, on considère une méthode de détection homogène pour l'adénosine en utilisant la spectroscopie UV. Une différence dans le profil de fusion des structures d'ADN causées par la présence d'adénosine dans la solution a été utilisée pour la détection de cette dernière. La courbe de fusion de la chaîne d'ADN 1D a montré deux pics correspondant à deux mécanismes de liaison différents. Le premier pic correspondant à la fixation de l'adénosine est affecté par la présence de cette dernière alors que le second pic correspondant à l'hybridation du brin complémentaire n'est pas affecté. La détection de l'adénosine a été obtenue en comparant ces deux pics. Le deuxième pic a également fourni une référence interne permettant de limiter notamment les variations dues aux différents tampons. Les modèles d'ADN utilisés pour cette méthode étaient basés sur la même structure de chaîne d'ADN 1D utilisée pour les expériences de SPRi. Cinq différents dimères dérivés des dimères S5, S6 et S8 ont été utilisés pour étudier l'influence de la force de liaison sur la détection. Deux des dimères ont été jugés appropriés pour la détection. L'optimisation du protocole et les défis rencontrés ont été abordés dans ce chapitre. Cette méthode de détection a montré une limite de détection de 1 µM.

4.1 Introduction

The UV-Vis spectroscopy of DNA duplex solution has been reported in many literatures to help determine the melting profile of the DNA duplex or realize detection of targets. [1–5] Other than these applications, in some simulation tools that predict the binding properties of the DNA strands, such as "DINAMelt", the simulation of UV absorbance is a vital element for determining the melting temperature of the strand mixture. Some other researchers used the change in the wavelength of the absorbed light to analyze the interactions that took place in the solution. [6–10] The principle and experimental methods for using UV-Vis spectroscopy to analyze the melting profile of the duplexes has been explained in Chapter 2. In this section, we listed some published detecting applications that used UV-Vis spectroscopy as a supplementary method for detection. By comparing the pros and cons of these methods, we will introduce our new detection method of Adenosine based on the melting profile obtained from UV-Vis spectroscopy.

Xue et al reported a one-step colorimetric detection of mercury cation at room temperature.[11] The scheme of the DNA/nanoparticle conjugate and the melting profile obtained from spectroscopy were shown in **Figure 4.1**. A DNA/nanoparticle conjugate was designed and the conjugate consisted of three parts, two different DNA probes functionalized on Au NPs and a DNA linker that can bind the two probes. The linker sequence contained several T-T DNA mismatches that were proven to affect the melting profile of the conjugate. With presence of Hg^{+} in the environment the three parts could form the DNA/nanoparticle conjugate at room temperature. If the Hg^{2+} was removed from the environment, due to mismatches formed in the DNA duplexes, the melting temperature was lower than the operating temperature, thus the formation of the conjugate was inhibited. The binding process was monitored by UV-Vis spectroscopy at wavelength 520 nm or 530 nm depending on the diameter (14 nm or 30nm) of the nanoparticles. Since the Hg^{2+} was the controlling element of the

conjugate, the melting profile of the solution was different depending on the presence of Hg^{+}, which was used for the detection of the mercury cation. Consequentially, the melting temperature of the conjugate without Hg^{2+} was decreased to 21 ℃, which was lower than the room temperature. In other words, without Hg^{2+}, the conjugate was not stable in solution. Furthermore, this changed the absorption of light and led to a change in the color of the solution, the detection could be realized by comparing the color with control solution.

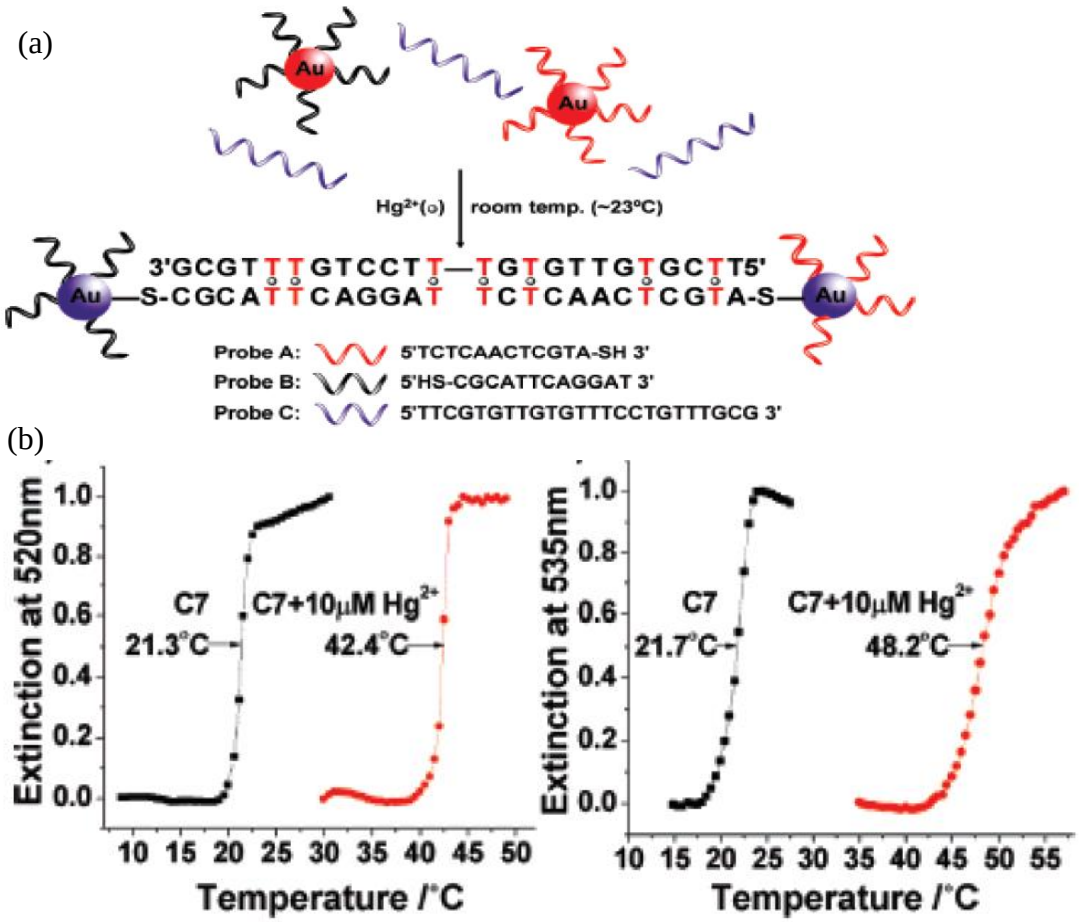

Figure 4.1 (a) the scheme of DNA/nanoparticle conjugate, Probe A and B were DNA probes functionalized on gold nano particles, Probe C was a linker binding the other two probes with presence of Hg^{+} at room temperature (23 ℃). (b) The normalized melting curve of the solution containing three probes, with (red) or without (black) Hg^{2+} (10 μM) in the solution. [11]

Xu and his team created a detecting model for copper cations similar to the mercury detection methods reported by Xue. [12] Two batches of Au NPs were prepared and functionalized with DNA probes. The first batch was modified with 30-propylthiol-terminated 40-mer oligonucleotides (template strand) and the second batch was functionalized with 30-propylthiolated and 50-alkylated 25-mer oligonucleotides that are complementary to half of the template DNA on the template particles. While mixed in solution, these nanoparticles formed polymeric networks because the sequences were complementary. A third oligonucleotide was added into the solution, it was an azidobutyrate labeled 15-mer oligonucleotide, and it was complementary to the other half of the template strand. Together, the three elements formed aggregates of Au NPs. The melting profile could have a shift in the melting temperature up to 12 ℃ depending on the concentration of Cu^{2+}. Once the solution was heated to 55 ℃, the aggregation of Au NPs would break if there was no Cu^{2+} in the solution. The solution with Cu^{2+}, on the other hand, maintained the aggregation because the melting temperature has shifted to higher temperature. The large extinction coefficient of the DNA Au NPs allowed detection through visual inspection.

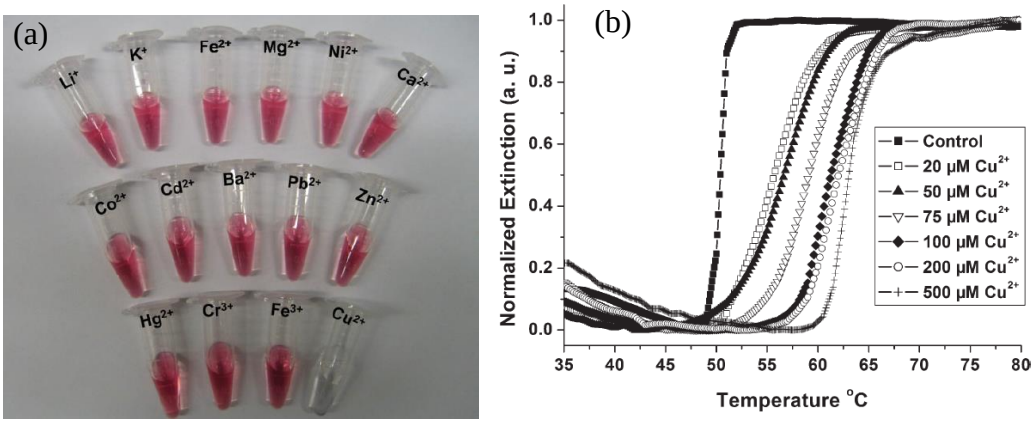

Figure 4.2 The colorimetric sensor reported by Xu [12]. (a) The solution with different ions and their color at 55 ℃. (b) The normalized extinction for solutions with different concentrations of copper cations. The curve shifted with the increase of Cu^{2+} concentration and indicated a different melting temperature.

Aptamers have also been used in UV-Vis spectroscopy for detection purpose. Song et al reported an Au NP-based colorimetric detection of kanamycin using a DNA aptamer. [13] Short DNA strands can be adsorbed to the surface of Au NPs even without modification. [14,15] The scheme of the Au NPs was displayed in **Figure 4.3**. When salt is added to a solution containing AuNPs, ssDNA aptamer-treated AuNPs with kanamycin aggregate and exhibit a color change from red to purple. Without kanamycin, the particles remained the same and were not aggregated. This was because the kanamycin suppresses the adsorption of the aptamer onto the surface of AuNPs by competitive binding with the aptamer. UV absorbance was used as a proof of concept experiment to show that this interaction was controlled by the presence of kanamycin in the solution (**Figure 4.3**). The melting temperature shifted higher due to the stronger binding from the interaction between kanamycin and the aptamers.

The three detection methods all used UV-Vis spectroscopy as a method to analyze the position, interaction and structures of the DNA and nanoparticles in the solution. In these three cases, a shift in the melting temperature was observed due to the change in the strength of binding. Despite the convenient detection directly through human eyes, the preparation of the Au NPs was costly and time-consuming. The UV-Vis spectroscopy also had one limitation that made it difficult to be used as the detection method. The melting temperature was influenced by the composition of the buffer, thus the value of the melting temperature obtained from the spectroscopy cannot be used directly for detection purpose.

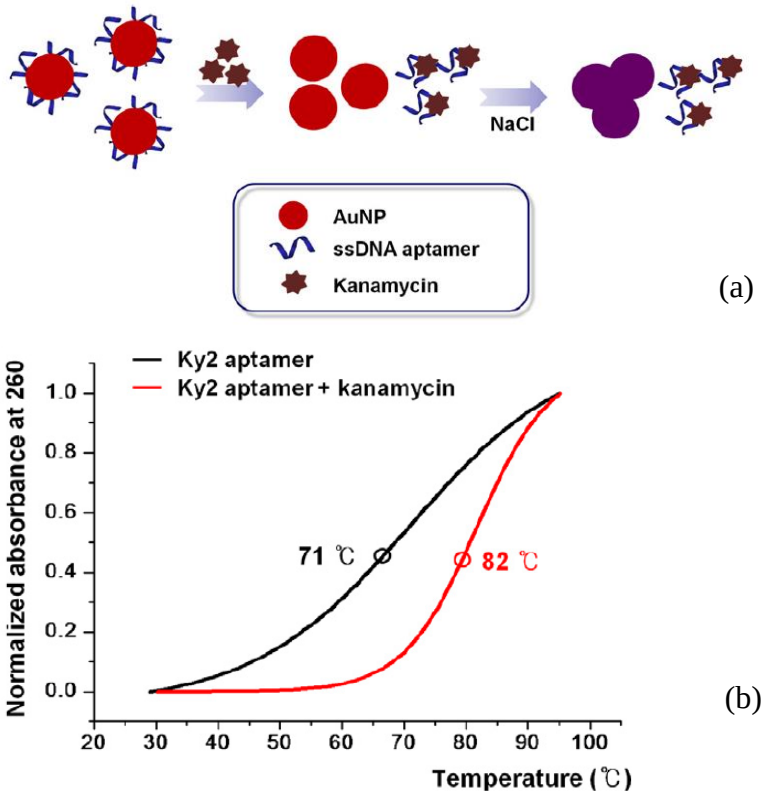

Figure 4.3 (a) The scheme of the Kanamycin sensor, ssDNA aptamers were adsorbed on the surface of Au NP. The Kanamycin in the solution isolated the aptamers from the gold particles and caused the particles to aggregate. (b) The normalized absorbance of 260nm light of aptamer solutions with or without kanamycin in the solution. The melting peak shifted with presence of the target.

As introduced in the first chapter, we designed DNA architectures that can be directly used for detection of Adenosine by analyzing their absorbance of UV light with 260nm wavelength. In addition to this, no nanoparticles or fluorescent labels were required during the preparation. The most intriguing benefit of this method was that by combining splited aptamer sequences with oligonucleotides, we introduced an internal reference in the system. The DNA architectures had two melting peaks: one corresponded to the hybridized oligonucleotide and the other corresponded to the Adenosine bridge. Instead of reading the melting temperature directly or compare the difference in the melting temperature with or without Adenosine, the difference between the two peaks were measured for the detection. This internal reference made

the detection more reliable, regardless of elements in the experimental environment influencing the melting temperature.

4.2 Sequence design of 1D DNA structures for UV spectroscopy

Our tests started with the sequences that were used in SPRi experiments along with some modification based on their properties observed during the detection with SPRi. Same as the sequences used for SPRi experiments, the duplexes were sorted into S5, S6 and S8 depending on the number of base pairs hybridized on one side of the Adenosine bridges. The S5 and S6 dimers were able to achieve detection with good selectivity and S8 dimer was used as a proof of concept in the SPRi experiments. Other than these sequences, the fully complementary S6 duplex (S6Z+S6cZc) was also used as positive control. In the SPRi experiment, we moved two bases in the oligonucleotide zip of S6 and S8 duplexes to strengthen the binding. In the UV spectroscopy experiments we used the same method to control the strength of binding.

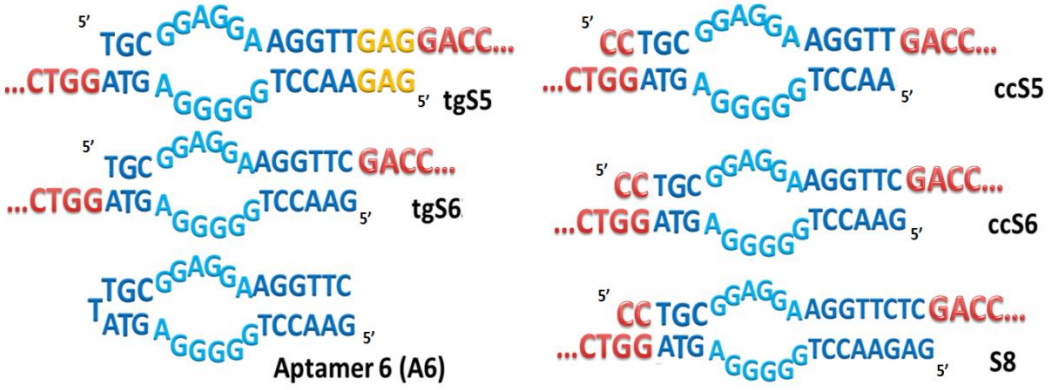

Figure 4.4 The scheme of the DNA structures used in UV spectroscopy. The dimers can be sorted into S5, S6 and S8 by the number of base pairs hybridized on the right side of the Adenosine bridges, or sorted by the starting two bases on the 5' of SxZ sequence by "CC" or "TG". The dimers start with "CC" had more balanced and stronger binding on both sides of the Adenosine bridge.

Based on the experience from SPRi experiments, the same S8 duplex and positive control (fully complementary S6 duplex) were kept to help proof of concept. As for the S5 and S6 duplexes, two different sequence designs with different binding strength were purchased in order to see the influence of binding strength. The duplexes without modification to enhance the binding started with two bases "TG" on the 5' of the SxZ strand and were named "tg-S5" or "tg-S6" for this reason. The duplexes for which we moved two "CC" bases from the 3' of the strand to its beginning of 5' to increase the binding strength were named "cc-S5" or "cc-S6". Moreover, in order to explain the benefit of using these split-aptamer based 1D DNA structures instead of the direct use of full aptamer, we also purchased full aptamer sequences corresponding to the splited aptamers. We named the aptamer from which the S6 dimers were design as A6 (short for aptamer 6). A6 was the two splited aptamers combined by the T base we removed while splitting the aptamer. A scheme of these DNA strands or duplexes were shown in **Figure 4.4**. The exact sequence could be found in the Appendix of the thesis.

4.3 UV spectroscopy for detection of Adenosine

4.3.1 The principle and internal reference of detection

In Chapter 3 we showed the melting curve of the 1D DNA chain obtained from fluorescent spectroscopy. Due to the competition between the fluorescent dye and Adenosine in the aptamer binding pockets only one peak corresponding to the hybridized oligonucleotide zip was found with fluorescent spectroscopy. As discussed in Chapter 2, the absorbance of UV was another way to determine the melting temperature of the DNA structures inside the solution since no fluorescent label was required and the formation of Adenosine bridges was not interfered. Hereby we

proposed a detection method for Adenosine using the melting profile obtained from UV spectroscopy. In Chapter 3 we already used the UV spectroscopy result as evidence that the 1D DNA chain we built existed in solution. In this section more details of these experiments will be explained and discussed.

The melting profile of the fully complementary S6 duplex was shown in **Figure 4.5** to verify our assumption that by self-assembling the 1D DNA chain through a self-repeating binding manner two melting peaks can be observed corresponding to the two different hybridized parts in the DNA chain. We observed two melting peaks in the melting curve of the fully complementary S6 duplex, the first one at 70 ℃ and the second one at 78 ℃. The two melting peaks were partly overlapped due to the small difference between the melting temperatures. This image suggested that 1D DNA chain structure will create two melting peaks corresponding to the two different bindings. While used in SPRi experiments the S5 dimers showed no signal without Adenosine and S6 dimers showed a small signal increase. And since the melting temperature represents the energy required to break the bindings, if the binding is more stable its melting temperature will be higher. In theory, the melting curve of S5 dimers without Adenosine should have only one peak corresponding to the hybridized oligonucleotide zip and two melting peaks can be observed with presence of Adenosine. In the case of S6 dimers, two melting peaks can be observed regardless the presence of Adenosine based on the SPR signal obtained without target. But the position of the first peak will be affected by Adenosine due to a change in the binding strength. These differences in the melting peaks caused by the presence of Adenosine can be used for detection purpose.

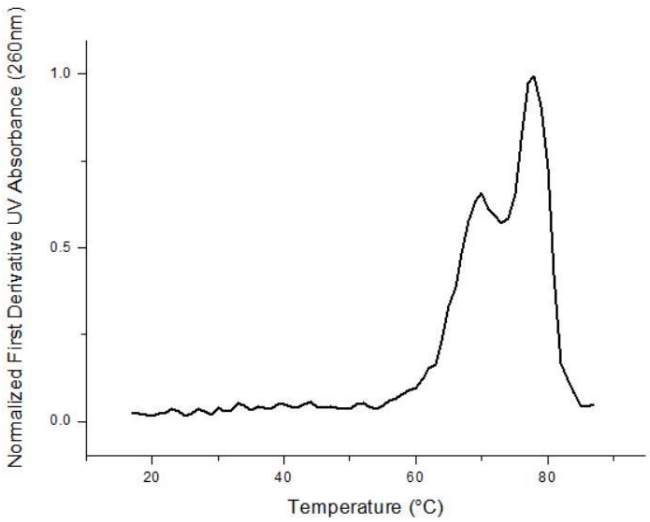

Figure 4.5 The melting profile of full complementary S6 dimers. The concentration of dimers was 0.9 μM. Two melting peaks were observed for the two hybridized parts, the first one at 70 ℃ and the second one at 77 ℃.

The melting profiles of tg-S6 dimers shown in **Figure 4.6** confirmed our theory about the change of melting peaks due to the Adenosine molecules in solution. The melting profile of its full aptamer A6 was compared in the same image. Based on the melting temperature simulation from "Mfold", the second peak in **Figure 4.6a** at higher temperature corresponded to the 24-mer hybridized oligonucleotide zip. The first peak corresponded to the Adenosine bridges. The first peak showed a clear shift in the melting temperature (6 ℃), the height of the peak was also increased. In the meantime, the second peak showed no shift in the melting temperature. On the other hand, by adding 100 μM Adenosine we observed a slight shift (less than 1 ℃) in the melting temperature of A6. The height of the peak was increased as well, but not on a large scale. This comparison between tg-S6 dimer and A6 full aptamer explained the importance of building the 1D DNA chain structure instead of using the aptamer directly for detection. In both cases the melting temperature corresponding to the Adenosine bridge shifted to higher temperature and the height of the melting peak increased. Besides the fact that the shift observed in the peaks of the 1D DNA chain was greater than the full aptamer, the more interesting benefit of using the 1D DNA

structure was the internal reference offered by the second melting peak. The melting curve of the full aptamer was influenced not only by the formation of Adenosine bridge but also differences in the buffer. Even the slight difference caused during the preparation or storage of the buffer can result in minor difference in the melting temperature measured from UV spectroscopy. The presence of Adenosine cannot be determined simply by the melting temperature of the full aptamer because the influences of other factors during the measurement were not ruled out. However, the 1D DNA chain used the difference between two melting peaks instead of the exact position of one melting peak for the detection of Adenosine. The melting temperature of the second peaks (with or without Adenosine) was the same because they were not influenced by Adenosine. The height of the peak was normalized so that the two peaks can completely overlap with each other. By comparing the heights and melting temperatures of two melting peaks obtained in the same buffer during the same measurement, the second melting peak served as an internal reference with which the influence of the buffer was ruled out.

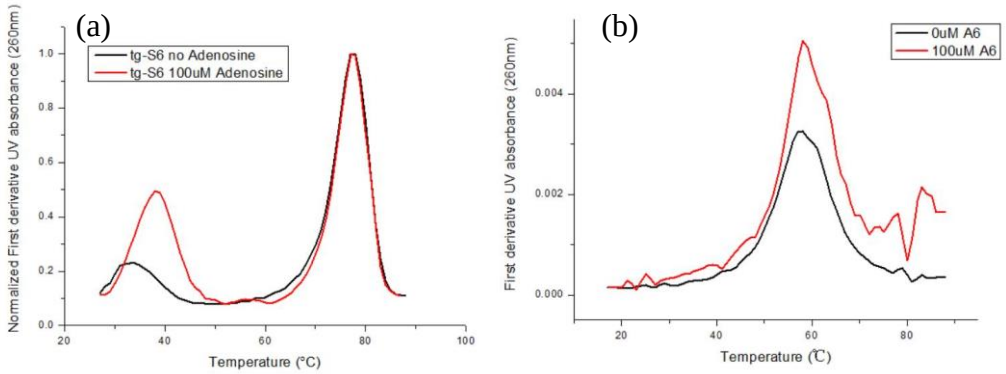

Figure 4.6 The melting profiles of tg-S6 dimers and its full aptamer sequence A6 with or without Adenosine. The concentrations of the DNA strands were 0.9 μM, the concentration of Adenosine was 100 μM. (a) the melting profile of tg-S6 dimer with and without Adenosine. Two melting peaks were observed for the duplex, the first peak on the left (around 40 ℃) correspond to the dissociation of Adenosine bridges, the second peak (78 ℃) correspond to the melting of the hybridized oligonucleotide zip. The first melting peak shifted 6 ℃ with the presence of Adenosine and the height of the peak was also increased; (b) the melting profile of A6 full aptamer with and without Adenosine. The full aptamer only had one peak and the melting temperature did not shift on a large scale (less than 1 ℃), only the increase in the height was observed.

4.3.2 Different elements affecting the melting profile

Measurement at low temperature

The melting profile of tg-S6 dimer has been shown in the last section. We performed UV spectroscopy of all the DNA structures proposed at 0.9 μM DNA concentrations in buffer without or with 100 μM Adenosine to compare the melting peaks. In the results of S6 and S8 series dimers we observed two melting peaks with good clarity in both cases with or without Adenosine. However, when it came to the measurement of melting profile of tg-S5 dimers we have encountered a problem with the low operating temperature. The result was shown in **Figure 4.7**.

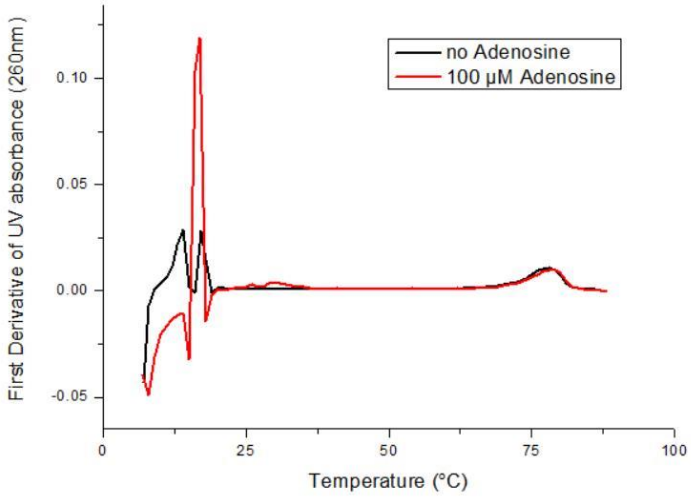

Figure 4.7 The melting profile obtained of tg-S5 dimers with and without Adenosine. The test started from 5 ℃ to 90 ℃, the concentration of the DNA was 0.9 µM, the concentration of Adenosine was 100 µM. A melting peak corresponding to the oligonucleotide zip was observed at 78 ℃, the melting curve showed great noise signal at low temperature around 10 ℃.

In the first attempt we observed only one peak correspond to the oligonucleotide zip with the presence of 100 µM Adenosine in the solution and huge amount of noise at low temperatures. The SPRi results have proven that the tg-S5 dimers can form DNA chain with Adenosine and the UV spectroscopy of other dimers have proven that we should observe two melting peaks for the 1D DNA chain structures. The problem was the low temperature from which the peak started. The noise at low temperature can be the result of two different effects: the precipitation of the solvent inside the cuvette or the condensation outside the cuvette. Therefore we proposed two methods to solve this problem, the first was to strengthen the binding in the split-aptamer dangling ends to increase its melting temperature to the detectable range and the second was to find a way to eliminate or minimize the noise when the system was operating at low temperatures.

The cc-S5 dimer was obtained after the modification on the oligonucleotide parts of tg-S5 sequences. The purpose was to move the first melting peak to higher temperature by enhancing the binding force near the Adenosine bridges. With this

modification we no longer experience difficulties in obtaining melting peaks with UV spectroscopy, however the dimer showed two melting peaks even without Adenosine due to the high binding strength. The melting curves of cc-S5 without Adenosine and with 100 μM Adenosine were compared in **Figure 4.8**. The first melting peak shifted due to the formation of Adenosine bridges but only by 2 ℃.The height of the peak has increased also. The 2 ℃ could prove the existence of Adenosine in the solution but was not considered good detecting performance. The result from this modification was not satisfying and we decided to solve the problem by improving the performance of the UV spectroscopy at low temperature.

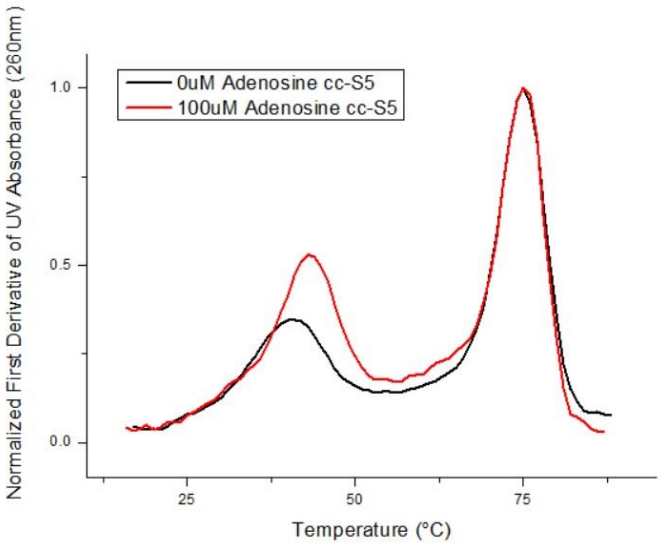

Figure 4.8 The melting profile of cc-S5 dimers with and without Adenosine. The concentration of the DNA was 0.9 μM, the concentration of Adenosine was 100 μM. Two melting peaks were observed in both experiments. The peak shifted and its height increased with the presence of Adenosine. The melting curve was smooth and with low noise.

To minimize the precipitation in the solution we added magnetic stirrers in the cuvette in the experiments of tg-S5 dimers so that the solvent was kept agitated during the heating and cooling processes. The condensation of the water in the air outside the cuvette was avoided by using an air pump to keep a circulation inside the reaction

chamber. Moreover, after the samples were loaded into the cuvette, they were placed in fridge for 10 mins so that when the cuvette was inserted into the chambers there was no initial difference between the temperature of the cuvette and the reaction chamber. Thanks to these modifications in the protocol, we were able to achieve better melting curve as shown in **Figure 4.9**. The melting profile of tg-S5 dimers gave a more intuitive result since the detection can be done by simply compare the number of the melting peaks. We observed only one peak corresponding to the oligonucleotide zip without Adenosine and two peaks with 100 μM Adenosine. Yet the noise still existed compared to the results obtained from other sequence designs, which gave a disadvantage in using S5 dimers for detection at low target concentration. The noise will increase the LoD on a large scale. It will be very promising if the noise of S5 dimers can be further decreased to have better detection limit.

Sequence design

In **Figure 4.9** the UV-Vis spectroscopies of tg-S5, cc-S5 tg-S6 and cc-S6 dimeres with and without Adenosine were displayed. The concentrations of the strands were 0.9 μM for all the experiments. Except for tg-S5 dimer without Adenosine, all other curves had two melting peaks. The second peak corresponding to the hybridization of oligonucleotide zip remained the same regardless of the concentration of Adenosine. The height of this peak was calibrated so that we can compare the height of the first peak. The tg-S5 dimer sample without Adenosine only showed one peak, this is because the binding strength for the 5 complementary bases in split-aptamer was too weak to create an isolate peak. But with Adenosine in the solution and the formation of Adenosine bridges, there was a clear peak observed at 27 ℃. The curve had more noise than the other three duplexes due the lower operating temperature.

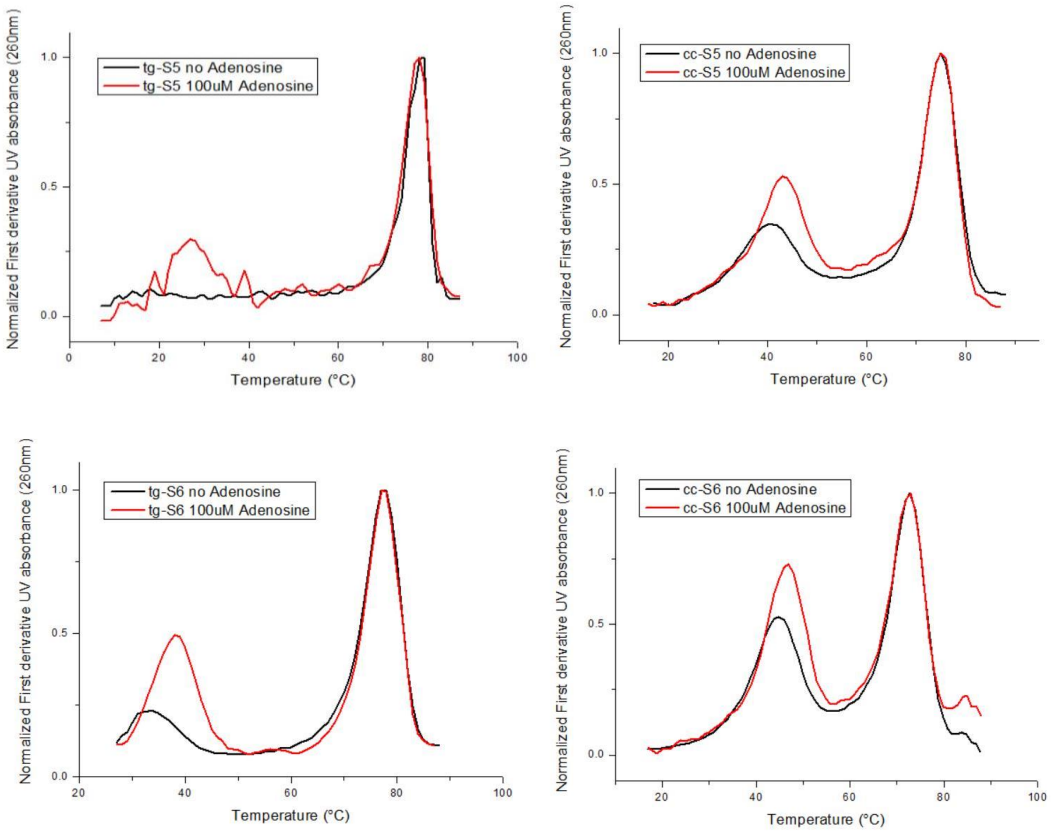

Figure 4.9 The melting profiles of tg-S5, cc-S5, tg-S6 and cc-S6 dimers with and without Adenosine. The concentration of the DNA was 0.9 μM. The concentration of the Adenosine was 100 μM. Only one peak was observed in the result of tg-S5 dimer. For other dimers the height of the second peak was calibrated to the same level, the first melting peak shifted with the presence of Adenosine and the height of the peak was increased as well.

Higher melting temperature indicated that the binding was stronger and required more energy to break. Based on the positions of the first melting peaks (P1), the strength of the binding followed the order cc-S6>cc-S5>tg-S6>tg-S5. The shift in the melting temperature was also higher for those strands with weaker bindings. The peak shifted from 34 ℃ to 39 ℃ for tg-S6 dimer, which was the biggest shift among the three duplexes, cc-S5 dimer only had 2 ℃ shift from 41 ℃ to 43 ℃. The cc-S6 dimer showed a shift from 45 ℃ to 47 ℃, the shift was same as cc-S5 dimer but at higher temperatures. The melting curve of S8 dimer was shown in **Figure 4.10**. The S8 dimers can form strong binding even without Adenosine in the solution. As a result

two peaks were observed regardless of the presence of Adenosine. The first melting peak shifted one by 1 ℃ from 52 ℃ to 53 ℃.

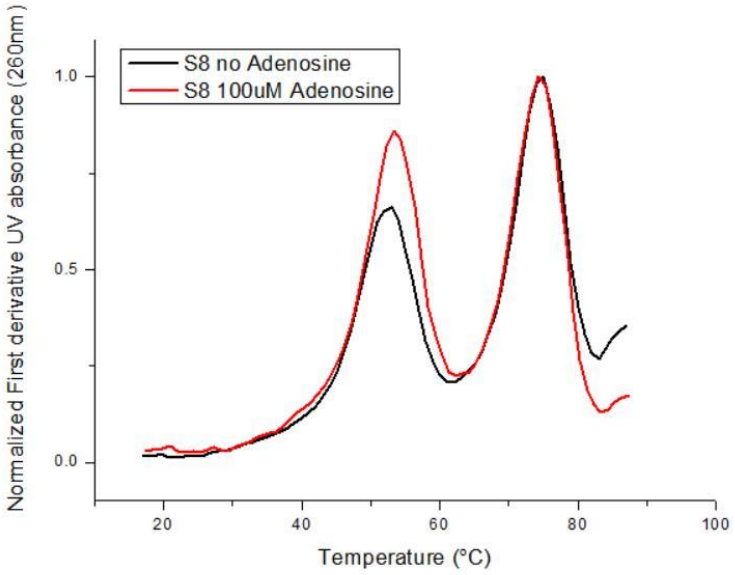

Figure 4.10 The melting profile of S8 dimers with and without Adenosine. The concentration of the DNA was 0.9 μM, the Adenosine concentration was 100 μM. Two melting peaks were observed, the second peak was calibrated and the first peak slightly shifted and the height of the peak increased with presence of Adenosine.

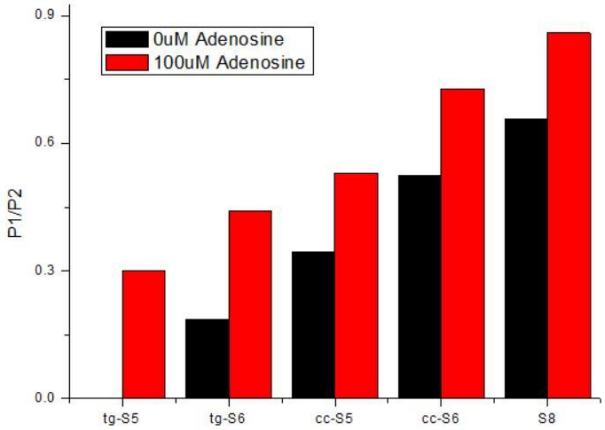

Figure 4.11 The ratio between the first melting peak corresponding to the Adenosine bridge (P1) and the second melting peak corresponding to the hybridized oligonucleotide zip (P2) for five different sequence designs. The black bars represented the samples without Adenosine and the red bars represented the samples with 100 μM Adenosine. The concentrations of the strands were 0.9 μM. S5 dimer only showed one melting peak, hereby the ratio was presented as 0.

As discussed before, not only the shift in the first melting peak corresponding to the Adenosine bridge (P1) could be used for detection purpose, the height of the peak could also be compared to determine the presence of Adenosine in the solution. In **Figure 4.11** the ratio between the heights of the first peak and the second peak were compared for the five duplexes. By comparison we drew the same conclusion that tg-S5 and tg-S6 dimers had the most noticeable difference with and without Adenosine. The other three sequence designs started with "CC" on the 5' of SxZ sequence did not have big shift in the melting temperature due to the strong binding near the Adenosine bridges. This modification has brought higher signal in SPRi experiments, but the strong binding was limiting its performance in this method by inhibiting the shift of the melting peak corresponding to the Adenosine bridges. Thus in choosing the sequences for the detection, duplexes with weaker binding such as tg-S5 dimer and tg-S6 dimer were more effective. And since tg-S5 dimer do not offer good detection limit due to the noise at low temperature, tg-S6 was chosen as the most suitable sequence design for this method.

Adenosine concentration

Having determined tg-S6 to be the best sequence design for this application, we further studied the influence of Adenosine concentration on both the height and shift of the peak. As explained in Chapter 2, the UV absorbance of the samples with Adenosine was achieved by subtracting the absorbance of reference sample (buffer + Adenosine) from the samples (buffer + DNA + Adenosine) to remove the absorbance of UV light caused by Adenosine molecules. While the sample and the reference sample were heated in two isolated chambers a gradient of Adenosine in the solution was created due to the heating. As a result the concentration of Adenosine through the light path showed turbulence. Based on the Beer–Lambert law the absorbance of UV light is proportional to the concentration of Adenosine, which means the turbulences

in the sample and its reference could create noise due to the difference in Adenosine concentration on the light path. If the concentration of Adenosine is higher than 100 μM the noise is no longer negligible compare to the absorbance of DNA structures and setting a maximum concentration of Adenosine for the UV spectroscopy at 100 μM.

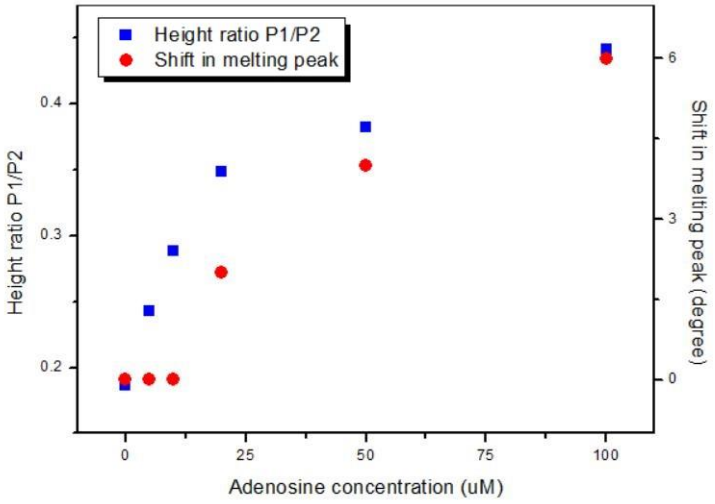

Figure 4.12 The result of tg-S6 dimer in various Adenosine concentrations (0, 5, 10, 20, 50, 100 μM). The concentration of dimers in all the samples was 0.9 μM. The ratio between the heights of two melting peaks (P1/P2) and the degrees shifted in P1 after addition of Adenosine in the environment were plotted against the Adenosine concentrations. At low concentration, the shift in the melting peak was insignificant compared to higher concentrations, whereas the ratio between the heights of the peaks was increased at a noticeable rate.

We tested the UV spectroscopy of Adenosine concentration from 0 μM to 100 μM (0, 5, 10, 20, 50, 100 μM) while the concentration of the DNA strands was kept at 0.9 μM. The results were shown in **Figure 4.12**, both the difference between the two peaks and the ratio between the heights of the two peaks (P1/P2) was plotted against the concentration of Adenosine. When the concentration of Adenosine was below 10 μM, the melting peaks showed no clear shift but the height of the peak still increased with an increase of Adenosine concentration. The melting peak shifted for 2 ℃ when the concentration of Adenosine increased to 20 μM. This shift further increased to 4 ℃ and 6 ℃ respectively when concentration of Adenosine was 50 μM and 100 μM.

The ratio between the heights of two peaks (P1/P2) increase from 0.18 to 0.35 when the concentration of Adenosine increased from 0 μM to 20 μM. This ratio continued to increase with Adenosine concentration and finally reached 0.44 with presence of 100 μM Adenosine in the solution. The increase of the ratio was more rapid at Adenosine concentrations lower than 20 μM. As the conclusion of these results, the shift in the first melting peak was only visible for solutions with more than 20 μM Adenosine. The detection of Adenosine molecules can be achieved by measuring the difference between the two melting temperatures if Adenosine concentration is higher than 20 μM. Meanwhile the detection could also be done by comparing the ratio between P1 and P2 regardless of the concentration of Adenosine because an increase in the height of the peak can be observed.

Difference of buffer

The benefit of the internal reference in our model was that the result will no longer be influenced by the difference in the buffer. We designed experiments to prove this point by comparing the UV-Vis spectroscopy with different buffers. To begin with, we tried to use buffer with same preparation protocol but not in the same batch and not on the same day. For the first test, the two peaks were at 33 ℃ and 77 ℃ without Adenosine. The first peak shifted to 38 ℃ with 100 μM of Adenosine in the solution. The value of all the peaks had 1 ℃ difference in the second test, the peaks without Adenosine were at 34 ℃ and 78 ℃, the peak shifted to 39 ℃ with 100 μM of Adenosine in the solution. Different buffers may result in different melting temperatures measured, but the difference between the two peaks remained the same. The result supported our claim that the internal reference is an important element enabling the detection of Adenosine regardless of the minor difference produced in the preparation of the buffer.

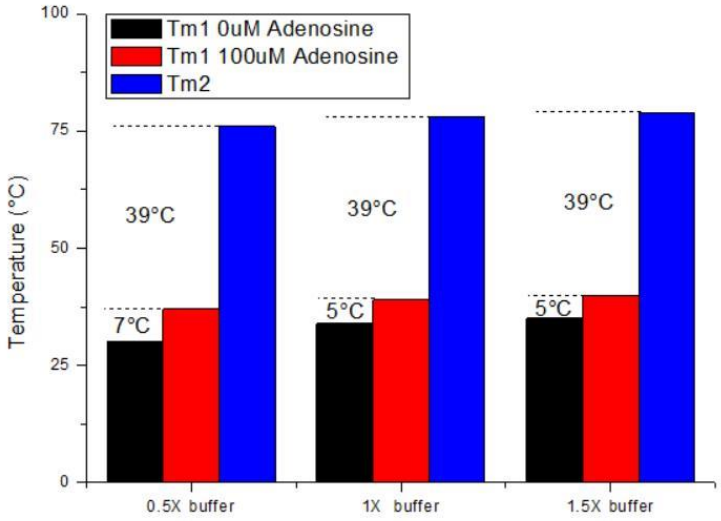

Figure 4.13 The melting peaks of tg-S6 dimer with different dilution of buffer. The concentrations of the DNA were 0.9 μM. The second melting peak (Tm2) kept the same for each buffer concentration and the first melting temperature (Tm1) was different based on the presence of Adenosine. Tm1 shifted 7°C for the sample 0.5X buffer and the other two shifted 5°C. The difference between Tm1 with 100 μM Adenosine and Tm2 was kept at 39°C for all three samples.

Furthermore, we diluted the buffer to see how the different salt concentration can affect the melting profiles. The 10X buffer was diluted into three different concentrations: 0.5X buffer, 1X buffer and 1.5X buffer. Six samples with different concentration of Adenosine and buffer were prepared. The first melting peak corresponding to the Adenosine bridge without Adenosine (Tm1 0uM), with 100 μM Adenosine (Tm1 100 μM) and the second melting peak corresponding to the oligonucleotide zip (Tm2) were listed in the same image in **Figure 4.13**. From the image we observed that no matter what concentration the buffer was, with presence of 100 μM Adenosine in the solution the difference between two melting peaks was kept at 39 ℃. The exact values of these melting peaks were not the same which suggested the measurement of melting temperature was affected by the concentration of salt in the buffer but the detection was still reliable thanks to the internal reference. We further noticed that the difference between the two melting peaks without Adenosine for these three buffers were 41 ℃ (0.5X buffer) or 39 ℃ (1X buffer and 1.5X buffer).

The bigger difference between the two peaks suggested that the binding strength was weaker in the case of 0.5X buffer without Adenosine. The reason was the lack of salt led to unsaturated formation of Adenosine bridges in the solution, whereas the other two buffers offered enough salt to saturate the formation of Adenosine bridges. Thus the internal reference can rule out the influence caused by the differences in the buffer, but the salt concentration need to be high enough to saturate the formation of Adenosine bridges.

DNA Strand concentration

The quality of the UV absorbance spectrum is related to the total amount of nucleobases in the solution. To achieve melting curve with less perturbation the concentration of DNA is ideal around 20-25 ng/μL. In the case of our 1D DNA chain structure, the best concentration of DNA strands for these experiments was 0.9 μM. Still we carried out a series of test to study the influence of DNA strand concentration. In **Figure 4.14** we showed the melting profile of solution prepared with same buffer and Adenosine concentration at 100 μM with four different concentrations of the tg-S6 dimer. The tests were not carried out under ideal DNA concentrations and the results contained noise. This noise was reduced by smoothing the curve with Savitzky–Golay filter. [16] The Savitzky–Golay filter did not change the position of the peaks and had no effect on the melting temperatures, but the height of the peaks were changed and the P1/P2 ratio was not as informative compared to the raw data.

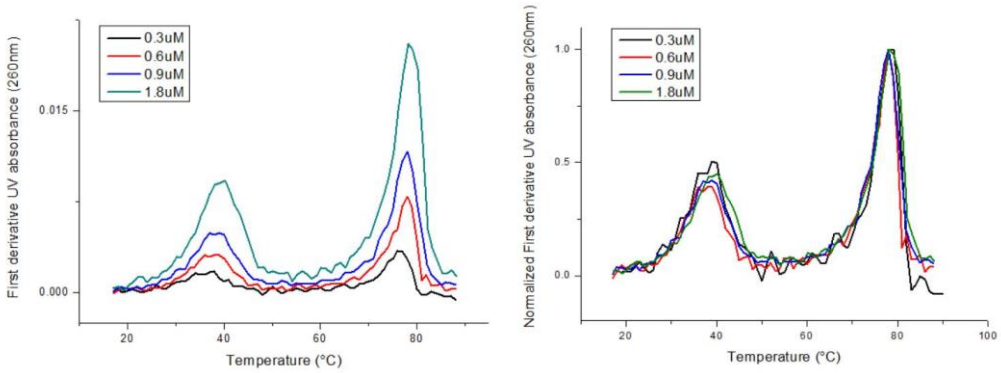

Figure 4.14 The spectroscopy of tgS6 dimer with 100 μM Adenosine in the solution. The concentration of the DNA duplex was changed from 0.3 μM to 1.8 μM. (a) the spectroscopy without calibration of the second peak. The heights of the peaks were increased with higher strand concentration. (b) The spectroscopy after calibration, the heights of the peaks were similar with small difference that are caused by the noise due to the imperfect strand concentrations.

The left image in **Figure 4.14** was the melting curve before calibration of the height of the second peaks. The two melting peaks exhibited a very small shift with the change of strand concentrations. On the other hand, the height of the peak has increased a lot with higher strand concentration. The heights of both peaks were increased with the Adenosine concentrations. By comparing the melting profile after the calibration of the second peak in the right image, we noticed the heights of the first peaks were similar to each other. The height of the peak did not show a clear relationship with the concentration of the strand, the difference was possibility the result of the noise caused by the imperfect strand concentration. The P1/P2 ratio obtained from curve smoothed with Savitzky–Golay filter was not a precise description of the melting profile. The conclusion we can draw from this image was that the concentration of the DNA strands affect the melting temperature and height of first melting peak in a limited range.

Heating-cooling protocol

We faced two difficulties while developing a protocol having a good balance in the accuracy, duration, resolution and repeatability. The first problem was the evaporation of the sample during the heating process and the second problem was the difference in the melting curve obtained in the heating and cooling processes. The 1.5 mL cuvette was filled with 1 mL of sample and the solution was evaporated during the heating process. Water droplets were formed on the inner wall of the cuvette above the solution, the concentration of the solution was increased due to the evaporation and as a result the absorbance of the UV was changed. In **Figure 4.15** the UV absorbance of same tg-S6 dimer sample during the heating processes of four heating-cooling cycles was displayed. The absorbance has increased slightly after each cycle, which suggested that the solution was more condensed due to the evaporation of water.

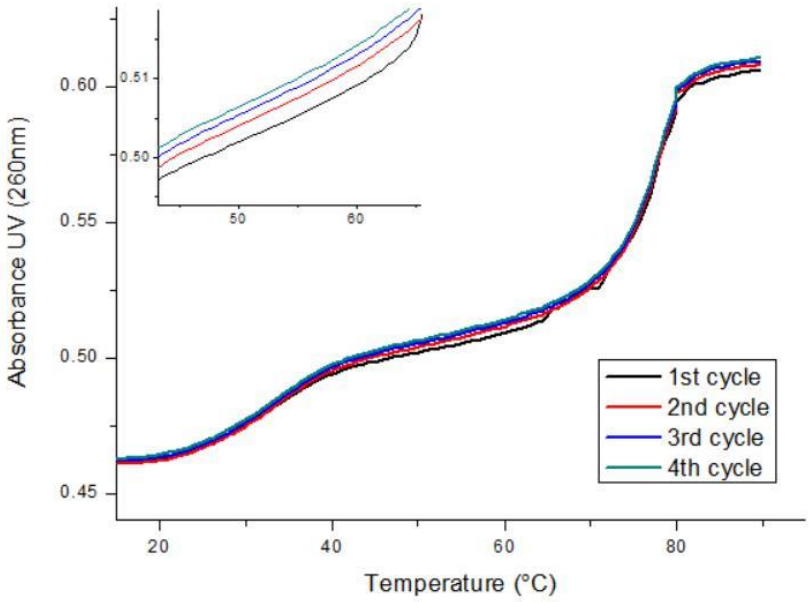

Figure 4.15 The UV absorbance of tg-S6 dimer in four heating processes during a 4-cycle analysis. The concentration of DNA was 0.9 μM, no Adenosine was presented. A closer look was offered in the window, value of the absorbance increased in small amount after each cycle.

Our attempt in filling the cuvette completely with sample solution and seal the cap with Para film to avoid evaporation was not successful. The volume of the solution was increased due to the raising temperature and the sample was overflowing outside the cuvette. Another method testd to minimize the effect of evaporation was to alter the heating protocol. The sample was heated at 1 ℃/min at temperatures below 80 ℃ and the heating rate was increased to 2 ℃/min so that the sample will spend less time at high temperature and in return reduce the effect brought by evaporation. The cooling rate during the cooling process was thus set at 2 ℃/min between 80 ℃ and 90 ℃ and 1 ℃/min at temperature below 80 ℃.

The heating and cooling rate influence the result not only in the evaporation but also in a difference between the heating and cooling process. The heating rate below 80 ℃ was programmed at 1 ℃ /min so that the four cycles of heating-cooling can be finished within 10h. In **Figure 4.16** we showed a 4-cycle heating-cooling spectroscopy of tg-S6 dimer with good repeatability and 2 ℃ difference in the heating and cooling was observed.

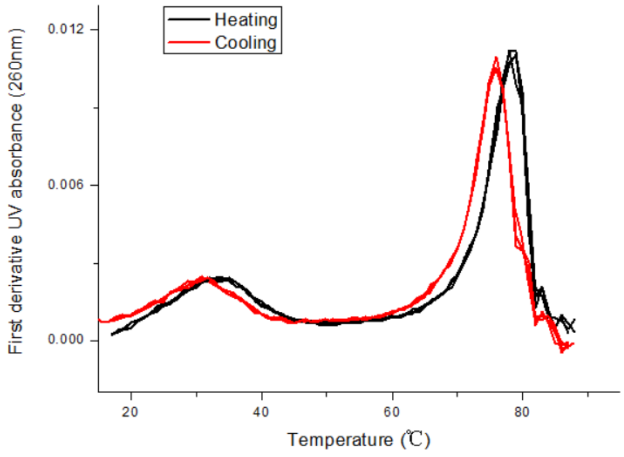

Figure 4.16 The four-cycle heating-cooling spectroscopy of 0.9 μM tg-S6 dimer without Adenosine. The two cycles showed good repeatability but the melting temperature obtained from the cooling process was 2°C lower than the melting temperatures obtained from the heating process. The difference was caused by the delay in the measurement.

The difference between the melting curve obtained from the heating and cooling processes was due to non-equilibrium in the hybridization-denaturation transition or formation of the Adenosine bridges. In **Figure 4.17** we showed a closer look at the melting peak corresponding to the oligonucleotide zip. A hypothetical melting curve (blue dash line) was added between the melting curves obtained from tg-S6 dimers during heating and cooling processes. We assume the hypothetical melting curve represented the real melting temperature of the oligonucleotide zip. While the sample was heated to 77 ℃ it will take around 1 min for 50% of the duplexes to be denatured into single strands (by definition of the melting temperature of DNA). As a result, when 50% of the duplexes were melted the temperature of the sample was already increased to 78 ℃ the UV absorbance suggesting that half of the duplexes were dissociated and the melting peak obtained during heating process was measured at 78 ℃. For similar reason, when the sample was cooled down 50% of the single strands started to hybridize into duplexes at 77 ℃ but by the time it was finished the temperature was already decreased to 76 ℃. This explained the 2 ℃ difference between the melting curves obtained during the heating and cooling processes.

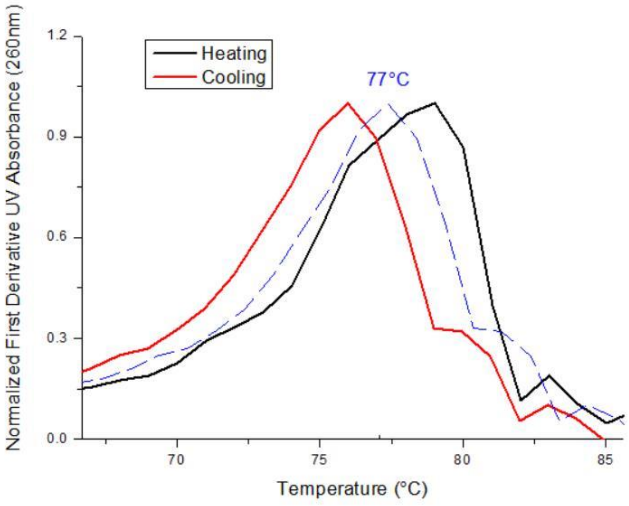

Figure 4.17 The details of the peaks obtained from heating and cooling process and corresponding to the oligonucleotide zip in 0.9 μM tg-S6 dimers without Adenosine. The two melting peaks had 2 ℃ difference. A hypothetical melting curve (blue dash line) was added in the middle of the two melting curves.

Thanks to the internal reference, this 2 ℃ difference between the heating and cooling did not have any impact on the detection. But still we offered a way to eliminate this difference. **Figure 4.18** presented the UV spectroscopy obtained at a heating/cooling rate of 0.2 ℃/min. After the absorbance was measured for each spot the solution was kept at the same temperature for 1 min before the heating or cooling continued. No difference between the heating and cooling peaks was discovered since we provided enough time for the DNA strands while changing structures but the experiment took much more time compared to the original heating/cooling rate. Another effect on changing the heating rate was having more spots in the curve and had a more detailed curve. But the oscillations in the first derivative plot were also amplified and increased the noise in the curve due to the long waiting time. How to decrease the noise while maintain good resolution and precision of the melting curve will be a vital part in the future studies.

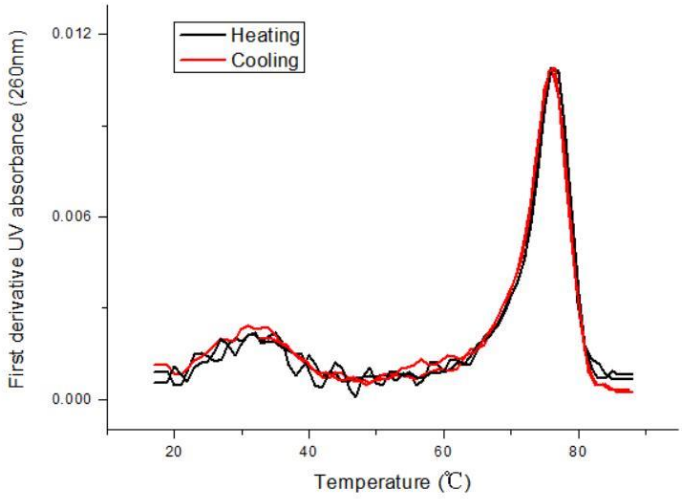

Figure 4.18 A two-cycle heating-cooling spectroscopy of 0.9 μM tg-S6 dimer without Adenosine at slow heating rate. No difference was observed between the melting curves obtained from the heating and cooling processes. The melting curves had more noise at low temperature range.

4.3.3 Selectivity and detection limit

Same as our SPRi experiments, Guanosine was used as negative control to verify the selectivity of the sensor. In **Figure 4.19** the three melting curves of tg-S6 dimer without any target and tg-S6 dimers with 100 µM Adenosine or 100 µM Guanosine were compared. As a result, the three melting curves all showed two melting peaks. The melting curves of tg-S6 dimer without target and with 100 µM Guanosine were similar, indicating the presence of Guanosine will not affect the position nor the intensity of the peaks. In comparison, the first melting peak observed for the sample with 100 µM Adenosine further confirmed the good selectivity of this method.

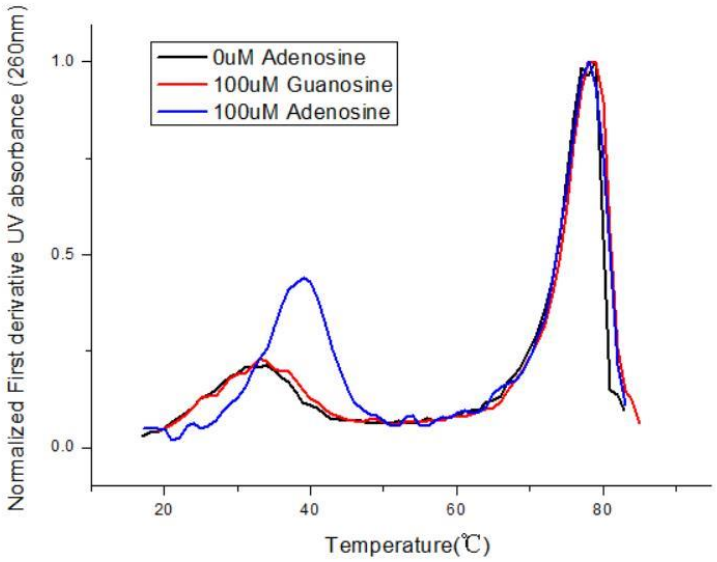

Figure 4.19 The melting curves of 0.9 µM tg-S6 dimer with 100 µM Guanosine, 100 µM Adenosine and with no target molecule (Adenosine or Guanosine) to verify the selectivity of the detection. All of the three curves showed two melting peaks, the second melting peak was calibrated. The first melting peaks for sample without target and 100 µM Guanosine showed small difference, the first melting peak of sample with 100 µM Adenosine shifted to higher temperature and had higher intensity.

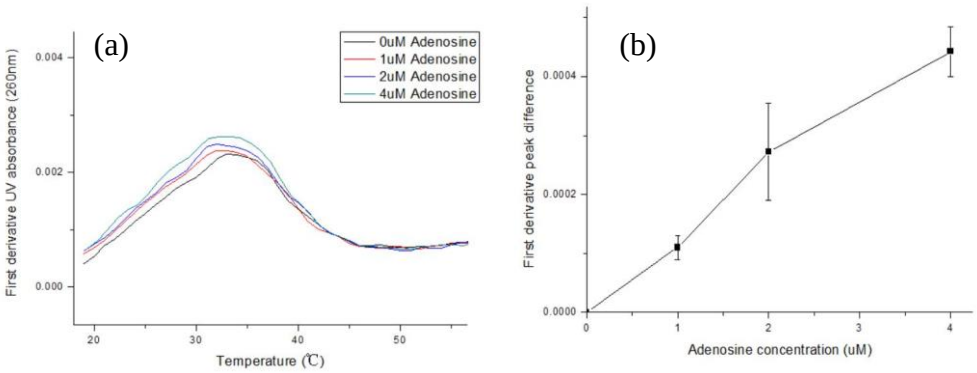

Figure 4.20 The detection limit of the detection: (a) The first melting peak of 0.9 μM tg-S6 dimer at low concentrations of Adenosine (0-4 μM), the height of the peak was increasing with the increase of Adenosine concentration. (b) The increase in the height of melting peak (P_x-P_0) plotted against Adenosine concentration with error bar. The signal/noise ratio can be calculated and was larger than 3.

To find the limit of detection (LoD) of this sensing method we made repeated heating-cooling cycles at low concentration of Adenosine and calculated the error bar. As mentioned before, the absorbance was influenced by the evaporation of solvent between each cycle. The improvement in the heating-cooling process reduced its influence but the difference between each cycle still existed. Despite these differences, the heights of the first peaks increased in all the cycles with the increase in Adenosine concentration (**Figure 4.20a**). The maximum of each peak corresponding to the Adenosine bridge was recorded and compared. A value ΔP was calculated with **Equation 4.1**.

$$\Delta P = P_x - P_0 \qquad \textbf{Equation 4.1}$$

Whereas P_x was the peak value for the curve with Adenosine in the buffer, the concentration was x μM, P_0 was the peak without Adenosine in the buffer. The calculation of ΔP allowed us to determine the LoD without the influence of the evaporation. This value represented the height of peak increased with the addiction of Adenosine and was defined as the signal of the detection. While the error bar of ΔP represented the perturbation in the signal and was the noise of the detection system. In other words the signal-noise ratio can be determined for the calculation of LoD. The

ΔP for each cycle was collected and its error bar was calculated and displayed in **Figure 4.20b**. The value of ΔP for these concentrations all exceeded 3 times the error bar, making the detection valid at relatively low Adenosine concentration (1 μM), the LoD of this method was close to 1 μM. This LoD is one order of magnitude lower than the LoD we determined for SPRi detection.

4.4 Conclusions

As discussed before, current methods using aptamers directly in solution had the limitations of strong dependence on fluorescent labels or Au NPs. These limitations cost more preparation procedures, time and money for the detection. UV-Vis spectroscopy was a supplementary method in some researches to help analyses the structure or status of DNA in the solution, but yet has not been often used directly for detection purpose. Our method using the UV-Vis spectroscopy of 1D DNA chain structure combining oligonucleotide and split-aptamer for detection of Adenosine has been proven effective. We have found solutions for difficulties encountered while using this method for detection, such as the evaporation of solvent and the operation at low temperature. Five different dimers were tested for their melting profiles and two of them (tg-S5 and tg-S6) were considered appropriate for detection purpose. The tg-S5 dimers showed only one melting peak corresponding to the oligonucleotide zip without the presence of Adenosine, and a new peak corresponding to the Adenosine bridges was observed with presence of Adenosine. The drawback of this sequence was the requirement of operating the system at low temperature. We have improved the protocol to minimize the influence of the low temperature but there was still room for improvement in reducing the noise and lowering the LoD. The tg-S6 dimers showed good selectivity and low noise level in detection, for these reasons this dimer was considered the optimized choice for detection. Two peaks were observed both

with and without Adenosine. After calibration of the second peak, the height of the first melting peak and its melting temperature could be used for the detection of Adenosine. The second melting peak served as an internal reference which eliminated the influence of changes in the buffer and environment and improved the accuracy of the detection. The detection can be simply achieved by measuring the difference between two different melting peaks at high target concentrations. The heights of the first peaks can be compared for detection at concentration of Adenosine below 20 μM. The method reached a detection limit of 1 μM, which was lower than the K_D of the aptamer (6 ± 3 μM). [17,18]

Reference

1. Taton, T. Andrew, et al. "The DNA-mediated formation of supramolecular mono-and multilayered nanoparticle structures." ***J Am Chem Soc*** 122.26 (2000): 6305-6306.

2. Storhoff JJ, Lazarides AA, Mucic RC, Mirkin CA, Letsinger RL, Schatz GC. What controls the optical properties of DNA-linked gold nanoparticle assemblies? ***J Am Chem Soc***. 2000;122(19):4640-4650. doi:10.1021/ja993825l.

3. Tomaszewska E, Soliwoda K, Kadziola K, et al. Detection limits of DLS and UV-Vis spectroscopy in characterization of polydisperse nanoparticles colloids. ***J Nanomater***. 2013;2013. doi:10.1155/2013/313081.

4. Cao YC, Jin R, Thaxton CS, Mirkin CA. A two-color-change, nanoparticle-based method for DNA detection. ***Talanta***. 2005;67(3):449-455. doi:10.1016/j.talanta.2005.06.063.

5. Xia F, Zuo X, Yang R, et al. Colorimetric detection of DNA, small molecules, proteins, and ions using unmodified gold nanoparticles and conjugated polyelectrolytes. ***Proc Natl Acad Sci U S A***. 2010;107(24):10837-10841. doi:10.1073/pnas.1005632107.

6. Hu YJ, Liu Y, Wang JB, Xiao XH, Qu SS. Study of the interaction between monoammonium glycyrrhizinate and bovine serum albumin. ***J Pharm Biomed Anal***. 2004;36(4):915-919. doi:10.1016/j.jpba.2004.08.021.

7. Kandagal PB, Ashoka S, Seetharamappa J, Shaikh SMT, Jadegoud Y, Ijare OB. Study of the interaction of an anticancer drug with human and bovine serum albumin: Spectroscopic approach. ***J Pharm Biomed Anal***. 2006;41(2):393-399. doi:10.1016/j.jpba.2005.11.037.

8. Hu Y-J, Liu Y, Zhao R-M, Dong J-X, Qu S-S. Spectroscopic studies on the interaction between methylene blue and bovine serum albumin. ***J Photochem Photobiol A Chem***. 2006;179(3):324-329. doi:10.1016/j.jphotochem.2005.08.037.

9. Li N, Ma Y, Yang C, Guo L, Yang X. Interaction of anticancer drug mitoxantrone with DNA analyzed by electrochemical and spectroscopic methods. ***Biophys Chem***. 2005;116(3):199-205. doi:10.1016/j.bpc.2005.04.009.

10. Zhang J, Chen L, Zeng B, Kang Q, Dai L. Study on the binding of chloroamphenicol with bovine serum albumin by fluorescence and UV-vis spectroscopy. ***Spectrochim Acta - Part A Mol Biomol Spectrosc***. 2013;105:74-79. doi:10.1016/j.saa.2012.11.064.

11. Xue, Xuejia, Feng Wang, and Xiaogang Liu. "One-step, room temperature, colorimetric detection of mercury (Hg2+) using DNA/nanoparticle conjugates." ***J Am Chem Soc*** 130.11 (2008): 3244-3245.

12. Xu X, Daniel WL, Wei W, Mirkin CA. Colorimetric Cu2+ detection using DNA-modified gold-nanoparticle aggregates as probes and click chemistry. ***Small***. 2010;6(5):623-626. doi:10.1002/smll.200901691.
13. Song KM, Cho M, Jo H, et al. Gold nanoparticle-based colorimetric detection of kanamycin using a DNA aptamer. ***Anal Biochem***. 2011;415(2):175-181. doi:10.1016/j.ab.2011.04.007.
14. Li H, Rothberg L. Colorimetric detection of DNA sequences based on electrostatic interactions with unmodified gold nanoparticles. ***Proc Natl Acad Sci U S A***. 2004;101(39):14036-14039. doi:10.1073/pnas.0406115101.
15. Li L, Li B, Qi Y, Jin Y. Label-free aptamer-based colorimetric detection of mercury ions in aqueous media using unmodified gold nanoparticles as colorimetric probe. ***Anal Bioanal Chem***. 2009;393(8):2051-2057. doi:10.1007/s00216-009-2640-0.
16. Schafer R. What Is a Savitzky-Golay Filter? [Lecture Notes]. ***IEEE Signal Process Mag***. 2011;28(4):111-117. doi:10.1109/MSP.2011.941097.
17. Andr é C, Xicluna A, Guillaume YC. Aptamer-oligonucleotide binding studied by capillary electrophoresis: Cation effect and separation efficiency. ***Electrophoresis***. 2005;26(17):3247-3255. doi:10.1002/elps.200500170.
18. Huizenga DE, Szostak JW. A DNA aptamer that binds adenosine and ATP. ***Biochemistry***. 1995;34(2):656-665. doi:10.1021/bi00002a033.

Chapter 5 Detection of Adenosine with 2D and 3D DNA structures

Dans ce chapitre, nous avons mis au point des structures d'ADN plus complexes en deux ou trois dimensions et validé leurs applications dans la détection des molécules d'adénosine. Une architecture 2D basée sur une jonction à trois voies en forme de Y et un assemblage 3D de type tétraèdre d'ADN ont été décorés avec des extrémités simples brins pendantes conduisant à un changement de structure en présence d'adénosine. Contrairement à la chaîne 1D obtenue en reliant les dimères par les extrémités, un large réseau d'ADN peut être formé à partir de ces briques élémentaires d'ADN 2D et 3D. Ces deux structures d'ADN ont été testées en utilisant les deux méthodes de détection rapportées aux chapitres 3 et 4. Les principaux résultats ont été exposés dans ce chapitre ainsi que des suggestions d'améliorations futures.

5.1 The construction of 2D and 3D DNA structures

5.1.1 Introduction

In Chapter 3 and 4 we described a 1D chain DNA structure built for the detection of Adenosine. By introducing this 1D structure we developed two detection methods that depend on neither Au NPs nor fluorescent label to create noticeable signal for detection of Adenosine. To further explore the potential of these detection methods, we designed 2D and 3D structures that are more complex in sequence design and have the possibility to form network through the split-aptamer dangling ends. DNA origami offers a "bottom-up" approach for fabrication of complicated DNA structures with good precision. [1–4] DNA has been proven to be a reliable building blocks for simple structures like Holliday junctions [5] and cubic cage [6], or complex structures such as aperiodic 2D nano-patterns, two-dimensional crystals [7,8], nanotubes [9–13], and three-dimensional wireframe nanopolyhedra [14–17], etc. The challenge remains in how to overcome the conformational flexibility of branched DNA structures. In the past two decades, a series of structural motifs have been reported to help stabilize the DNA structure. [18–20] A long DNA single strand known as the scaffold is folded into the desired structure with these motifs. Each motif is specially designed to bind different places in the scaffold. In earlier studies, the constructions of DNA structures were assembled by multiple short DNA oligonucleotides. The manufacture of DNA structures enables the design and fabrication of many devices. The improvement made in the field of DNA origami provided more versatility in sophisticated devices bearing features on the nanometer scale. The most appealing advantage of DNA origami is its experimental simplicity and fidelity of the folding process. The traditional way of assembling DNA structures with multiple single strands requires very precise stoichiometry and purification of individual oligonucleotides. By folding the scaffold with short staple strands DNA origami alleviated the stoichiometry concerns. Moreover, the staple strands can be synthesized without additional purification. [21] The strands can be chemical modified to introduce new functionalities into the DNA structure.

In Chapter 1 we already gave examples of complex 2D DNA structures formed by DNA origami technique (**Figure 1.15**). The application can be further extended to 3D domains. According to the paper published by Kjems, Gothelf and their coworkers, the extension from two-dimensional structures to three-dimensional structures could be done by connecting several planar origami sub-structures at the edge. [22] Each plane holds an angle to its adjacent planes to form the 3D super structure. The structures formed by this approach are hollow structures, whereas Shih reported another approach that forms dense 3D structures by parallel arrangement of helices into a honeycomb lattice. [23] This method is generally more applicable but has lower yield and is more time consuming. The yield of this method was improved by the same group in the following work. They reported a more compact design in which layers of helices packed on a square lattice to form 3D origami. [24] The examples of the 3D structures formed by these two approaches were shown in **Figure 5.1**.

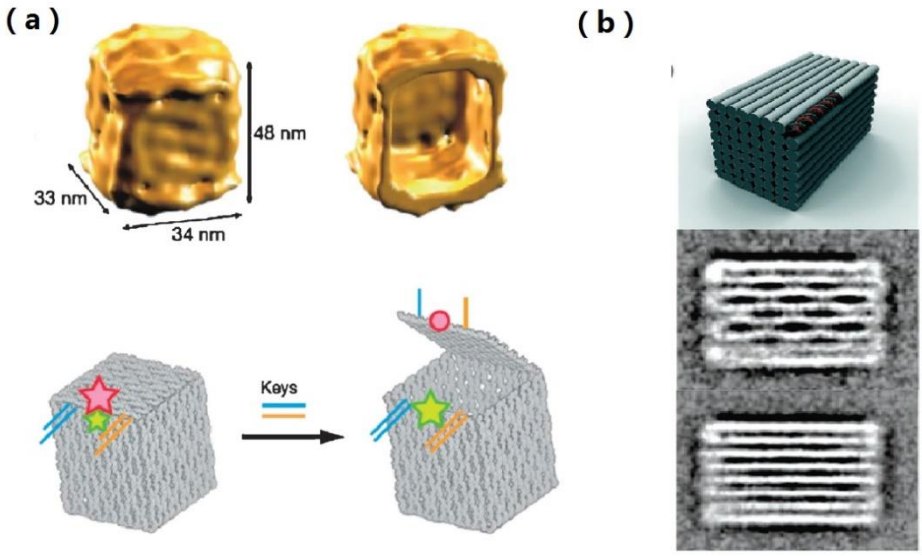

Figure 5.1 The 3D DNA structures form by two different approaches. (a) 3D box structures formed by adjacent planes and fixed with DNA keys. The cryo-TEM image showed a clear cavity in the structure, indicating a hollow structure. (b) 3D structure formed by stacking layers of helices on square lattice. The structure is dense compared to the first approach. [22,23]

In this study we proposed to use DNA structures to free the detection methods from the limitations of Au NPs or fluorescent label. The DNA structures were combined with split-aptamer dangling ends to introduce a controlling element that can alter the DNA structure with the concentration of Adenosine. In the beginning of our exploration to this new field, we decided to build less complicated DNA structures that could be formed with multiple single strands through self-assembly. The sequence design and DNA structures will be discussed in the following sections. Another interest in the DNA structures we proposed is the possibility to form a network of DNA through the connection of Adenosine bridges. Cooperativity effect is common during phase transitions of large chain molecules made of many identical or near-identical subunits. It is a phenomenon that the subunits are acting dependently on each other and creating an influence on its performance. In our case, we assume the multiple hybridization process forming the 2D three-way junction or 3D tetrahedron will have a chance in achieving better results due to this effect. [25,26]

5.1.2 Sequence design of 2D DNA structure

The Y shape structure we built was a 2D DNA three-way junction structure formed by three DNA single strands. A similar Y shape DNA structure formed by oligodeoxynucleotides was reported by Nishikawa et al. [27] The Y shape DNA structure leaves three branches where split-aptamer dangling ends could be added. Wang et al reported a detection method using a similar Y shape DNA structure. The Au NPs were firstly asymmetrically functionalized with PEG and oligonucleotides (probe 1 and 2). In the presence of a linker oligonucleotide containing the aptamer sequence, the two probes formed the Y shape DNA structure. Due to the asymmetric functionalization the majority of the Au NPs will form into dimers. This process came with a change in the color from red to blue. The stability of the sensor was greatly increased because of the controlled formation of Au NP dimers instead of big

aggregates. With the presence of the target, the linker will fold with the target and break the Au NP dimers, the color of the solution changed from blue to red for detection.

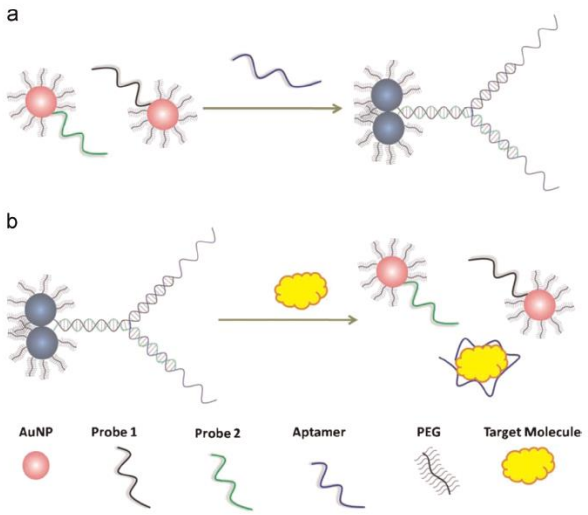

Figure 5.2 The scheme of a biosensor using a DNA three-way junction, (a) probe 1 and 2 were functionalized on Au NPs, with the aptamer linker, it will form a three-way junction and force the gold nanoparticles to form Au NP dimers and change the color of the solution from red to blue. (b) The linker will fold with the target and the Au NP dimers will break and change the color of solution from red to blue. [27]

The Y shape structure was developed from the DNA structures reported by Leontis. [28] The variations of Y shape sequence designs are shown in **Figure 5.3**, the number of split-aptamer dangling ends could be controlled by varying the strands mixed in the DNA solution. The original Y structure had no dangling ends. By changing the mixture of strands we built other Y shape structures with one and three split-aptamer dangling ends. The Y shape DNA with one dangling end could interact with the corresponding splited aptamer probes functionalized on the gold surface, while the Y shape DNA with three dangling ends could first form a network by connecting these dangling ends in the solution before they interact with the probes on gold surface. As discussed in Chapter 3, we used three different aptamers and their splits for the detection of Adenosine. Among the three sets of split-aptamer, the S8 split-aptamers will form binding regardless of the presence of Adneosine. S5 and S6

split-aptamers could be used for detection but they both have its flaws. The shortcoming of S6 split-aptamers was that a small portion of the splits can be binded without Adenosine. The S5 split-aptamers were free from this problem, in other words, no binding was detected without the presence of Adenosine. However the limitation of S5 lies in the low signal achieved due to the weak binding. Thus we decided to start the experiments with S6 split-aptamer as the dangling end to make sure the binding is strong enough to form the network of 2D DNA structures. Once the protocol for building these structures and protocols of detection have been improved, the split-aptamer dangling ends could be switched to S5 split-aptamer to achieve higher signal-noise ratio.

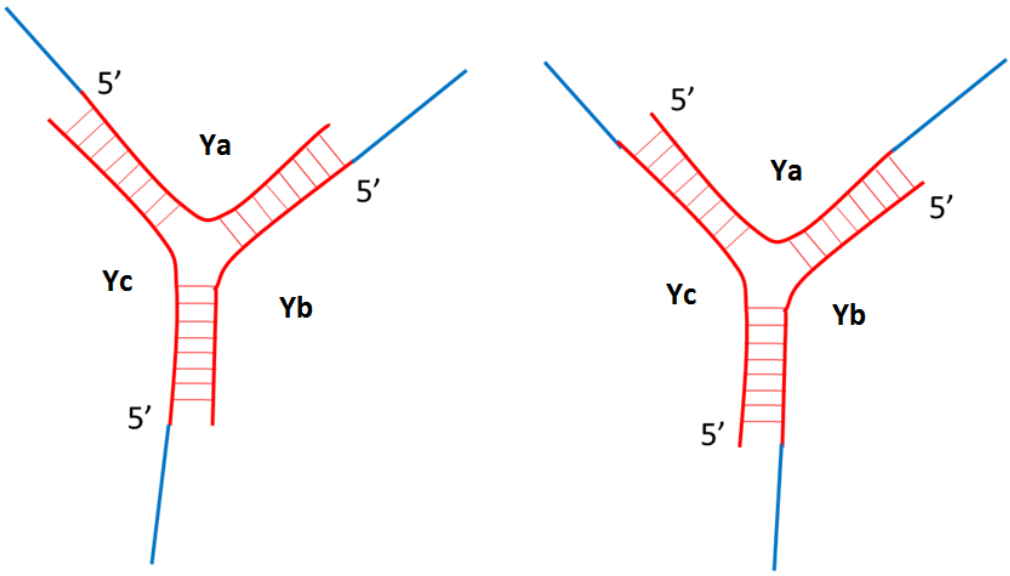

Figure 5.3 the two possible ways to attach the three split-aptamers to form a network of 2D Y shape DNA structure. The original Y structure was hybridized by three strands (the red color Ya, Yb and Yc). In order to form binding between the "Y"s, split-aptamer dangling ends can be added to the 5' or 3' positions as shown in the image. The number of the split-aptamer added can be controlled by switching the sequences.

Same as the 1D chain structure, the sequence design of the Y shape requires a melting profile simulation to select the most suitable structures. There are six possible

positions to add the split aptamer dangling ends (**Figure 5.3**): the 5' and 3' end of the three branches forming the Y shape. Considering the fact that there are two splited aptamer dangling ends and the Y shape is formed by three strands, the possible combinations to form a Y shape DNA structure with three dangling ends were listed in **Table 5.1**. Each combination contained three strands (Strand A, Strand B and Strand C). These three strands consisted of two parts: the oligonucleotide forming the framework of the Y (Ya, Yb, Yc) and split-aptamer (S6 and S6*). If the sequence starts with S6 on its 5' and finishes with Ya on its 3', then it is named S6Ya. Twelve possible combinations were listed and their melting profiles were shown in **Table 5.2**.

Design	Strand A	Strand B	Strand C
1	S6*Ya	S6Yb	S6Yc
2	S6*Ya	S6Yb	S6*Yc
3	YaS6	YbS6*	YcS6
4	YaS6*	YbS6*	YcS6
5	S6Ya	S6*Yb	S6Yc
6	S6Ya	S6*Yb	S6*Yc
7	YaS6	YbS6	YcS6*
8	YaS6*	YbS6	YcS6*
9	S6*Ya	S6*Yb	S6Yc
10	YaS6	YbS6*	YcS6*
11	S6Ya	S6Yb	S6*Yc
12	YaS6*	YbS6	YcS6

Table 5.1 The 12 possible combinations of different Strand A, B and C forming a Y shape DNA structures with three split-aptamer dangling ends

Design	Strand A+B	Strand B+C	Strand A+C	Strand A	Strand B	Strand C
1	60.3	51.7	55.8	57.4	60.2	65.8
2	60.3	51.7	56.4	57.4	60.2	59.2
3	59.6	51.3	55.8	59.6	53.2	51.3
4	59.6	51.3	55.8	57.4	53.2	51.3
5	59.7	52.5	55.8	58	53.2	65.8
6	59.7	52.5	56.4	58	53.2	59.2
7	59.3	51.6	55.8	59.6	56.7	59.2
8	59.3	51.6	55.8	57.4	56.7	59.2
9	60.3	52.5	55.8	57.4	53.2	65.8
10	59.6	51.6	55.8	59.6	53.2	59.2
11	59.7	51.7	56.4	58	60.2	59.2
12	59.3	51.3	55.8	57.4	56.7	51.3

Table 5.2 The sequence designs of 12 possible Y structures with three dangling ends and their melting temperature simulations. Each design contained Strand A, B and C to form the framework of the Y shape, depending on the position and sequence of the split-aptamer dangling ends, each strand had 4 possible choices. There were 12 combinations of these strands. The simulated melting temperatures of the duplex formed by each strands (Strand A+B, Strand B+C, Strand A+C) were listed with the simulated melting temperatures of the self-folding secondary structures and were compared to eliminated the inapportate sequence designs. The sequences that had the most stable self-folding secondary structure were marked red and those with the least stable self-folding secondary structure were marked green.

In **Table 5.2**, we first listed the melting temperature of the structure formed by each two single strands and then compare them to the melting temperatures of the secondary structure formed by self-folding of the each three strands. The name of the strands in the column Strand A, B and C were corresponding to the sequence design listed in **Table 5.1**. The highest melting temperature in each column was marked red while the lowest melting temperature in each column was marked green. The simulation for 2D structure was more complicated than the 1D chain for several reasons. First, more strands were involved in the self-assembly of DNA structure, which brought more possible secondary structures. The second reason is that the 2D structure was formed by the interaction between three strands, thus the simulation cannot offer the real melting temperature of the Y shape DNA structure, but only the melting temperatures of the duplexes formed by these three strands. The increase in

complexity of the sequence designs has brought a problem for the sequence engineering for our case. The melting temperatures of the duplex formed by Strand A and C for the 12 potential combinations were around 56 ℃, which was lower than the self-folded structures of four possible sequences that can be used as Strand A. It is likely that secondary structures formed by self-folding of Strand A are formed superior than the duplex formed by Strand A and C. However, the difference in the two melting temperatures was not more than 4 ℃. More importantly, the melting temperature of the 2D DNA structure was anticipated to be a value in the range of the three melting temperatures obtained from the simulation. We approved the sequence design regardless of this flaw, so that the feasibility can be further tested with experiments. We first looked into column "Strand C" because it can best narrow down the choices. Other than the three designs marked in green which correspond to the strand "YcS6", all the melting temperatures were close to 60 ℃. After "YcS6" was first selected to be the Strand C, Design 3 was ruled out due to the very stable secondary structure of the corresponding Strand A. Design 4 and 12 were selected to be the final sequence designs, the number of split-aptamer dangling ends could be controlled by replacing the strands with Ya, Yb or Yc.

Based on these simulation results, we determined two 2D Y shape DNA structures with three split-aptamer dangling ends. The sequences include YaS6*, YbS6, YbS6* and YcS6. The details of the sequences could be found in the Appendix of the thesis.

Characterization of 2D DNA structure

The final sequence design was based on a series of melting simulation of the duplexes formed by each two strands among the three ssDNA forming the Y structure. Judging from the results, during the cooling process after denaturation Strand A and B will first hybridize due to its highest melting temperature. The not hybridized part of Strand A will then hybridize with half of Strand C. In the end, Strand C and B were

hybridized to finally form the Y shape DNA structure. However, the real formation process involved more complex interactions between the three strands at the same time and the binding process can be more unified. On the other hand, the simulation results left the doubt in whether the self-folding secondary structure of Strand A will have a negative impact on the formation of 2D structure. Due to these two reasons the characterization of the DNA structures existing in the mixture of the three strands was necessary.

The melting temperature was first measured by fluorescent spectroscopy and UV-Vis spectroscopy to compare with the simulation results. In **Figure 5.4** the melting profiles of the Y structures with different number of dangling ends obtained from UV spectroscopy were displayed. As a result, the 2D Y structure without dangling end or with one dangling end showed only one melting peak while the Y structure with three dangling ends showed two melting peaks. Furthermore, we could see in **Figure 5.5** that the three duplexes formed by the strands forming the one of the Y structure (YaS6*+YbS6+YcS6) had three different melting temperatures respectively at 53℃, 58℃ and 71℃. These results were not the same as the simulated melting temperature due to the influence of the split-aptamer dangling ends that were not hybridized. The simulation software was targeting fully hybridized DNA structures, the free dangling ends brought variations into the final results. In **Figure 5.4** it was clear that formation of the original Y structure without dangling ends only had one melting peak. The Y structure with one dangling end had the same melting profile because there was only one split-aptamer in the DNA structure and no Adenosine bridge can be formed without the other half of the splited aptamer. This suggested that the 2D Y shape structure was formed in a one-step process with the three strands despite the different melting temperatures of the three duplexes. In the case of the Y network, there were two different split-aptamer dangling ends, the “Y”s were binded through the Adenosine bridge with presence of Adenosine in solution. In

the tests on 1D DNA structures, when there was no Adenosine presented in the solution the 1D chain with S6 dangling ends shown a first melting peak due to the stronger binding compared to S5 dangling ends. The same result was observed in the 2D DNA structures, the S6 split-aptamer dangling ends also partly hybridized with each other and created a melting peak even without Adenosine. (**Figure 5.4**) The melting profile was similar to the 1D DNA chain, two melting peaks were observed respectively for the Adenosine bridges and the Y shape structures. The first peak in **Figure 5.4** at 44 ℃ corresponded to the melting temperature of Adenosine bridges. This value was higher than the melting temperature of the Adenosine bridges in the 1D chain reported in Chapter 4 (38 ℃). The reason causing this difference in the melting temperature was the more stable structure of the Y network. The second peak at 67 ℃ corresponded to the formation of Y structures was 10 ℃ lower than the 1D duplex. This value was higher than two duplexes shown in **Figure 5.5** (53 ℃, 58 ℃) and lower than the other duplex (71 ℃). This melting temperature of the Y shape DNA structure without split-aptamer dangling ends was measured with fluorescent spectroscopy for confirmation. We used a Step-one real time PCR system that allows observation of the fluorescent signal during the heating process of solution and can be used for DNA melting curve measurement after mixing the DNA solution with fluorescent dye. 0.32 μM DNA strands were mixed in fluorescent buffer. The solution was first denatured at 95 ℃ for 5 mins and cooled down to 10 ℃. The fluorescent signal was recorded over time during a second heating process. The melting curve of the Y shape DNA structure was the same as the melting temperature obtained from UV spectroscopy at 67 ℃. The three duplexes formed by Ya, Yb and Yc showed different melting temperatures, which confirmed the result that the Y shape structure can be formed in a one-step process regardless of the three different melting temperatures of the duplexes.

From **Figure 5.4** we observed that the two peaks were overlapped in the range around 50 ℃. The normalized first derivative for the Y network showed another peak at 44 ℃ other two samples with only one peak. The small difference between the two peaks may be a factor limiting the shift in the melting temperature after the formation of the Adenosine bridges.

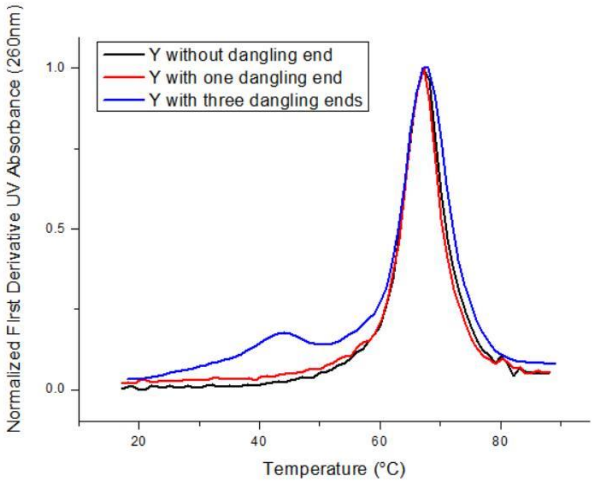

Figure 5.4 The melting profiles of the 2D Y structure with different number of split – aptamer dangling ends obtained from UV spectroscopy. The strand concentration was 0.9 μM, the buffer was 1X SPR buffer and no Adenosine was presented in the solution. The 2D Y shape DNA structure without dangling ends (Ya+Yb+Yc) and with one dangling end (Ya+YbS6+Yc) showed one peak corresponding to the three-way junction while the "Y" with three dangling ends (YaS6*+YbS6+YcS6) formed a network and showed two melting peaks, one corresponding to the three-way junction and the other corresponding to the network formed through Adenosine bridges.

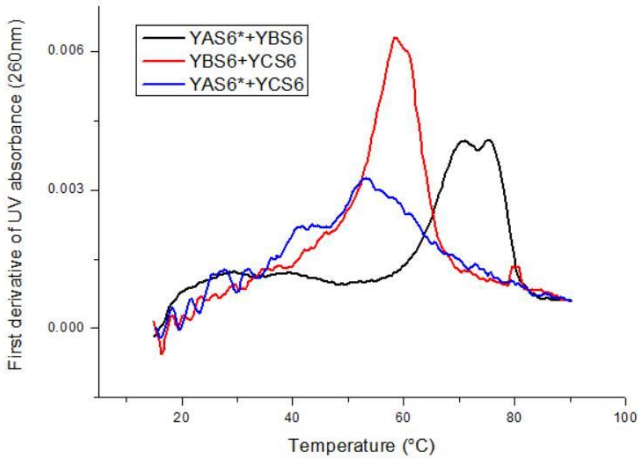

Figure 5.5 The melting profiles of the three duplexes formed the by YaS6*, YbS6 and YcS6. The three duplexes had a melting peak respectively at 53 ℃, 58 ℃ and 71 ℃.

Gel electrophoresis was used for the characterization of 7 DNA structures that can be formed with the 7 sequences we used for building the Y structures (Ya, Yb, Yc, YaS6*, YbS6, YbS6*, YcS6). A DNA ladder was used to measure the approximate size of the DNA structures formed. The sequences in each sample were listed in Tabel 5.3 All the samples showed one band around 50 bps, which corresponded to the Y structure. Sample 1 and 7 had a band representing DNA structure with smaller size, which was caused by the excessive single strands in the solution. We observed a band representing bigger DNA structure than the Y structure at approximately 100 bps. It can be an aggregated DNA cluster or a unwanted secondary structure, thus the use of this combination in the detection was avoided.

	Strand A	Strand B	Strand C	Number of dangling ends
1	YaS6*	YbS6	YcS6	3
2	YaS6*	YbS6*	YcS6	3
3	Ya	Yb	Yc	0
4	YaS6*	Yb	Yc	1
5	Ya	YbS6	Yc	1
6	Ya	YbS6*	Yc	1
7	Ya	Yb	YcS6	1

Table 5.3 The strands in the samples analyzed with gel electrophoresis and their number of split-aptamer dangling ends.

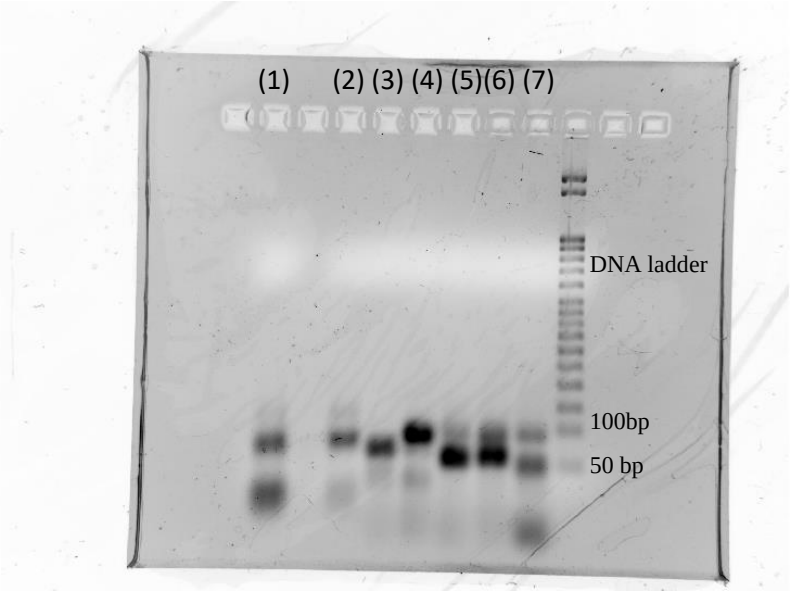

Figure 5.6 The Agarose gel electrophoresis result of different Y structures listed in Table 5.3. Each well contained 10 pmol sample in 15 μL. A DNA ladder was used to help estimate the size of the structures. The samples showed a band around 50 bps according to the DNA ladder, sample 1 and 7 also showed a band corresponding to the single strands. Sample 6 and 7 showed a possible secondary structure which is larger than the 2D Y structure.

5.1.3 Sequence design of 3D DNA structure

A variety of 3D DNA structures have been reported by researchers all over the world, including DNA lattice, cubic, tetrahedron, etc. [29–32] We designed a 3D DNA tetrahedron structure based on the single step synthesis method reported by Goodman et al. [32] DNA with such structures have been used in many applications such as drug delivery and detection. In many sensor applications the space created by the pyramid was improving the sensitive of the detection. [33] Other examples using this structure to capture the drug inside the pyramid and deliver them to the correct human organ. [34–37] The structures were then dissociated to release the drug at minimum damage to health tissue, especially for diseases like cancer whereas the drug can be harmful to human body.

The tetrahedron was formed by four single strands, each 55-mer strand consisted of three 17-mer oligonucleotide and two 2-mer hinges. The hinges were not hybridized with other bases, their purpose was to separate the 17-mer oligonucleotide so that the DNA strand can bend successfully at the four vertices of the tetrahedron. This 3D structure has two enantiomers but the shape and properties of the DNA are not affected. The four single strands forming the tetrahedron were named Ta, Tb, Tc and TD. The split-aptamer dangling ends can be added on either the 5' end or the 3' end of the Tx (x=a, b, c, d) strand. The mixture of these four strands with dangling end can form a DNA tetrahedron with split-aptamer on each vertex. There are 16 possible sequences to be simulated for their melting profiles. These sequences were named by the same rules as the 2D Y shape structure during the sequence design process. For instance, the sequence start with S6 dangling end on the 5' and followed by Ta oligonucleotide was named S6TA. After the sequences were finalized, the four strands were referred as T1, T2, T3 and T4. The 16 sequences and the melting temperature of their self-folding structures were listed in **Table 5.4**. Each of the sequences was represented by the number in the table during the sequence design process for simplification.

Design	Name	Tm(°C)	Design	Name	Tm(°C)
1	S6*Ta	43.4	9	TaS6*	48.9
2	S6*Tb	58.2	10	TbS6*	56.1
3	S6*Tc	53.0	11	TcS6*	49.0
4	S6*Td	52.9	12	TdS6*	56.4
5	S6Ta	47.9	13	TaS6	51.8
6	S6Tb	49.2	14	TbS6	44.1
7	S6Tc	49.1	15	TcS6	52.6
8	S6Td	51.6	16	TdS6	55.2

Table 5.4 The 16 potential sequences that can be used to form the tetrahedron DNA structure with four split-aptamer dangling ends and the melting temperature simulated for their self-folding secondary structures.

The 16 sequences can be sorted into four categories, the candidates for T1 (1, 5, 9, 13), T2 (2, 6, 10, 14), T3 (3, 7, 11, 15) and T4 (4, 8, 12, 16). In order to successfully build the tetrahedron we need to pick one strand in every category. The four strands can form six duplexes by different combinations, all the possible structures were simulated and their melting temperatures were compared in **Table 5.4** to search for the best choices. The four strands (T1, T2, T3 and T4) can form six duplexes by hybridizing each pairs of them. The possible structures of these six duplexes were separated into six tables whereas the columns were the four possible choices for one strand and the rows for the other strand. The melting temperature of the self-folding structure for each strand was noted in the brackets. First, the structures that had lower melting temperature compared to the self-folded structures of the two single strands were marked red in the table. These strands were first removed from the candidates. The second step was to mark the strands that had close melting temperatures between the duplex and self-folded structures in blue color. These strands will only be considered in absence of better choices. These two steps eliminated Strand 2, 8, 10, 12 and Strand 16 was noted as an unfavorable strand. Based on Table T1+T4 and Table T2+T4, Strand 4 and 6 were selected to be the final sequence design of T2 and T4. The last step was to search for the best choices for T1 and T3. Strand 1 and 15 offered the most stable duplexes (the melting temperatures marked green) among the 8 strands, thus they were chosen as the final sequence T1 and T3. In conclusion, Strand 1, 4, 6 and 15 were chosen to be the four strands forming the tetrahedron DNA structures with split-aptamer dangling ends based on the simulation results of the melting profiles. Details of these sequences can be found in the Appendix of the thesis.

T1+T2	1 (43.7)	5 (47.9)	9 (48.9)	13 (51.8)
2 (58.2)	55.9	55.9	55.9	55.9
6 (49.2)	55.9	55.9	56.8	55.9
10 (56.1)	55.9	49.3	55.9	55.9
14 (44.1)	55.9	55.9	55.9	55.9

T1+T3	1 (43.7)	5 (47.9)	9 (48.9)	13 (51.8)
3 (53.0)	63.9	63.9	60.8	63.9
7 (49.1)	63.9	63.9	60.8	63.9
11 (49)	63.9	63.9	60.8	63.9
15 (52.6)	67.2	67.2	63.1	67.2

T1+T4	1 (43.7)	5 (47.9)	9 (48.9)	13 (51.8)
4 (52.9)	57	56.2	56.5	56.5
8 (51.6)	51.1	51.2	49.7	49.7
12 (56.4)	56.4	55.7	55.8	55.8
16 (55.2)	56.4	55.7	55.8	55.8

T2+T3	2 (58.2)	6 (49.2)	10 (56.1)	14 (44.1)
3 (53.0)	63.2	63.2	63.2	63.2
7 (49.1)	63.3	63.3	63.3	63.3
11 (49)	63.3	63.3	63.3	63.3
15 (52.6)	63.3	63.3	63.3	63.3

T2+T4	2 (58.2)	6 (49.2)	10 (56.1)	14 (44.1)
4 (52.9)	64.2	64.2	64.7	59.4
8 (51.6)	64.2	64.2	64.7	59.4
12 (56.4)	65.1	65.1	65.5	60.0
16 (55.2)	65.5	65.5	65.9	60.2

T3+T4	3 (53.0)	7 (49.1)	11 (49)	15 (52.6)
4 (52.9)	67.1	67.1	67.1	67.1
8 (51.6)	67.1	67.1	57.4	67.1
12 (56.4)	67.1	67.1	67.1	67.1
16 (55.2)	67.1	67.1	67.1	67.1

Table 5.5 The simulated melting temperatures of the duplexes formed by the 16 sequences listed in Table 5.4. The four sequence forming the tetrahedron can form six duplexes, each duplex had 16 possible combination of sequence designs. The simulated melting temperature of the self-folding secondary structures of the 16 strands was added in the brackets to determine which structures were not stable. The duplexes that had lower melting temperature compared to the self-folding structure was marked red as not stable. If the two temperatures were close they were marked blue.

Characterization of 3D DNA structure

While we were studying the original Y shape DNA structure we observed only one melting peak suggesting that the 2D structure was formed by the three strands all at the same time, rather than a complex formation process in multiple steps. The detection of Adenosine with UV spectroscopy is only possible with structures that can be formed in such one-step process. If multiple melting peaks exist for the DNA structures, they will not be able to act as the internal reference. The four strands forming the 3D DNA tetrahedron structures were first tested for their melting profile to check if they can be used in UV spectroscopy for detection.

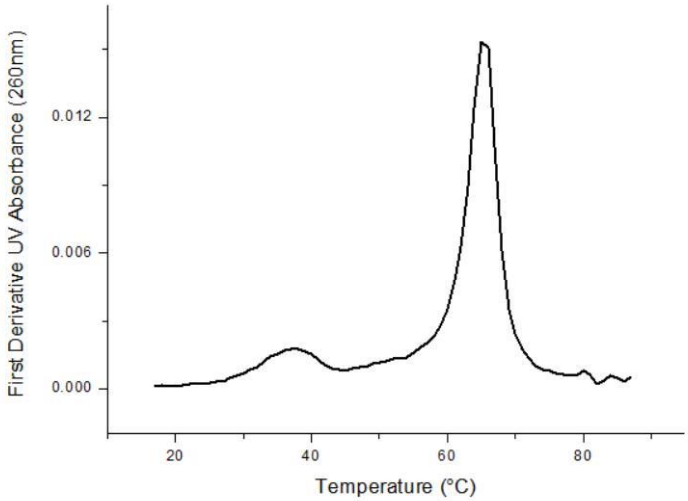

Figure 5.7 The melting profile of 3D DNA tetrahedron with four split-aptamer dangling ends, the strand concentration was 0.3 μM and no Adenosine was present in the solution. Two peaks were observed respectively at 37 ℃ and 65 ℃. The first melting peak corresponded to the formation of Adenosine bridges and the second melting peak corresponded to the tetrahedron structure. Same as the Y shape DNA structure, only one peak was observed for the formation of tetrahedron DNA structure.

In **Figure 5.7** we can see the melting profile of the mixture of the four strands we designed in sequence engineering. The concentration of each strand was 0.3 μM so that the amount of UV light absorbed by the solution remained in the most suitable experiment range. Same as 1D or 2D designs, the first peak corresponded to the formation of Adenosine bridges. The melting temperature was observed at 38 ℃,

which was close to the melting temperature measured using the 1D DNA chain. Despite the fact that the six duplexes can be formed by these four strands had six different simulated melting temperatures, we observed only one peak corresponding to the tetrahedron (the second peak on the right side). These two clear peaks made sure that this 3D tetrahedron DNA structure with split-aptamer dangling ends could be used for detection of Adenosine with UV spectroscopy. Our conclusion was supported by the melting curve of the same tetrahedron (without any dangling end) reported by Armitage et al. The UV melting curve they reported showed a melting temperature at around 64 ℃, very similar to our result. [35]

5.2 Detection of Adenosine with 2D DNA structure

5.2.1 Detection of Adenosine using SPRi

The 1D DNA chain structure has been used for the detection of Adenosine and its SPR results were discussed in Chapter 3. We discovered that the grafting density have a great impact on the number of Adenosine bridges formed on each probe. In condensed grafted spots the DNA chain was shorter than those spot with low grafting density. This indicated the fact that the growing process of DNA structure on the probes is strongly affected by the morphology of the gold surface. Simply put, the interaction between complex DNA structures and the immobilized probes will be suppressed without sufficient space. The 2D Y shape structure is larger in size in comparison with the 1D chain structure. Moreover, the 2D structure takes more space due to the increase in dimension. The reason we proposed this 2D structure was to take advantage of its greater mass effect in SPR experiments in order to achieve stronger signal. The possibility of forming network between the Y structures may even further increase the signal. The key point in developing the SPR detecting

protocol for this 2D DNA structure lies in balancing the advantage of larger mass effect and the disadvantage of the suppress in the interaction between Y shape DNA structures and the probes due to its bigger size. Unfortunately, the study on the whole system was not finished due to the limitation in time. Many details in the protocol still have room for improvement and we will discuss the possible solutions to solve the current existing problems after a presentation of the results.

Binding mechanism and detection principle

The 1D chain structure started with an initial probe Z on the surface so that it can hybridize with one monomer forming a duplex and create a specialized probe for S5, S6 or S8 dimers. In the case of the 2D structure only S6 split-aptamers were used as the dangling ends of the Y shape DNA, thus the initial probe Z was switched to 10T-S6 or 10T-S6* probes. 10T-S6 and 10T-S6* probes were the two S6 split-aptamers with 10 “T”s on its 5’ to separate the split-aptamer and gold surface, both probes were thiolated on the 5’ to enable functionalization. The sequence details could be found in the Appendix. This saved the hybridization process (Step 2 in **Figure 3.6**) which took nearly three hours to finish. The change of the probe immobilized on gold surface greatly saved the time needed for the preparation of each measurement. However, the hybridization process was the key enabling the calculation of average number of duplexes attached on each probe. We are no longer able to quantify the number of Y shape DNA interacting with the probes. The interactions of the 2D structures with the probes were displayed in **Figure 5.8**.

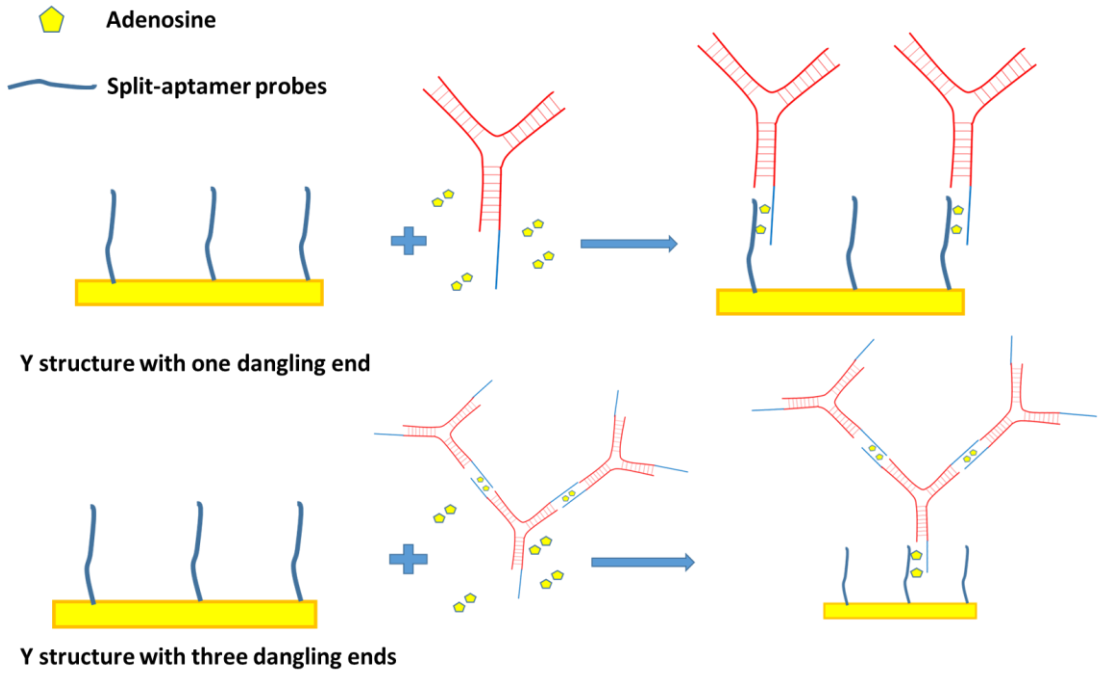

Figure 5.8 The interactions of the 2D Y shape DNA structures on gold surface. The gold surface was functionalized with split-aptamer probes. In the case of Y structure with one dangling end, the Y shape structure will bind onto the surface with the help of Adenosine molecules in the solution and create SPR signal. In the case of Y structure with three dangling ends, the "Y"s will first bind with each other through the Adenosine bridges formed by the dangling ends in solution and create a network. This network then bind onto the surface with Adenosine in the solution, the greater mass of the network will provide higher signal.

The Split-aptamer S6 or S6* were functionalized on the gold prism with the same protocol as the Z probes, the grafting densities were also controlled from 0.4 pmol/cm^2 to 8 pmol/cm^2. When the Y shape structure with one dangling end was first formed in the solution and then injected with Adenosine into the chamber, the dangling end will form Adenosine bridge with the probes and produce a detectable SPR signal. In the case of the 2D network, the three dangling ends on the Y structure will connect with each other with the help of Adenosine molecules and form a network before the injection. The network can also bind with the probes through the dangling ends that are not occupied in formation of the network.

The SPR results and key parameters

The probes on the gold surface were switched to split-aptamer in the study of 2D DNA structures. The negative control remained the NC sequence used in the 1D SPR experiments. The first test with these probes and negative controls revealed one problem in the negative control probes. The ΔR of the negative control spots increased 5% during the injection of the Y structure with one split-aptamer dangling end (Ya+YbS6+Yc), which was an abnormal phenomena. Theoretically the NC probes were not able to hybridize with any of the three strands and the creation of such huge signal was unexpected. The mechanism for this interaction was unclear and we proposed to solve this problem by switching the negative control probes. The signal of the initial probe Z used in the SPR test for the 1D chain remained unchanged during the injection of the Y structures. For this reason, probe Z was used as the alternative negative control for the SPR experiments using 2D DNA structures. Same as the SAMs formation protocol of the 1D tests, S6 and S6* split-aptamer strands thiolated on the 5' were diluted with probe Z and functionalized on the gold surface.

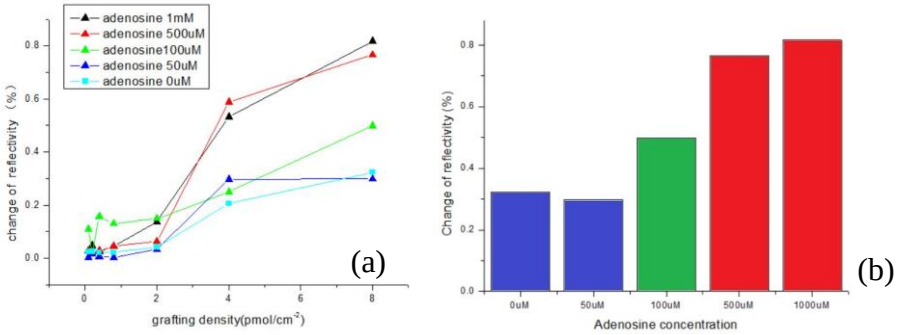

Figure 5.9 The SPR signal obtained from Y structure with one split-aptamer dangling end (Ya+YbS6*+Yc) on gold prism functionalized with10T-S6 probes. The strand concentration was kept at 1 μM while the Adenosine concentrations varied from 0 μM to 1mM. (a) The signal obtained for different Adenosine concentrations at different grafting densities. (b) The signal obtained on the spots with grafting density of 8 pmol.cm^{-2}. When Adenosine concentration was 0 μM a signal OFF was observed, the signal for 50 μM Adenosine was similar. When Adenosine concentration was 100 μM the signal increased and showed good detection. The target was saturated in tests with 500 μM and 1mM Adenosine and the signals were similar.

Due to the limited time, we were not able to report a fully developed protocol for the SPR experiments of the 2D structure. We made several tests varying the Adenosine concentration and strand concentration in the injection. The SPR signal obtained with different concentrations of Adenosine were displayed in **Figure 5.9**. We tested Adenosine concentration from 0 μM to 1mM, the grafting density of the spots was from 0.4 to 8 pmol.cm^{-2} and the concentration of DNA strands were kept at 1 μM. The signals showed an increasing trend with the increase of grafting density. In Chapter 3 we reported an increase in the signal for the 1D chain with S6 dangling ends even without any Adenosine in the solution, which created a higher signal OFF but brought an increase in the signal. In **Figure 5.9** we observed the same signal increase in the test without Adenosine. When the concentration was increased to 50 μM the signal was similar to the test without Adenosine. This indicated that the increase of signal brought by 50 μM of Adenosine was insignificant compared to the signal OFF created by the hybridization of S6 dangling ends. The signal was noticeable when the concentration of Adenosine was further increased to 100 μM. Based on these results, the detection limit of the current protocol was between 50 and 100 μM. This LoD was not satisfying for sensing techniques and will be one of the major concerns in further improvement. The concentration of Adenosine was further increased to 500 μM and 1mM. Their similar results proved that the Adenosine concentration has reached saturation at 500 μM. The maximum signal obtained from these two experiments was 0.8%, which was lower than the signal (2.2%) obtained from the 1D DNA chain with S6 split-aptamer dangling ends. On the other hand, the signal OFF obtained without Adenosine was also lowered from 0.8% of the 1D S6 DNA chain to 0.3% and their signal ON/OFF ratio was similar to each other (2.6).

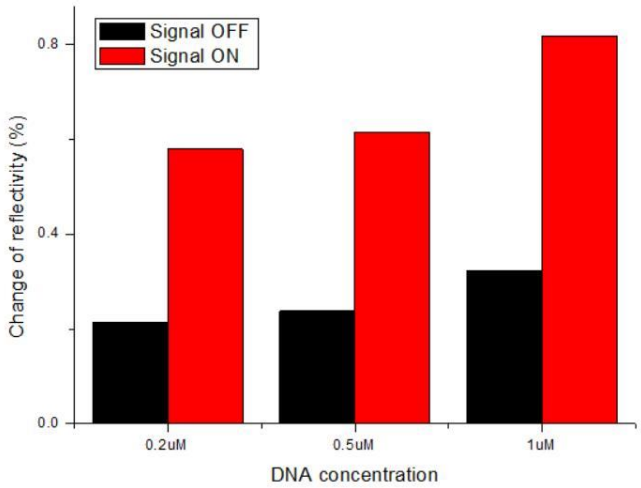

Figure 5.10 The SPR signal ON and signal OFF obtained from Y structure with one split-aptamer dangling end (Ya+YbS6*+Yc) on gold prism functionalized with 10T-S6 probes. The signal ON was obtained from injection of DNA strands with 1mM Adenosine, the signal OFF was obtained from injection of DNA strands without Adenosine. The grafting densities of the spots were 8 pmol.cm^{-2}. The strand concentration varied from 0.2 μM to 1 μM. The signal ON and signal OFF both increased with higher concentration of Adenosine molecules. The ratio between signal ON and signal OFF was kept around 2.6 for these three samples.

In **Figure 5.10** the SPR results of 0.2 μM, 0.5 μM and 1 μM strands with and without Adenosine in the solution were compared. The SPR signals were decreased with lower concentration of the Y structures. The signal OFF without Adenosine decreased from 0.3% (1 μM Y structure) to 0.2% (0.2 μM Y structure), meanwhile the Signal ON was decreased from 0.8% (1 μM Y structure) to 0.6% (0.2 μM Y structure). The signal ON/OFF ratio remained close to 2.6 regardless of the change in the strand concentrations.

The signal obtained from 2D structures with only one split-aptamer dangling ends was lower than the signal obtained from 1D DNA structure with the same dangling ends. The greater mass effect brought by the bigger molecular weight of the Y structure was not enough to compensate the bigger space it required on the gold surface. Other than the greater mass effect, the possibility to form a network was also one benefit of this Y structure. In **Figure 5.11** the SPR signal of two possible Y

networks were compared. The first one that had S6 dangling end on Yb strand was referred as Y_1 (YaS6*+YbS6+YcS6) and the second one that had S6* dangling end on Yb strand was referred as Y_2 (YaS6*+YbS6*+YcS6). Both 10T-S6 and 10T-S6* probes were functionalized on the gold prism because the Y structure had two different split-aptamer dangling ends.

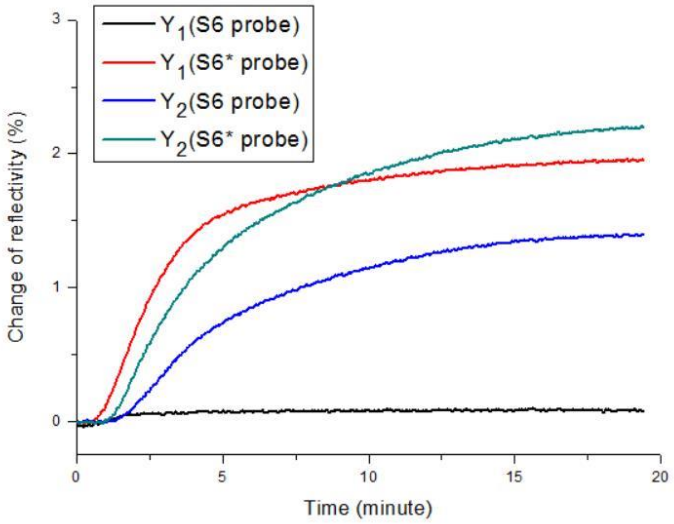

Figure 5.11 The SPR signal obtained for two different Y networks on different probes. Y_1 (YaS6*+YbS6+YcS6) had two S6 and one S6* split-aptamer dangling ends, Y_2 (YaS6*+YbS6*+YcS6) had two S6* and one S6 split-aptamer dangling ends. The strand concentration was 1 μM, grafting density of the spots was 8 pmol.cm^{-2} and Adenosine concentration was 1mM for all the tests. Y_1 did not create much signal on 10T-S6 probes (0.5%), but the signal on S6* was at a higher level (1.8%). The Y_2 network created higher signal on both probes, 2.2% on the 10T-S6* probes and 1.4% on the 10T-S6 probes.

The two Y networks showed different performance on different probes. Y_1 had two S6 dangling ends and one S6* dangling end, which was likely the reason why the network did not create much signal on 10T-S6 probes. For same reason, Y_2 also created less signal on 10T-S6* probes (1.4%) compared to 10T-S6 probes (2.2%). Moreover, the signals created with Y_2 were greater than the signal created with Y_1. The connection of the Y network on the probes was more favorable to the structures having more S6* dangling ends in the Y structures. The most important conclusion

draw from **Figure 5.11** was the signal can be improved more than two times by building a network between the "Y"s. The most suitable combination of the Y network and probes was Y_2 network and 10T-S6* probes, this combination will create the highest signal.

5.2.2 Detection of Adenosine using UV spectroscopy

We explained in Chapter 4 a detection method using the two melting peaks of the 1D DNA chain structure and the difference between them to detect the presence of Adenosine. According to **Figure 5.4** the original 2D Y shape DNA structure without dangling ends has shown only one melting peak. In theory the principle of detection explained in Chapter 4 applies to the 2D DNA structure as well, since two peaks were expected for the S6 split-aptamer dangling ends and the Y shape structure. The Y structures with one dangling ends were not able to form binding because the other half of the splited aptamer was missing in the solution, thus only the Y structures with three split-aptamer dangling ends were tested for this method. However the formation of the network and the interactions between each "Y"s will affect the melting and cooling process in a different manner compared to the 1D chain. Experiments have shown that the 2D structure could be used for detection of Adenosine but less effective compared to the 1D chain.

Depending on the split-aptamer dangling ends connected with Yb, there are two kinds of Y structures with three dangling ends. Their UV spectroscopies were shown in **Figure 5.12**, two melting peaks were observed as expected. The first melting peak (Tm1) corresponded to the Adenosine bridge and the second peak (Tm2) corresponded to the Y shape DNA structure. The two kinds of Y network solutions were tested with and without Adenosine. The melting profile exhibited the same increase in the intensity of Tm1 as the 1D DNA chain. The intensity of the first melting peak of Y_1 was smaller than the peak of Y_2. This indicated that the bindings

provided by Y_2 were stronger than Y_1, which also matches the SPR results that higher signal was obtained with Y_2. The shift in the value of Tm1 was not observed in the case of 2D network, this was probably due to the stable hive-like network formed by the split-aptamer dangling ends. The higher melting temperature (44 ℃) compared to the Adenosine bridge melting temperature observed in 1D tg-S6 duplex (38 ℃) also suggested that the network between the dangling ends has greatly increased the binding strength. The strength of binding was close to the 1D cc-S6 duplex whose first melting peak was at 45 ℃. We also observed a shoulder in the second melting peak of Y_2. The shoulder existed in the sample with and without Adenosine, thus we assumed it was due to a duplex formed with higher stability than the Y structure. The difference between Y_1 and Y_2 was the YbS6 and YbS6* used as Strand B which suggested the YbS6* strand was crucial to the formation of this structure. Based on the gel electrophoresis result shown in **Figure 5.6**, it also has the possibility to be the secondary structure observed in sample 6.

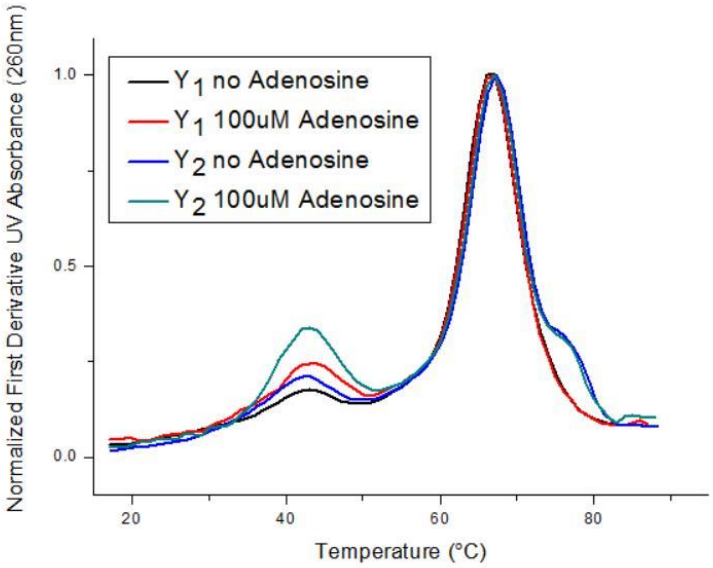

Figure 5.12 The UV spectroscopy of two different Y networks with and without Adenosine. The melting peaks were at 44 ℃ and 66 ℃. The first melting peak did not shift with presence of Adenosine like the 1D detection model, but the intensity of the peak still increased. The intensities for Y_2 network with and without Adenosine were all higher than Y_1 network. The melting curve of Y_2 also presented a shoulder at high temperature.

In conclusion, the 2D network could be used for the same detection method reported in Chapter 4. The detection was only possible by comparing the height of the peak but not the shift in Tm1. The strong binding between the networks was the limiting factor for this application.

5.2.3 Potential methods for improvement

The work on the 2D DNA structures was not yet completed, there were still many flaws we wish to overcome to achieve better performance with this detecting method. Here we offer some thoughts about the possible approaches to solve the current problems and improve the results.

In theory the SPR experiments using the Y structures can also start with hybridization of Z probes with S6*Zc (like the 1D model) and use the split-aptamer dangling ends to capture the "Y"s on the surface. In the beginning of **Section 5.2.1** we mentioned that the negative control "NC" used in 1D model showed an unexpected interaction with the Y shape DNA structures. As a result, initial probe was switched from Z to 10T-S6 and 10T-S6* probes to avoid the interaction between the "NC" probes and the Y shape DNA structures and to simplify the preparation of the experiments. But without the hybridization of the initial probes, we lost the reference to calculate the number of DNA structures connected to each probe. In order to regain this analytical tool, a new negative control needs to be designed so that Z strand can be used again as the initial probe on the surface. It can be a potential research interest in the future work.

Second, SPRi is a multi-parametric detection method which offers many possibilities for improvement. In our work we only briefly made several tests on the Adenosine concentration and strand concentration. We have learnt that Adenosine reached saturation after 500 μM in the solution, but the threshold lied between 100 μM and 500 μM of Adenosine concentration. More tests will be needed to find this

threshold. Moreover, the signal OFF reduced with the strand concentrations. Although the SPR signal will also decrease will the strand concentration, we could find a certain concentration whereas the signal OFF was suppressed to a lower value while the SPR signal remained noticeable for detection purpose. There are other parameters we could alter for further improvement, such as the injection speed of the sample solution and split-aptamer dangling end used on the "Y"s. Decreasing the injection speed may be helpful for the binding process because the 2D structure was more complicated due to the interactions between the "Y"s and it can take longer time than the 1D DNA chain needed to bind to the surface. The LoD of the 2D Y structures were proven to be higher than 50 μM, which was not to our satisfaction. We have proven the 2D structure can successfully formed and can be used for detection with the S6 dangling ends. Based on the experience with the 1D chain, we believe the detection limit can be effectively lowered by switch the dangling ends from S6 to S5.

In the tests of Y structures we used 10T-S6 probes on gold prism to catch the S6* dangling end on the Y structure. But the experiments with the 2D network provided prove that 10T-S6* probes had better signal compared to 10T-S6 probes. One way to improve the performance of detection using Y structure with only one dangling end is to use 10T-S6* probes on the surface to capture the Y structures instead of 10T-S6 probes.

In the aspect of the UV spectroscopy experiments, the 2D structures have proven to be able for detection but were not the ideal choice compared to the tg-S6 duplex. Their melting profiles were similar to cc-S6 duplex, which showed an increase in the intensity of the melting peak but not much shift with presence of Adenosine. By switching the S6 split-aptamer to S5 split-aptamer may provide better detection due to the weaker bonding in S5 split-aptamers.

5.3 Detection of Adenosine with 3D DNA structure

5.3.1 Detection of Adenosine using UV spectroscopy

The melting profile of the tetrahedron 3D DNA structure was shown in **Figure 5.6**, two peaks were observed at 37 ℃ and 65 ℃. The lower melting temperature for the Adenosine bridges compared to the cc-S6 duplex and 2D Y DNA network made it more promising in detection purpose. The melting profiles measured for samples with different Adenosine concentrations were presented in **Figure 5.13**. The first melting peak was shifting with the increased concentration of Adenosine as well as an increase in the intensity of melting peak. The peak shifted 4 ℃ with the presence of 100 μM Adenosine in the solution. These results proved that this 3D structure was a suitable sequence engineering for detecting Adenosine with UV spectroscopy. The two melting peaks also suggested that the tetrahedrons were binded with each other through the Adenosine bridges and formed a network.

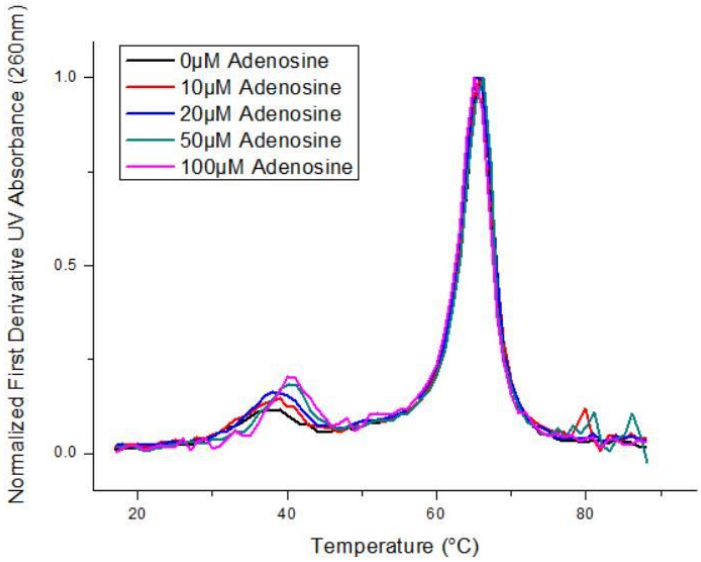

Figure 5.13 The melting profile obtained with UV spectroscopy of 3D DNA tetrahedron network. The Adenosine concentration varied from 0 μM to 100 μM while concentration of each strand was kept at 0.3 μM. The first melting peak shifted from 37 ℃ to 41 ℃ with the increase of Adenosine, the intensity of the peak also increased. The second peak was not shifted at 65 ℃.

The LoD was also measured by performing experiments with lower Adenosine concentrations. The DNA tetrahedron was tested in solutions with 1 μM, 2μM and 5μM of Adenosine. The same calculation with **Equation 4.1** was made to determine the LoD. The maximum height of Tm1 obtained at these three Adenosine concentrations minus the maximum height of Tm1 obtained without Adenosine was calculated, the error bar was made by comparing four heating process in the cycles. The ΔP and their calculated error bars were shown in **Figure 5.14**.

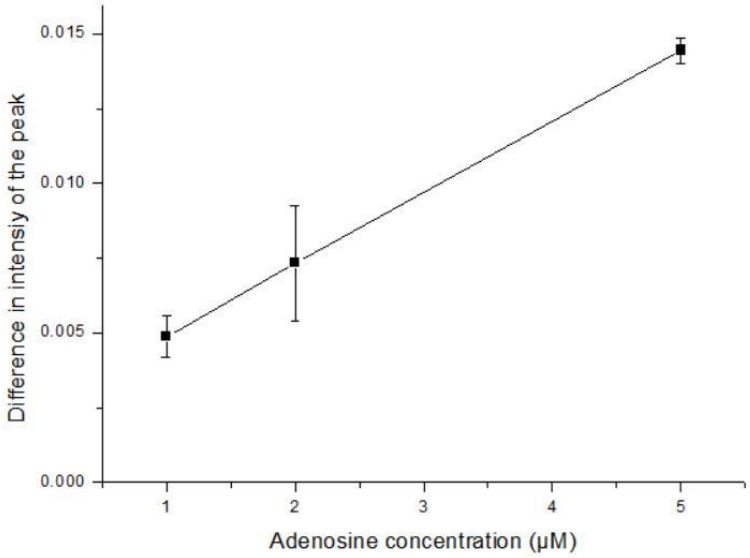

Figure 5.14 The difference between the maximum values in the melting peak of the 3D DNA tetrahedron network at various Adenosine concentrations and the maximum value in the melting peak of the 3D DNA tetrahedrons with split-aptamer dangling ends without Adenosine molecule. This difference ΔP represented the height of the peak increased due to the formation of Adenosine bridges. The experiments were repeated for four cycles, which allowed the calculation of the error bar. The ΔP was higher than 3 times the value of error bar, which gave a LoD in the range of 1 μM.

The ΔP displayed in **Figure 5.14** showed a highly linear increase with the Adenosine concentrations. The error bars was smaller than 1/3 of the ΔP, which suggested that the detection was reliable. The LoD of UV spectroscopy detection method for Adenosine molecules was 1 μM, which was same as the 1D tg-S6 DNA

chain. The 3D DNA tetrahedron was proven to be an effective structure design for this application.

In the limited tests we made with the 3D structures the 3D tetrahedron DNA displayed good performance for detection of Adenosine using UV spectroscopy. The melting profiles were similar to tg-S6 duplex, which was the ideal choice for detection of Adenosine using 1D DNA chain. The melting peak Tm1 showed a clear shift in the melting temperature and increase in the intensity with the presence of Adenosine. The detection limit was proven to be in the range of 1 μM. Based on these facts, the 3D tetrahedron DNA structure with four split-aptamer dangling ends was suitable for detection of Adenosine.

5.3.2 Potential methods for improvement

Due to the limitation of time, the SPRi experiment on the 3D DNA network was only started. The future work on this 3D DNA structure will be focused on its application in SPRi for detection. In the first experiments we noticed that the 3D network will bind with probe Z with similar manner as the 2D Y shape DNA bind with probe NC. To avoid this problem, in further studies probe 10T-S6 or 10T-S6* should be immobilized as the initial probe and probe NC as the negative control. Earlier study in our group has found that the 3D tetrahedron without any split aptamer tend to aggregate at a concentration of 1 μM. To avoid this aggregation in the solution before the network interact with the probes on the gold surface, the concentration of the DNA strands should be controlled and other parameters need to be improved to create a well-developed protocol.

The 3D structure has shown a good LoD while used in UV spectroscopy for the detection of Adenosine. The results have shown that the intensities of the peaks were increasing with the concentration of the targets. The LoD was limited by the perturbations in the melting peak. The next step to achieve better detection with UV spectroscopy lies in the further elimination of the noise and improves the resolution of the melting curve.

Reference

1. Seeman NC. Nucleic acid junctions and lattices. ***J Theor Biol***. 1982;99(2):237-247. doi:10.1016/0022-5193(82)90002-9.
2. FU TJ, Seeman NC. Dna Double-Crossover Molecules. ***Biochemistry***. 1993;32(13):3211-3220. doi:10.1021/bi00064a003.
3. Li X, Yang X, Qi J, Seeman NC. Antiparallel DNA double crossover molecules as components for nanoconstruction. ***J Am Chem Soc***. 1996;118(26):6131-6140. doi:10.1021/ja960162o.
4. Seeman NC. DNA in a material world. ***Nature***. 2003;421(6921):427-431. doi:10.1038/nature01406.
5. Liu Y, West SC. Happy Hollidays: 40th anniversary of the Holliday junction. ***Nat Rev Mol Cell Biol***. 2004;5(11):933-937. doi:10.1038/nrm1501.
6. Chen JH, Seeman NC. Synthesis from DNA of a molecule with the connectivity of a cube. ***Nature***. 1991;350(6319):631-633. doi:10.1038/350631a0.
7. Winfree E, Liu F, Wenzler LA, Seeman NC. Design and self-assembly of two-dimensional DNA crystals. ***Nature***. 1998;394(6693):539-544. doi:10.1038/28998.
8. Rothemund PWK, Papadakis N, Winfree E. Algorithmic self-assembly of DNA Sierpinski triangles. ***PLoS Biol***. 2004;2(12). doi:10.1371/journal.pbio.0020424.
9. Yan H, Park SH, Finkelstein G, Reif JH, LaBean TH. DNA-templated self-assembly of protein arrays and highly conductive nanowires. ***Science***. 2003;301(5641):1882-1884. doi:10.1126/science.1089389.
10. Rothemund PWK, Ekani-Nkodo A, Papadakis N, Kumar A, Fygenson DK, Winfree E. Design and characterization of programmable DNA nanotubes. ***J Am Chem Soc***. 2004;126(50):16344-16352. doi:10.1021/ja044319l.
11. Mathieu F, Liao S, Kopatsch J, Wang T, Mao C, Seeman NC. Six-helix bundles designed from DNA. ***Nano Lett***. 2005;5(4):661-665. doi:10.1021/nl050084f.
12. Liu D, Park SH, Reif JH, LaBean TH. DNA nanotubes self-assembled from triple-crossover tiles as templates for conductive nanowires. ***Proc Natl Acad Sci U S A***. 2004;101(3):717-722. doi:10.1073/pnas.0305860101.
13. Yin P, Hariadi RF, Sahu S, et al. Programming DNA Tube Circumferences. ***Science*** . 2008;321 VN-(5890):824-826. doi:10.1126/science.1157312.
14. Goodman RP, Schaap IAT, Tardin CF, et al. Rapid chiral assembly of rigid DNA building blocks for molecular nanofabrication. ***Science***. 2005;310(5754):1661-1665. doi:10.1126/science.1120367.
15. Zhang YW, Seeman NC. Construction of a Dna-Truncated Octahedron. ***J Am Chem Soc***. 1994;116(5):1661-1669. doi:10.1021/ja00084a006.
16. He Y, Ye T, Su M, et al. Hierarchical self-assembly of DNA into symmetric supramolecular polyhedra. ***Nature***. 2008;452(7184):198-201. doi:10.1038/nature06597.

17. Zhang C, Su M, He Y, et al. Conformational flexibility facilitates self-assembly of complex DNA nanostructures. ***Proc Natl Acad Sci U S A***. 2008;105(31):10665-10669. doi:10.1073/pnas.0803841105.

18. SantaLucia J, Hicks D. The thermodynamics of DNA structural motifs. ***Annu Rev Biophys Biomol Struct***. 2004;33:415-440. doi:10.1146/annurev.biophys.32.110601.141800.

19. Lu XJ, Shakked Z, Olson WK. A-form conformational motifs in ligand-bound DNA structures. ***J Mol Biol***. 2000;300(4):819-840. doi:10.1006/jmbi.2000.3690.

20. He Y, Mao C. Balancing flexibility and stress in DNA nanostructures. ***Chem Commun***. 2006;(9):968-969. doi:10.1039/b513962g.

21. Review T. Advances in DNA-based nanotechnology themed issue Guest editors Eugen Stulz , Guido Clever , Mitsuhiko Shionoya and. 2011;40(12).

22. Andersen ES, Dong M, Nielsen MM, et al. Self-assembly of a nanoscale DNA box with a controllable lid. ***Nature***. 2009;459(7243):73-76. doi:10.1038/nature07971.

23. Douglas SM, Dietz H, Liedl T, Högberg B, Graf F, Shih WM. Self-assembly of DNA into nanoscale three-dimensional shapes. ***Nature***. 2009;459(7245):414-418. doi:10.1038/nature08016.

24. Ke Y, Douglas SM, Liu M, et al. Multilayer DNA origami packed on a square lattice. ***J Am Chem Soc***. 2009;131(43):15903-15908. doi:10.1021/ja906381y.

25. Gibbs-Davis JM, Schatz GC, Nguyen ST. Sharp melting transitions in DNA hybrids without aggregate dissolution: Proof of neighboring-duplex cooperativity. ***J Am Chem Soc***. 2007;129(50):15535-15540. doi:10.1021/ja073034g.

26. Moody EM, Bevilacqua PC. Folding of a Stable DNA Motif Involves a Highly Cooperative Network of Interactions. ***J Am Chem Soc***. 2003;125(52):16285-16293. doi:10.1021/ja038897y.

27. Nishikawa M, Matono M, Rattanakiat S, Matsuoka N, Takakura Y. Enhanced immunostimulatory activity of oligodeoxynucleotides by Y-shape formation. ***Immunology***. 2008;124(2):247-255. doi:10.1111/j.1365-2567.2007.02762.x.

28. Leontis NB, Kwok W, Newman JS. Stability and structure of three-way DNA junctions containing unpaired nucleotides. ***Nucleic Acids Res***. 1991;19(4):759-766. doi:10.1093/nar/19.4.759.

29. Seeman NC. Nanomaterials based on DNA. ***Annu Rev Biochem***. 2010;79:65-87. doi:10.1146/annurev-biochem-060308-102244.

30. Bai X, Martin TG, Scheres SHW, Dietz H. Cryo-EM structure of a 3D DNA-origami object. ***Proc Natl Acad Sci U S A***. 2012;109(49):20012-20017. doi:10.1073/pnas.1215713109.

31. Ke Y, Sharma J, Liu M, Jahn K, Liu Y, Yan H. Scaffolded DNA origami of a DNA tetrahedron molecular container. ***Nano Lett***. 2009;9(6):2445-2447. doi:10.1021/nl901165f.

32. Goodman RP, Berry RM, Turberfield AJ. The single-step synthesis of a DNA tetrahedron. ***Chem Commun (Camb)***. 2004;44(April):1372-1373. doi:10.1039/b402293a.
33. Carneiro KMM, Greschner AA. Recent advances in self-assembled DNA nanosensors. ***Am J Nano Res Appl Spec Issue Nanomater Nanosensors Chem Biol Detect***. 2015;3(1):1-7. doi:10.11648/j.nano.s.2015030101.11.
34. Jiang Q, Song C, Nangreave J, et al. DNA origami as a carrier for circumvention of drug resistance. ***J Am Chem Soc***. 2012;134(32):13396-13403. doi:10.1021/ja304263n.
35. Özhalici-Ünal H, Armitage BA. Fluorescent DNA nanotags based on a self-assembled DNA tetrahedron. ***ACS Nano***. 2009;3(2):425-433. doi:10.1021/nn800727x.
36. Yang XH, Huang JH, Wang Q, Wang KM, Yang LJ, Huo XQ. A one-step sensitive dynamic light scattering method for adenosine detection using split aptamer fragments. ***Anal Methods***. 2011;3(1):59-61. doi:10.1039/c0ay00709a.
37. Chang M, Yang C-S, Huang D-M. Aptamer-Conjugated DNA Icosahedral Nanoparticles As a Carrier of Doxorubicin for Cancer Therapy. ***ACS Nano***. 2011;5(8):6156-6163. doi:10.1021/nn200693a.

Conclusion et perspectives

Les objectifs de ce travail sont de construire des structures d'ADN auto-assemblées avec des extrémités pendantes avec l'aptamère scindés comme un déclencheur pour contrôler un changement dans les structures d'ADN et d'utiliser de telles structures d'ADN dans le développement de nouvelles méthodes de détection pour les petites molécules qui ne dépendent pas d'une amplification du signal avec des nanoparticules d'or ou des labels fluorescents. Nous avons synthétisé avec succès les unités d'ADN de 1D à 3D (duplex, forme Y à trois voies et tétraèdre) avec des extrémités pendantes avec l'aptamère scindés. Ces unités peuvent encore construire des structures plus complexes avec la présence en solution de molécules d'adénosine en raison de l'interaction entre les aptamères scindés et l'adénosine. Les structures complexes (chaîne d'ADN 1D, réseau ADN 2D et 3D) ont été utilisées comme méthode d'amplification du signal pour de nouveaux aptasenseurs.

Dans cette thèse, nous avons démontré deux nouvelles méthodes de détection pour les molécules d'adénosine: une détection hétérogène avec SPRi et une détection homogène avec spectroscopie UV. La SPRi est une méthode de détection capable de détecter le changement de masse sur la surface de l'or en temps réel en analysant la réflectivité de la solution. Notre méthode profite de l'effet massique de grandes structures d'ADN comme moyen d'amplification du signal. Deux modèles de séquence 1D différents ont été prouvés pour cette application et le protocole a été amélioré pour obtenir un signal plus fort. L'influence de la densité de greffage des sondes a été étudié, elle a eu un impact tant sur l'intensité du signal que sur le nombre de ponts d'adénosine sur chaque sonde. Une limite de détection de 10 µM a été obtenue pour cette méthode. Le réseau 2D formé par des structures d'ADN en forme de Y a également été testé en utilisant cette méthode. Le résultat a montré avec succès la détection d'adénosine et la formation du réseau a augmenté le signal SPR de l'ADN unique de forme Y par deux fois. Cependant, en raison de la limitation du temps, le protocole de cette méthode de détection n'a pas été complètement optimisé. La deuxième méthode de détection utilise la courbe de fusion calculée à partir de l'absorbance UV de la solution pour détecter le changement de structure d'ADN en raison de la présence d'adénosine. La courbe de fusion des structures d'ADN complexes 1D à 3D avait deux pics de fusion, l'un correspondant au pont d'adénosine et l'autre correspondant aux oligonucléotides hybridés. Le second pic de fusion a servi de référence interne pour éliminer l'influence du tampon sur le résultat. Le déplacement et l'intensité accrue observée dans le premier pic de fusion en raison de la présence d'adénosine ont été utilisés pour la détection. Une limite de détection de 1 µM a été obtenue par cette méthode. Le réseau 3D formé par les tétraèdres s'est avéré être le choix idéal pour cette méthode.

L'intérêt pour le travail futur de ce projet réside dans l'amélioration de la détection à l'aide de réseaux 2D et 3D. Les deux méthodes de détection ont été bien développées pour la structure de la chaîne d'ADN 1D et ont encore des possibilités d'amélioration pour les réseaux d'ADN 2D et 3D. Un autre objectif peut être de modifier le protocole contre d'autres cibles de petites molécules, telles que la cocaïne, ochratoxin A, acides aminés, etc. Les méthodes de détection étaient basées sur l'interaction entre les cibles et les extrémités pendantes de l' aptamère scindés. La cible de la détection peut être changée en modifiant les extrémités pendantes de l' aptamère scindés vers une autre cible tout en restant le cadre des structures d'ADN construites par les unités d'ADN simples. Nous avons également commencé des travaux préliminaires sur la caractérisation de la structure de l'ADN en utilisant l'AFM. Une image du réseau a déjà été capturée, mais la résolution nécessaire pour caractériser des structures d'ADN avec une taille aussi petite est encore un défi.

Conclusion and perspective

The purposes of this work are to build self-assembled DNA structures with split-aptamer dangling ends as a trigger to control a change in the DNA structures and to use such DNA structures in developing new detection methods for small molecules that do not depend on signal amplification with gold nanoparticles or fluorescent labels. We have successfully synthesized DNA units with split-aptamer dangling ends from 1D to 3D (duplex, Y shape three-way junction and tetrahedron). These units can further construct more complex structures with the presence of Adenosine molecules in the solution due to the interaction between split-aptamers and Adenosine. The complex structures (1D DNA chain, 2D and 3D DNA network) were used as a signal amplification method for new aptasensors.

In this thesis we have demonstrated two new detection methods for Adenosine molecules: a heterogeneous detection with SPRi and a homogeneous detection with UV spectroscopy. SPRi is a detection method that can sense the change of mass on gold surface in real-time by monitoring the reflectivity of the solution. Our method takes advantage of the mass effect of large DNA structures as a way for signal amplification. Two different 1D sequence designs were proven suitable for this application and the protocol has been improved to achieve stronger signal. The influence of the grafting density of the probes was studied, it had an impact in both the strength of signal and the number of Adenosine bridges on each probe. A detection limit of 10 μM was achieved for this method. The 2D network formed by Y shape DNA structures was also tested using this method. The result has shown success in the detection of Adenosine and the formation of the network increased the SPR signal of the single Y shape DNA by two fold. However, due to the limitation of time the protocol of this detection method has not been completely optimized. The second detection method uses the melting curve calculated from the UV absorbance

of the solution to detect the change of DNA structure due to the presence of Adenosine. The melting curve of the 1D to 3D complex DNA structures had two melting peaks, one corresponding to the Adenosine bridge and the other corresponding to the hybridized oligonucleotides. The second melting peak served as an internal reference to eliminate the influence of the buffer on the result. The shift and increased intensity observed in the first melting peak due to the presence of Adenosine was used for detection. A detection limit of 1 μM was achieved by this method. The 3D network formed by tetrahedrons was also proven to be ideal choice for this method.

The interest in the future work of this project lies in improving the detection using 2D and 3D networks. The two detection methods have been well-developed for the 1D DNA chain structure and still have room for improvement for the 2D and 3D DNA networks. Another objective can be altering the protocol against other small molecule targets, such as cocaine, ochratoxin A, amino acids, etc. The detection methods were based on the interaction between the targets and the split-aptamer dangling ends. The target of detection can be switched by altering the split-aptamer dangling ends towards another target while remaining the framework of the DNA structures built by the simple DNA units. We have also started some primary work on characterizing the DNA structure using AFM. An image of the network has already been captured but the resolution of characterizing DNA structures with such small size is still a challenge.

Appendix

Buffer used in the experiments:

Buffer	Composition
SPR buffer	HEPES 10 mM, $MgCl_2$ 5mM, NaCl 150mM, pH=7.4
Grafting buffer	HK_2PO_4 1M pH 9,25
Fluorescent buffer[1]	0.32X SYBR Green, HEPES 10 mM, $MgCl_2$ 5mM, NaCl 150mM
Fluorescent buffer[2]	1X SYBR Green, HEPES 10 mM, $MgCl_2$ 5mM, NaCl 150mM

Fluorescnet buffer [1]: The buffer used for fluorescent spectroscopy with Step-one real time PCR system

Fluorescnet buffer [2]: The buffer used for fluorescent spectroscopy with Fluoromax 4 spectrofluorometer

Oligonucleotide used in the experiments

1D DNA structure experiments (SPRi)

Name	Sequence (5' to 3')
S5Z	TGCGGAGGAAGGTTGAGGACCATCGTGCGGGTAGGTAGACC
S5*Zc	GAGAACCTGGGGGAGTAGGTCTACCTACCCGCACGATGGTC
S6Z	CCTGCGGAGGAAGGTTCGACCATCGTGCGGGTAGGTAGA
S6*Zc	GAACCTGGGGGAGTAGGTCTACCTACCCGCACGATGGTC
S8Z	CCTGCGGAGGAAGGTTCTCGACCATCGTGCGGGTAGGTAGA
S8*Zc	GAACCTGGGGGAGTAGGTCTACCTACCCGCACGATGGTC
S6cZc	GAACCTTCCTCCGCAGGTCTACCTACCCGCACGATGGTC
NC	HS-TGCGATCGCAGCGGTAACCTGACC
Z	HS-GGTCTACCTACCCGCACGATGGTC

1D DNA structure experiments (UV spectroscopy)

Name	Sequence (5' to 3')
tg-S5Z	TGCGGAGGAAGGTTGAGGACCATCGTGCGGGTAGGTAGACC
cc-S5Z	CCTGCGGAGGAAGGTTGACCATCGTGCGGGTAGGTAGA
tg-S5*Zc	GAGAACCTGGGGGAGTAGGTCTACCTACCCGCACGATGGTC
cc-S5*Zc	AACCTGGGGGAGTAGGTCTACCTACCCGCACGATGGTC
tg-S6Z	TGCGGAGGAAGGTTCGACCATCGTGCGGGTAGGTAGACC
cc-S6Z	CCTGCGGAGGAAGGTTCGACCATCGTGCGGGTAGGTAGA
S6*Zc	GAACCTGGGGGAGTAGGTCTACCTACCCGCACGATGGTC
S8Z	CCTGCGGAGGAAGGTTCTCGACCATCGTGCGGGTAGGTAGA
S8*Zc	GAACCTGGGGGAGTAGGTCTACCTACCCGCACGATGGTC
S6cZc	GAACCTTCCTCCGCAGGTCTACCTACCCGCACGATGGTC
A6	GAACCTGGGGGAGTATTGCGGAGGAAGGTTC

2D DNA structure experiments

Name	Sequence (5' to 3')
Ya	CAGGCCACTTACGGCTCAGCCTCAGCTGAAA
Yb	CTTGATATCTTGCTGGAGCCGTAAGTGGCCTG
Yc	TTTCAGCTGAGGCTGATCCAGCAAGATATCAAG
YaS6*	CAGGCCACTTACGGCTCAGCCTCAGCTGAAAGAACCTGGGGGAGTA
YbS6	CTTGATATCTTGCTGGAGCCGTAAGTGGCCTGTGCGGAGGAAGGTTC
YbS6*	CTTGATATCTTGCTGGAGCCGTAAGTGGCCTGGAACCTGGGGGAGTA
YcS6	TTTCAGCTGAGGCTGATCCAGCAAGATATCAAGTGCGGAGGAAGGTTC
10T-S6	HS-T_{10}GCGGAGGAAGGTTC
10T-S6*	HS-T_{10}GAACCTGGGGGAGTA

3D DNA structure experiments

Name	Sequence (5' to 3')
T1	GAACCTGGGGGAGTAACATTCCTAAGTCTGAAACATTACAGCTTGCTACAC GAGAAGAGCCGCCATAGTA
T2	TGCGGAGGAAGGTTCTATCACCAGGCAGTTGACAGTGTAGCAAGCTGTAAT AGATGCGAGGGTCCAATAC
T3	TGCGGAGGAAGGTTCTCAACTGCCTGGTGATAAAACGACACTACGTGGGAA TCTACTATGGCGGCTCTTC
T4	GAACCTGGGGGAGTATTCAGACTTAGGAATGTGCTTCCCACGTAGTGTCGTT TGTATTGGACCCTCGCAT